A LEAST-SQUARES/ GALERKIN SPLIT FINITE ELEMENT METHOD FOR INCOMPRESSIBLE AND COMPRESSIBLE NAVIER-STOKES EQUATIONS

by

RAJEEV KUMAR

Presented to the Faculty of the Graduate School of

The University of Texas at Arlington in Partial Fulfillment

of the Requirements

for the Degree of

DOCTOR OF PHILOSOPHY

THE UNIVERSITY OF TEXAS AT ARLINGTON

August 2008

ACKNOWLEDGEMENTS

I would first like to thank my advisor Dr. Brian Dennis for his able guidance, constant encouragement and support throughout the course of this research. I would also like to thank Dr. Zhen Xue Han for many valuable suggestions. I would also like to express my gratitude to Dr. Kent Lawrence, Dr. Chaoqun Liu, Dr. Guojun Liao and Dr. Zhen Xue Han for kindly accepting to be members of the supervising committee.

I am greatly indebted to my CFD lab colleague Takahiro Sonoda for many valuable discussions and insightful suggestions. I would also like to thank my other CFD lab colleagues Weiya Jin, Tao Heng Pan, Wei Han, Rachaneewan Charoenwat, Ai Ueno, Satoshi Ukai, Chinmay Adhvaryu, James Ruiz, Harsh Shah and Kamal Chauhan for all their friendship and cooperation.

This work was partially funded by Texas Space Grant Consortium, their role is duly acknowledged.

To my parents, brothers and sisters and late grand father, my eternal thanks for their continuous encouragement and support during my studies.

To my new-born daughter Nivedita for being such a nice baby and staying healthy which helped my studies go smoothly.

Last but not least, I would like to specially thank my wife Alpna Kumar for her support, patience, and words of encouragement and inspiration during my studies.

July 15, 2008

ABSTRACT

A SPLIT LEAST-SQUARES/ GALERKIN SPLIT FINITE ELEMENT METHOD FOR INCOMPRESSIBLE AND COMPRESSIBLE NAVIER-STOKES EQUATIONS

RAJEEV KUMAR, PhD.

The University of Texas at Arlington, 2008

Supervising Professor: Dr. Brian Dennis

Over the years Galerkin finite element method along with its variants has been used to solve incompressible and compressible Navier-Stokes equations. The Galerkin method which is more suited for self-adjoint type system of equations like in solid mechanics and heat conduction struggles when applied to non self-adjoint type systems like one encountered in fluid dynamics. Velocity and pressure variables have to be approximated using functions which belong to different spaces and must satisfy the tough LBB condition.

The least-squares finite element method (LSFEM), which is based on minimizing the l^2-norm of the residual, has many attractive advantages over Galerkin

finite element method (GFEM). It is now well established as a proper approach to deal with the convection dominated fluid dynamic equations. The least-squares finite element method has a number of attractive characteristics such as the lack of an *inf-sup* condition and the resulting symmetric positive system of algebraic equations unlike GFEM. However, the higher continuity requirements for second-order terms in the governing equations force the introduction of additional unknowns through the use of an equivalent first-order system of equations or the use of C^1 continuous basis functions. These additional unknowns lead to increased memory and computing time requirements that have limited the application of LSFEM to large-scale practical problems, such as three-dimensional compressible viscous flows.

A simple finite element method is proposed that employs a least-squares method for first-order derivatives and a Galerkin method for second order derivatives, thereby avoiding the need for additional unknowns required by a pure LSFEM approach. When the unsteady form of the governing equations is used, a streamline upwinding term is introduced naturally by the least-squares method. Resulting system matrix is always symmetric and positive definite and can be solved by iterative solvers like pre-conditioned conjugate gradient method. The method is stable for convection-dominated flows and allows for equal-order basis functions for both pressure and velocity. The stability and accuracy of the method are demonstrated with preliminary results of several benchmark problems solved using low-order C^0 continuous elements.

TABLE OF CONTENTS

LIST OF ILLUSTRATIONS

LIST OF TABLES

CHAPTER 1

INTRODUCTION

Problems in physics and engineering generally can be modeled through a system of partial differential equations. In general, the partial differential equations cannot be solved analytically; therefore a numerical method is required to obtain solutions. Early work on numerical solution of partial differential equations can be traced to the use of finite difference methods in 1940s. Difficulties and frustration associated with using finite difference methods on more difficult and geometrically challenging problems inspired the development of finite element methods (FEM).

1.1 Finite Element Methods: Historical Background

In mid-1950s, engineers began to solve continuum problems in elasticity using small, discrete "elements" to describe the overall behavior of simple elastic bars. Hence the finite element method was introduced into aircraft industry. However the credit to coin the term *finite element* for these discrete "elements" goes to Clough [1]. Since then finite element methods has emerged as one of the most powerful numerical methods devised so far. Its widespread acceptance in the field of science and engineering is due to its attractive attributes like ease in negotiating complex geometries, the consistent treatment of the differential-type boundary conditions, easy programmability and most importantly the sound mathematical foundations. Due to its versatility and rich

mathematical basis, it soon spread from the structural mechanics, its original field of application to non-structural areas like heat conduction, electromagnetism and fluid mechanics etc. Earliest application of FEM to field problems like heat conduction, irrotational fluid flow involving Laplace and Poisson equations were done by Zienkiewicz et al [2] and Oden [3]. Heat transfer problems with complex boundaries are discussed in details by Huebner [4].

In the past, finite element method was synonymous with Galerkin finite element method (GFEM). GFEM which is based on method of weighted residuals was highly successful in solid/ structural mechanics, the field of its origin. GFEM worked equally well in other situations like heat conduction that is governed by diffusion type equations. The reason for this success was, when applied to problems governed by self-adjoint elliptic or parabolic partial differential equations, GFEM leads to symmetric stiffness matrices. In such cases the difference between finite element solution and the exact solution is minimized with respect to the energy norm. Practically Galerkin formulation is optimal in problems governed by self-adjoint equations. In such cases, there exists a quadratic functional the minimum of which corresponds to satisfying the partial differential equation governing the problem. For example, in structural mechanics the equilibrium position of a structure corresponds to the minimum of the quadratic functional expressing the total potential energy of the structure. Similarly in heat conduction, the thermal equilibrium achieved by solving the Laplace or Poisson equation actually corresponds to the minimum of the quadratic functional expressed in terms of thermal flux which is representation of the total energy of the system at that

moment. This success of GFEM in above mentioned fields provided strong case for its use in fluid dynamics. Similar success was expected in fluid dynamics too.

1.2 Introduction of Finite Element Methods into Fluid Mechanics

1.2.1 Early Problems with Convective Terms in Fluid Mechanics

Finite element methods were introduced to fluid mechanics with great expectations in 1970s. The great expectation that the significant success of GFEM in structural dynamics and heat conduction problems would be replicated in fluid dynamics did not realize. Early application of finite element technique to viscous fluid flow was given in 1971 by Baker [5]. Finite element methods make use of a spatial discretization and a weighted residual formulation to reach a system of equations. GFEM is the most widely used among these weighted residual formulations, where weight and interpolation functions are identical. But in fluid dynamics, convection operators present in the non-Lagrangian formulation of the governing equations render the system of equation non-symmetric and the best approximation property in energy norm which made GFEM a success in structural mechanics is lost. Consequently, solutions to non self-adjoint fluid dynamic problems by GFEM are often corrupted by spurious node to node oscillations. This problem has motivated the development of alternatives to the GFEM which preclude oscillations without requiring mesh or time-step refinement.

1.2.2 Upwind Differencing

It is well known that the GFEM gives rise to central difference type approximation of the differential operator, leading to instability. This lead to the first

alternative formulation in early 1970s that tried to reproduce in the finite element context the effect of **upwind differencing** used in finite difference context to stabilize the oscillatory results by a central difference scheme. The upwind derivative of the convective term introduces a numerical dissipation, in addition to the physical dissipation. It was however noticed that the upwind treatment of the convective term leads to excessively dissipative results. This not fully satisfactory approach paved the way for more convincing finite element procedures.

An initial upwind FEM was presented by Christie et al. [6] for the one dimensional convection-diffusion equation, by modifying weighting functions to achieve the upwind effect. Essentially, the element upstream of a node is weighted more heavily than the element downstream of a node. This method was later generalized to the two dimensional case by Heinrich et al. [7]. Since the modified weighting function is used, it no longer remains the same as the interpolating function. Therefore these formulations fall in the category of **Petrov-Galerkin methods**, where weighting functions and interpolating functions are from different spaces. Hughes [8] in 1978 suggested that the upwind effect can also be achieved through a modification of the numerical quadrature for the convective term. Hughes and Atkinson [9], using a different approach, derived an optimal upwind from a variational principle, demonstrating that upwind methods can be developed from a firm theoretical basis. Many other researchers like Heinrich and Zienkiewicz [10], Griffiths and Mitchell [11] gave successful upwind formulations. Most of these upwind formulations give exact solutions for one-dimensional problems but when generalized to multi-directional flow

situations some of these formulations are far from optimal. They generate solutions that exhibit excessive diffusion in perpendicular to flow direction. Thus there was a need for more refined upwind schemes.

1.2.3 The Streamline Upwind Petrov-Galerkin Formulation

The extension to multidimensional domains of the concept of modified weighting functions is not easy. The crucial issue is that the diffusion should be added in the flow direction only, and not transversely. The reason is that the convective transport takes place along the streamlines and adding diffusion transversely to the flow leads to overly diffusive results because of excessive crosswind diffusion. Brooks et al. [12] in 1982 came up with **Streamline Upwind Petrov-Galerkin (SUPG)** formulation, where the added dissipation has anisotropic nature, acting just in flow direction. This is achieved through standard Galerkin weighting functions by adding a streamline upwind perturbation, which acts just in the flow direction. This method successfully incorporates streamline upwind concept, which precludes the possibilities of excessive crosswind diffusion while eliminates artificial diffusion that plagues many upwind schemes by consistent Petrov-Galerkin formulation. The method is easy to implement and does not require higher order weighting functions. Johnson [13] and Nävert [14] constructed multi-dimensional version of SUPG for advection diffusion. The SUPG method provided by Brooks et al. [12] was generalized to hyperbolic systems of conservation laws by Hughes et al. [15] with emphasis of high speed flows with shocks. SUPG is an excellent method for problems with smooth solutions, but introduces localized oscillations about sharp internal and boundary layers. Hughes et al. [16] added

a discontinuity capturing term that provides additional control over gradients, but this was restricted to scalar convection-diffusion equation. Later in Hughes et al. [17] the discontinuity capturing term was generalized to multidimensional systems.

1.3 Finite Element Methods for Navier-Stokes Equations

When it comes to finite element methods for solving incompressible viscous flows, most of the methods developed over the decades are based on velocity-pressure formulations because of its simpler boundary conditions and easy extension to three-dimensions. Most commonly used velocity-pressure formulations are **mixed Galerkin method,** the **penalty method** and the **segregated method**.

1.3.1 The Mixed-Galerkin Method

In mixed Galerkin method, lack of diffusive term in the continuity equation makes the advective-diffusive Navier-Stokes system of equations an incomplete parabolic one and has so-called singular behavior. This singularity stems from the fact that pressure is not one of the unknowns in the continuity equation. The continuity equation is a kinematic constraint instead of an equal-footing governing equation such as momentum equations [18]. Pressure is the Lagrange multiplier of the system. In order to construct a solution, pressure (the Lagrange multiplier), and the velocities (the solution of the governing equations) should be defined in different function spaces.

Zienkiewicz and Wu [19] explained the numerical manifestation of this singularity on the basis of the structure of the linear algebraic system of the discretized flow equations. The block in the global coefficient matrix corresponding to momentum

equations is usually positive definite. Whereas the block corresponding to continuity equation has null diagonal, that makes the overall global matrix singular.

Importantly, for compressible flows, there are additional unknowns like temperature and density. Pressure now is related to temperature and density through the equation of state, and thereby can be eliminated from the flow equations. This is common practice in high speed compressible flow computations. For low speed compressible flows, however pressure fluctuation rather than the pressure itself, becomes the unknown and equation of state becomes a reciprocal correlation between temperature and density [20]. Pressure (fluctuation) is no longer directly related to them. Therefore pressure (fluctuation) can not be eliminated from the list of unknowns. Similar to incompressible flows, pressure (fluctuation here) does not appear in continuity equation and the singularity problem emerges again.

Various methods were developed to overcome this singularity problem. One way is to ensure that the coefficient matrix with null diagonal sub matrix is not singular. Only certain combinations of approximation functions for velocities and pressure ensure that. These combinations must satisfy the Ladyzhenskaya-Babuška-Brezzi (LBB) condition for the existence of solutions [21, 22]. Although for two dimensional problems quite a few such combinations are available, most of these combinations are tough to implement. For three dimensional problems, this difficulty becomes even more severe. Another difficulty is that the matrix associated mixed-Galerkin method is **non-symmetric due to presence of convection terms** in the Navier-Stokes equations and **non-positive definite due to uncoupled nature of incompressibility constraint**.

Therefore direct solvers like Gaussian elimination rather than iterative solvers like pcg method have to be applied.

1.3.2 The Penalty Method

In the penalty method, pressure is pre-eliminated by penalizing the continuity equation. Considerable saving in computation time and memory can be achieved since only velocities are involved. Pressure is recovered by using the perturbed mass-conservation equation. This recovered pressure may exhibit oscillations due to ill-conditioning of pressure matrix. Another disadvantage is that for small values of penalty parameter there may be loss of accuracy and for large values the scheme may not converge at all.

1.3.3 The Segregated Method

The segregated method [23, 24] adopts a well-known SIMPLE-type algorithm. Since computation of velocity and pressure are decoupled, considerable saving in computation time and memory ca be effected. But the pressure values computed may be inaccurate due to lack of proper pressure boundary conditions for pressure correction equation.

1.4 The Least-Squares Finite Element Method

Least squares finite element method (LSFEM) recently developed by Jiang et al. [25-27] seems to overcome these difficulties by providing a symmetric positive definite system of equations and freedom from meeting LBB condition. However, higher continuity requirements for second-order terms in the governing equations force the introduction of additional unknowns by use of an equivalent first-order system of

equations or the use of C^1 continuous basis functions. These additional unknowns lead to increased memory and computing time requirements that have limited the application of LSFEM to large-scale practical problems, such as three-dimensional compressible viscous flows.

1.5 The Proposed Least-Squares/Galerkin Split Finite Element Method

A novel and simple finite element method is proposed in this work that employs a least-squares method for first-order derivatives and a Galerkin method for second order derivatives, thereby avoiding the need for additional unknowns required by a pure LSFEM approach. This method doesn't need to satisfy the LBB condition. Galerkin part of the method exploits the benefit of integration by parts. When the unsteady form of the governing equations is used, a streamline upwinding term is introduced naturally by the least-squares method. Resulting system matrix is always symmetric and positive definite and can be solved by iterative solvers like pre-conditioned conjugate gradient method. The method is stable for convection-dominated flows and allows for equal-order basis functions for both pressure and velocity. The stability and accuracy of the method are demonstrated with preliminary results of several benchmark problems solved using low-order C^0 continuous elements [28]. The method has been successfully applied to incompressible flows and results have been accepted for publication [29].

1.6 Layout of the Dissertation

The novel finite element method proposed in this thesis is essentially based on Galerkin finite element methods (GFEM) and least-squares finite element methods (LSFEM) which are sub categories of the broader method of weighted residuals.

Chapter 2 discusses method of weighted residuals with emphasis on Galerkin and least squares finite element methods, both explained in the context of one dimensional applications. Chapter 3 contains the formulation of the proposed least-squares/ Galerkin split finite element method (LSGSFEM) explained on convection diffusion equation. This chapter also contains stability analysis for LSGS method, application to convection diffusion benchmarks and results. Chapter 4 contains formulation of LSGSFEM for incompressible Navier-Stokes equations and the results from its application to standard benchmark problems. Chapter 5 contains LSGS formulation for incompressible buoyancy-driven flows with Boussinesq-approximation and results from natural convection benchmark. Chapter 6 contains high speed compressible flow formulation of LSGSFEM and results from few benchmarks. Future works are discussed in Chapter 7 followed by a brief summary in chapter 8.

CHAPTER 2

FINITE ELEMENT METHODS: SOME FUNDAMENTALS

2.1 Introduction

Finite element methods originated from structural engineering or solid mechanics where it was realized that it was a form of Rayleigh-Ritz problem. The relation between these two methods comes from considering the variational form of a problem. For example, the solution *u(x)* of the Euler equation

$$-\frac{d}{dx}\left(p(x)\frac{du(x)}{dx}\right)+q(x)u(x)=f(x) \tag{2.1}$$

also corresponds to minimum of quadratic functional [30]

$$F(u)=\int_0^1\left[p(x)(u'(x))^2+q(x)(u(x))^2-2f(x)u(x)\right]dx \tag{2.2}$$

Therefore, instead of solving for the differential equation (2.1) to determine *u(x)*, an alternative but equivalent solution would be the *u(x)* which minimizes the functional of (2.2). The idea in Rayleigh-Ritz problem above is to approximate the solution by a finite number of functions $u(x)=\sum_i^m q_i N_i(x)$ and to determine the unknown coefficients q_i, which minimize the functional of (2.2).

In finite element methods the solution is also approximated by a finite number of functions which are typically ***local*** in nature as opposed to ***global*** functions used in Rayleigh-Ritz approach above. Generally in finite element methods the ***integral form***

(which is called the Galerkin formulation) rather than ***functional form*** is obtained through which the problem is reduced to a system of algebraic equations which could be solved numerically. Important connection between the Rayleigh-Ritz method and the finite element method was made when it was realized that the integral form of the finite element method was exactly the same as the functional form used in the Rayleigh-Ritz method.

This relation between the finite element method and the Rayleigh-Ritz method was very significant as it provided the finite element method a sound mathematical foundation. Initially this relation also proved somewhat misleading by implying that a functional form is needed to formulate the problem. This is, actually, not the case, as we don't need functional form but need integral formulation which can be effected in a very general way using the method of weighted residuals (MWR).

2.2 Method of Weighted Residuals

Method of weighted residuals (MWR) existed as an approximation technique for obtaining approximate solutions to linear and nonlinear partial differential equations even before the development of the finite element methods. It offers means to formulate the finite element equations.

Application of MWR mainly involves two steps. The first step is to assume the general functional behavior of the dependent field variable in some way as to satisfy the given differential equation and the boundary conditions. This approximation function, when substituted into the differential equation and boundary conditions results in some

error called ***residual***. This residual is required to vanish in some average sense over the entire solution domain.

The second step is to solve the equation (or equations) resulting from the first step and thereby specialize the general functional form to a particular function, which then becomes the approximate solution sought.

To describe the method of weighted residuals, let us consider a problem where we want to determine an approximate functional representation for a field variable u governed by the differential equation

$$\mathcal{L}(u) - f = 0 \tag{2.3}$$

in the domain Ω bounded by surface Γ, on which proper boundary conditions are prescribed. The function f is a known function of independent variables. It is assumed that the exact solution u(x, t) can accurately be represented by the approximate solution of the form

$$\tilde{u}(x,t) = u_0(x,t) + \sum_i^m \hat{u}_i N_i(x) \tag{2.4}$$

where $N_i(x)$ are analytic functions called the trial (or expansion) functions, m the number of degrees of freedom, $\hat{u}_i$ are the m unknown coefficients and $u_0(x,t)$ is selected to satisfy the initial and boundary conditions. Substitution of the approximate solution (2.4) into equation (2.3) produces a non-zero residual, $\mathcal{R}$

$$\mathcal{L}(\tilde{u}) - f = \mathcal{R} \tag{2.5}$$

The MWR seeks to determine the m unknown $\hat{u}_i$ in such a way that the residual $\mathcal{R}$ over the entire domain tends to zero. This is accomplished by forming a weighted average of the error and specifying that this weighted average vanishes over the solution domain. We choose m linearly independent weighting functions w_i and then impose a condition that

$$\int_\Omega w_i[\mathcal{L}(\tilde{u}) - f]d\Omega = \int_\Omega w_i \mathcal{R} d\Omega = 0, \qquad i = 1, 2, \ldots\ldots\ldots m \qquad (2.6)$$

then the weighted residual $w_i\mathcal{R}$ tends to zero in some sense and it is from this expression that the technique gets its name MWR. The nature of the scheme is determined by the choice of the expansion function $N_i(x)$ and the weighting function w_i. A list of important computational methods derived by different choices of the weighting functions is given in the following table.

Table 2.1 Various Choices of Weighting Functions and the Methods Produced

Weighting Function, $w_j(x)$	Method
$w_j(x) = \delta(x - x_j)$	Collocation
$w_j(x) = \begin{cases} 1 & \text{inside } \Omega^j \\ 0 & \text{inside } \Omega^j \end{cases}$	Finite volume (Subdomain)
$w_j(x) = \dfrac{\partial \mathcal{R}}{\partial \hat{u}_j}$	Least-squares
$w_j(x) = x^j$	Method of moments
$w_j(x) = N_j(x)$	Galerkin
$w_j(x) = \Psi_j(x) \quad (\neq N_j(x))$	Petrov-Galerkin

The MWR that is used the most to derive finite element method is Galerkin or Bubnov-Galerkin method, in which weighting functions are chosen to be same as the

approximating functions, i.e. $w_j(x) = N_j(x)$. There are many other choices in which $w_j(x) \neq N_j(x)$, these methods are called Petrov-Galerkin methods. One of the Petrov-Galerkin methods is more famous as Least-squares method in which $w_j(x) = \frac{\partial \mathcal{R}}{\partial \hat{u}_j}$. A brief introduction of the two of the methods which are important constituents of the LSGS method follows.

2.2.1 The Galerkin Finite Element Method

Galerkin formulation has been explained by considering the Poisson equation here, which arises in many areas like irrotational fluid flow, steady state heat conduction etc. Poisson equation in one-dimension is

$$\mathcal{L}(u) \equiv \frac{d^2u}{dx^2} + f = 0 \tag{2.7}$$

in domain $\Omega = \{ x \mid 0 < x < 1\}$ with boundary conditions: $u(0) = g_D$ and $\frac{du}{dx}(1) = g_N$. The boundary condition g_D specifies a condition on the solution and is referred to as Dirichlet (or essential) boundary condition, whereas the boundary condition $\frac{du}{dx}(1) = g_N$ specifies a condition on the derivative of the solution and is referred to as Neumann (or Natural) boundary condition.

In Galerkin method, the weighting functions are chosen to be the same as the approximating functions i.e. $w_j(x) = N_j(x)$. We first approximate the unknown exact solution $u(x)$ by $\tilde{u}(x)$, which has the form

$$\tilde{u}=\sum_{i=1}^{m} N_i(x)\hat{u}_i \tag{2.8}$$

Where N_i is the element interpolation function and m is the number of nodes per element. Applying a weighting function to the equation (2.7) and casting it in integral form gives

$$\int_{x_1}^{x_2} N_i(x)\left[\frac{d^2\tilde{u}}{dx^2}+f\right]dx=0 \tag{2.9}$$

where x_1 and x_2 are the end points of the line element . Integration by parts is applied to above equation to obtain

$$N_i\frac{\mathrm{d}\tilde{u}}{\mathrm{d}x}\bigg|_{x_1}^{x_2}-\int_{x_1}^{x_2}\frac{\mathrm{d}\tilde{u}}{\mathrm{d}x}\frac{\mathrm{d}N_i}{\mathrm{d}x}dx+\int_{x_1}^{x_2} f(x)\,N_i(x)\,\mathrm{d}x=0 \tag{2.10}$$

This equation is the weak form of equation (2.9). The solution $u(x)$ must have C^1 continuity in the original boundary value problem (2.7) as must $\tilde{u}(x)$ in the Galerkin integral of equation (2.9), but in the weak form (2.10), the continuity requirement on $\tilde{u}(x)$ is C^0. Also the integration by parts has brought the natural boundary condition into the formulation. Using the definition (2.8), we have

$$\frac{\mathrm{d}\tilde{u}}{\mathrm{d}x}=\sum_{i=1}^{m}\frac{\mathrm{d}N_i}{\mathrm{d}x}\hat{u}_i=\left[\frac{\mathrm{d}N_i}{\mathrm{d}x}\right]\{\hat{u}\}^e \tag{2.11}$$

where $\{\hat{u}\}^e$ is the column vector of the nodal unknowns of the element. Now the weak-form becomes

$$\int_{x_1}^{x_2}\left[\frac{\mathrm{d}N}{\mathrm{d}x}\right]\frac{\mathrm{d}N_i}{\mathrm{d}x}dx\{\hat{u}\}^e=N_i\frac{\mathrm{d}\tilde{u}}{\mathrm{d}x}\bigg|_{x_1}^{x_2}+\int_{x_1}^{x_2} f\,N_i\,\mathrm{d}x=0 \qquad i=1,2 \tag{2.12}$$

The first term on the RHS is the boundary condition term, and applied at global level once the matrix system is assembled over full domain. So at element level we have system of equation as

$$[ke]\{\hat{u}\}^e = \{fe\}^e \tag{2.13}$$

Where $[ke] = \int_{x_1}^{x_2} \left[\frac{\mathrm{d}N}{\mathrm{d}x}\right] \frac{\mathrm{d}N_i}{\mathrm{d}x} dx$ and $\{fe\}^e = \int_{x_1}^{x_2} f\, N_i \,\mathrm{d}x$ are the element stiffness matrix and the element force vector respectively. In the present one-dimensional case with linear element (i.e. $m = 2$) we have

$$[ke] = \int_{x_1}^{x_2} \begin{bmatrix} \frac{\mathrm{d}N_1}{\mathrm{d}x}\frac{\mathrm{d}N_1}{\mathrm{d}x} & \frac{\mathrm{d}N_1}{\mathrm{d}x}\frac{\mathrm{d}N_2}{\mathrm{d}x} \\ \frac{\mathrm{d}N_2}{\mathrm{d}x}\frac{\mathrm{d}N_1}{\mathrm{d}x} & \frac{\mathrm{d}N_2}{\mathrm{d}x}\frac{\mathrm{d}N_2}{\mathrm{d}x} \end{bmatrix} dx \text{ and } \{fe\}^e = \int_{x_1}^{x_2} \begin{Bmatrix} f\, N_1 \\ f\, N_2 \end{Bmatrix} \mathrm{d}x \text{ respectively.}$$

The element stiffness matrix [*ke*] and vector {*fe*} are assembled to get the global stiffness matrix and force vector. During the assembly of the matrices the natural boundary condition terms $\frac{\mathrm{d}\tilde{u}}{\mathrm{d}x}$ in the equation (2.12) cancel at all interior nodes of the domain, leaving only the natural boundary conditions to be specified at the end nodes.

2.2.2 The Least-Squares Finite Element Method

Least-squares finite element method is one of the methods of weighted residuals in which weight function is taken as $w_j(x) = \frac{\partial \mathcal{R}}{\partial \hat{u}_j}$. In other words l^2-norm of the residual is minimized in this method. Consider the one dimensional transient advection equation given as:

$$\frac{\partial U}{\partial t} + (\vec{V} \cdot \nabla) U = 0 \tag{2.13}$$

where U is the property being convected at a velocity $\vec{V}$ with u, v and w as its components in x, y and z directions respectively. Before application of the finite element method in space, the time derivative of (2.13) is discretized with a simple backward-Euler method.

$$\frac{U^{n+1}-U^{n}}{\Delta t}+\vec{V}\cdot\nabla U^{n+1}=0 \tag{2.14}$$

In the least-squares approach, the l^2-norm of the differential equation is minimized with respect to unknown coefficients over the solution domain, Ω. Applying the l^2-norm to (2.14) and minimizing the functional with respect to U^{n+1} leads to the weak statement.

$$\int_{\Omega}\left(\frac{\{N\}}{\Delta t}+(\vec{V}\cdot\nabla)\{N\}\right)\left(\frac{\{N\}}{\Delta t}+(\vec{V}\cdot\nabla)\{N\}\right)^{T} d\Omega\{U^{n+1}\}= \int_{\Omega}\left(\frac{\{N\}}{\Delta t}+(\vec{V}\cdot\nabla)\{N\}\right)\frac{\{N\}^{T}}{\Delta t}\{U^{n}\}d\Omega \tag{2.15}$$

where the row vector $\{N\}$ contains the basis functions N_j used to approximate the solution over the domain as $U(x,y,z)=\sum_j N_j(x)U_j=\{N\}^T\{U\}$.

The weak statement can be expanded and written in matrix form

$$\left(\frac{[M]}{\Delta t}+([C]+[C]^{T})+\Delta t\vec{V}^{T}\vec{V}[K]\right)\{U^{n+1}\}=\left(\frac{[M]}{\Delta t}\right)\{U^{n}\} \tag{2.16}$$

where the individual matrix contributions are given by

$$\begin{aligned}[M]&=\int_{\Omega}\{N\}\{N\}^{T}d\Omega\\ [C]&=\int_{\Omega}\{N\}\{(\vec{V}\cdot\nabla)N\}^{T}d\Omega\\ [K]&=\int_{\Omega}[\nabla N][\nabla N]^{T}d\Omega\end{aligned} \tag{2.17}$$

Equation (2.16) clearly shows that the resulting system of equations is symmetric, a quality that is not achievable for Galerkin finite element methods or even finite difference or finite volume methods. In addition, one can notice an upwind diffusion term that is implicit to the least-squares approach. The upwind diffusion is often useful for smoothing non-monotone solutions that occur before and after any sharp gradients that appear in the flow direction. These advantageous features of LSFEM have been well exploited for generating adaptive grid in order to capture shocks. A least-squares method based moving-node grid adaptation technique was used by Taghaddosi et al [31] to capture shocks in inviscid transonic and supersonic flows. The advantageous features of LSFEM with adaptive grids were used by Xue and Liao [32] to capture shocks while solving Burgers equations. Cai and Liao [33] also used LSFEM for grid generation on moving domains. Fleitas et al [34] demonstrated the need for a properly over determined system of equations in the context of LSFEM. They used overlapping elements with mesh free concept to create enough residual equations to achieve a properly over determined system of equations. There are no tunable parameters in the LSFEM approach, such parameters often appear in stabilized Galerkin methods and are difficult to determine in general.

CHAPTER 3

THE LEAST-SQUARES GALERKIN SPLIT FINITE ELEMENT METHOD: A NOVEL METHOD

3.1 Introduction

The least-squares finite element method (LSFEM), due to several attractive characteristics such as lack of an *inf-sup* condition and the resulting symmetric positive system of algebraic equations etc., is now well established as a proper approach to deal with the convection dominated fluid dynamic equations. However, problems arising due to the higher continuity requirements for second-order terms in the governing equations have limited the application of LSFEM to large-scale practical problems, such as three-dimensional compressible viscous flows.

A simple finite element method is proposed that employs a least-squares method for first-order derivatives and a Galerkin method for second order derivatives, thereby avoiding the additional unknowns required by a LSFEM approach. When the unsteady form of the governing equations is used, a streamline upwinding term is introduced naturally by the component least-squares method. Resulting system matrix is always symmetric, positive definite and can be solved by iterative solvers like pre-conditioned conjugate gradient method. The method is stable for convection-dominated flows and allows for equal-order basis functions for both pressure and velocity. The method is described below in the context of one-dimensional convection-diffusion equation

$$\frac{\partial T}{\partial t} + \vec{V}.\nabla T - k\nabla^2 T = 0 \tag{3.1}$$

Here T is the property being transported by the equation, k the thermal conductivity. The numerical difficulty with this equation (unstable solutions, asymmetric matrix) is due to the presence of first order of first order terms. Therefore one way of avoiding these difficulties was to solve first order terms using LSFEM for half of the time step and then solve for second order terms using Galerkin method in the second half of the time step. This gave the split time formulation that preceded the current LSGS formulation.

3.2 The Split Time Preliminary Formulation

This formulation was based on actually splitting the time derivative into two halves and solving first and second order terms in the governing equation separately using LSFEM and GFEM respectively. To explain this, consider the convection-diffusion equation (3.1), which after first order splitting in time can be written as

$$\frac{T^{n+1} - T^{n+\frac{1}{2}}}{\Delta t} + \frac{T^{n+\frac{1}{2}} - T^{n}}{\Delta t} = -\vec{V} \cdot \nabla T + k\nabla^2 T \tag{3.2}$$

and we can write

$$\frac{T^{n+\frac{1}{2}} - T^{n}}{\Delta t} - k\nabla^2 T = 0 \tag{3.3}$$

$$\frac{T^{n+1} - T^{n+\frac{1}{2}}}{\Delta t} + \vec{V} \cdot \nabla T = 0 \tag{3.4}$$

as the diffusion and convection steps respectively. Galerkin method applied to diffusion equation gives

$$\int_\Omega w\left(\frac{T^{n+\frac{1}{2}}-T^n}{\Delta t}-k\nabla^2 T\right)d\Omega=0 \tag{3.5}$$

After applying integration by parts to second order terms and θ-discretization we get

$$\int_\Omega\left(w\left(\frac{T^{n+\frac{1}{2}}-T^n}{\Delta t}\right)+k\theta\nabla w\nabla T^{n+\frac{1}{2}}+k(1-\theta)\nabla w\nabla T^n\right)d\Omega=0 \tag{3.6}$$

Galerkin method uses same basis for weighting and approximating functions i.e. we can write $w = \sum_i T_i N_i$ and $T = \sum_i T_i N_i$ and final variational form can be written as

$$\left(\frac{[M]}{\Delta t}+\theta k[K_D]\right)\{T^{n+\frac{1}{2}}\}=\left(\frac{[M]}{\Delta t}+(1-\theta)k[K_D]\right)\{T^n\} \tag{3.7}$$

Similarly the convection equation (3.4) can be θ-discretized as

$$\frac{T^{n+1}-T^{n+\frac{1}{2}}}{\Delta t}+\theta\vec{V}\cdot\nabla T^{n+1}+(1-\theta)\vec{V}\cdot\nabla T^{n+\frac{1}{2}}=0 \tag{3.8}$$

and after applying LSFEM , it can be written as

$$\begin{aligned}\left(\frac{[M]}{\Delta t^2}+\frac{\theta}{\Delta t}\left([C]+[C]^T\right)+\theta^2\vec{v}\vec{v}^T[K_D]\right)\{T^{n+1}\}=\\ \left(\frac{[M]}{\Delta t^2}+\frac{\theta}{\Delta t}[C]-\frac{(1-\theta)}{\Delta t}[C]^T-\theta(1-\theta)\vec{v}\vec{v}^T[K_D]\right)\{T^{n+\frac{1}{2}}\}\end{aligned} \tag{3.9}$$

In these equations

$$[C]=\int_\Omega\{N\}\{\vec{V}.\nabla N\}^T d\Omega \tag{3.10a}$$

$$\begin{aligned}[M]&=\int_\Omega\{N\}\{N\}^T d\Omega\\ [K_D]&=\int_\Omega\{\nabla N\}\{\nabla N\}^T d\Omega\\ [K_{UP}]&=\int_\Omega\{\vec{V}\cdot\nabla N\}\{\vec{V}\cdot\nabla N\}^T d\Omega\end{aligned} \tag{3.10b}$$

Equations (3.7) and (3.9), due to assumption that $T^{n+\frac{1}{2}} = \frac{T^{n+1} + T^n}{2}$, can be combined to form a single equation which for $\theta = 1$ can be written as

$$\left([M] + \Delta t([C] + [C]^T) + \Delta t^2 [K_{UP}] + \frac{k\Delta t}{2}[K_D]\right)\{T^{n+1}\} = \left([M] - \frac{k\Delta t}{2}[K_D]\right)\{T^n\} \tag{3.11}$$

But the assumption made above is not very sound as it is not necessary that $T^{n+\frac{1}{2}}$ is simple mean of T^{n+1} and T^n always. Therefore more robust formulation was constructed which is named least-squares Galerkin split finite element method.

3.3 The Least-Squares/Galerkin Split Finite Element Formulation

In the context of numerical difficulties caused by the first order terms in convection equation it has been seen that LSFEM produces a symmetric system of equations that yields a stable solution. Therefore, in LSGS formulation we apply the LSFEM to these terms only to determine the proper weighting function to apply to the full equation or to determine the Euler-Lagrange formulation which is equivalent to Galerkin method applied to a modified differential equation. First let us discretize time derivative and use θ-discretization for 1st order spatial derivative in model equation (3.1) as

$$\frac{T^{n+1} - T^n}{\Delta t} + \theta \vec{V}.\nabla T^{n+1} = (1-\theta)\vec{V}.\nabla T^n \tag{3.12}$$

Application of LSFEM to above transient convection equation yields

$$\begin{aligned} &\int_\Omega \left(\{N\} + \theta\Delta t(\vec{V}.\nabla)\{N\}\right)\left(\{N\} + \theta\Delta t(\vec{V}.\nabla)\{N\}\right)^T d\Omega \{T^{n+1}\} = \\ &\qquad \int_\Omega \left(\{N\} + \theta\Delta t(\vec{V}.\nabla)\{N\}\right)\left(\{N\} - (1-\theta)\Delta t(\vec{V}.\nabla)\{N\}\right)^T d\Omega \{T^n\} \end{aligned} \tag{3.13}$$

and Euler-Lagrange equation in matrix form for this weak statement becomes

$$\left([M]+\theta\Delta t\left([C]+[C]^T\right)+\theta^2\Delta t^2[K_{UP}]\right)\{T^{n+1}\}= \left([M]+\theta\Delta t[C]-(1-\theta)[C]^T-\theta(1-\theta)\Delta t^2[K_{UP}]\right)\{T^n\} \tag{3.14}$$

where matrices [*M*], [*C*] and [K_{UP}] are defined in (3.10). This is equivalent to a stabilized Petrov-Galerkin formulation using the weight function

$$\{N\}+\theta\Delta t\vec{V}.\nabla\{N\} \tag{3.15}$$

Applying this weight function to the residual of the original equation (3.1), we get

$$\int_\Omega\left(\{N\}+\theta\Delta t(\vec{V}.\nabla)\{N\}\right)\left(\{N\}+\theta\Delta t(\vec{V}.\nabla)\{N\}-\theta\Delta tk\nabla^2\{N\}\right)^T d\Omega\{T^{n+1}\}= \int_\Omega\left(\{N\}+\theta\Delta t(\vec{V}.\nabla)\{N\}\right)\left(\{N\}-(1-\theta)\Delta t(\vec{V}.\nabla)\{N\}+(1-\theta)\Delta tk\nabla^2\{N\}\right)^T d\Omega\{T^n\} \tag{3.16}$$

Integrals involving second order derivatives are resolved using integration by parts and subsequent terms still having second order terms are neglected. Above integrals lead to the final form of the LSGS formulation for transient convection-diffusion equation

$$\left([M]+\theta\Delta t\left([C]+[C]^T\right)+\theta^2\Delta t^2[K_{UP}]+\theta\Delta tk[K_D]\right)\{T^{n+1}\}= \left([M]-(1-\theta)[C]+\theta\Delta t[C]^T-\theta(1-\theta)\Delta t^2[K_{UP}]-(1-\theta)\Delta t[K_D]\right)\{T^n\} \tag{3.17}$$

When we have $\theta = 1$, we get fully implicit scheme

$$\left([M]+\Delta t\left([C]+[C]^T\right)+\Delta t^2[K_{UP}]+\Delta tk[K_D]\right)\{T^{n+1}\}=\left([M]+\Delta t[C]^T\right)\{T^n\} \tag{3.18}$$

and for $\theta = 1/2$, we get semi-implicit time accurate formulation

$$\left([M]+\frac{\Delta t}{2}\left([C]+[C]^T\right)+\frac{\Delta t^2}{4}[K_{UP}]+\frac{\Delta tk}{2}[K_D]\right)\{T^{n+1}\}= \left([M]-\frac{1}{2}[C]+\frac{\Delta t}{2}[C]^T-\frac{\Delta t^2}{4}[K_{UP}]-\frac{1}{2}\Delta t[K_D]\right)\{T^n\} \tag{3.19}$$

The element stiffness matrix produced by preliminary split time formulation (3.11) and the SLGSFEM (3.18) are characteristically the same, except for factor of 2 in last term

which does not change the behavior of the system. Therefore the stability analysis for split formulation in the following section is also valid for LSGSFEM.

3.3.1 Stability Analysis of LSGS Method

Stability analysis has been carried out on the equivalent split time formulation as it produces characteristically the same element stiffness matrix as LSGS formulation. We first compute the component amplification factors (see Appendix A) G_1 and G_2 for diffusion and convection step respectively with the help of table 3.1 of reference [35]. The overall amplification factor then is

$$G = G_1 \cdot G_2 = \frac{1 + 4(1-\theta)d\sin^2\xi/2}{1 + 4\theta d\sin^2\xi/2} \cdot \frac{1 - i(1-\theta)C\sin\xi - 2(1-\theta)C\sin^2\xi/2}{1 + i\theta C\sin\xi + 2\theta C\sin^2\xi/2} \tag{3.20}$$

For Euler backward Scheme, $\theta = 1$, So

$$G = \frac{1}{1 + 4d\sin^2\xi/2} \cdot \frac{1}{1 + iC\sin\xi + 2C\sin^2\xi/2}, \quad \text{For stability } |G| \le 1$$

$$\Rightarrow \; 1 + 2C\sin^2\xi/2 + iC\sin\xi \ge 1$$
$$\left(1 + 2C\sin^2\xi/2\right)^2 + \left(C\sin\xi\right)^2 \ge 1 \tag{3.21}$$

after simplification the stability condition becomes

$$C\left(\sin^2\xi/2 + \cos^2\xi/2\right) \ge 0 \tag{3.22}$$

which is always true, Therefore backward Euler scheme is unconditionally stable.

Similarly, for $\theta = 1/2$, the Crank-Nicolson scheme, equation (3.20) becomes

$$G = \frac{1 - C\sin\xi si\left(\sin\xi in + i\ \cos\xi os\right)}{1 + C\sin\xi si\left(\sin\xi/2 + i\ \cos\xi/2\right)}$$

For stability $|G| \le 1$, this leads to stability condition as

$$\left|1-C\sin\xi si\left(\sin\xi in+i\ cos\xi os\right)\right|\leq\left|1+C\sin\xi si\left(\sin\xi/2+i\ cos\xi/2\right)\right| \qquad (3.23)$$

which is always true, therefore Crank-Nicolson scheme is also unconditionally stable.

3.4 Application of LSGS Method to Convection-Diffusion Benchmarks

The LSGSFEM has been validated by solving a couple of following two-dimensional convection-diffusion benchmark problems.

3.4.1 Benchmark Problems

3.4.1.1 Transient Solute Transport Problem

The first problem is of evaluating transient solute transport in a two-dimensional semi-infinite isotropic porous medium (half plane) with a step change in concentration along the inlet during one-dimensional flow. Solute transport in porous media, a phenomenon of practical importance in engineering, agriculture and hydrology takes place by advection and dispersion. This benchmark problem was taken from a work by Leij and Dane [36]. Transport in a homogenous and isotropic medium during one dimensional steady state flow with two-dimensional diffusion is given by

$$\frac{\partial C}{\partial t}+u\frac{\partial C}{\partial x}-D_L\frac{\partial^2 C}{\partial x^2}-D_T\frac{\partial^2 C}{\partial y^2}=0 \qquad (3.4.1)$$

where C is the solute concentration, t the time, u the pore water velocity, D_L and D_T are the coefficients of longitudinal and transverse diffusion respectively. The solution domain is a half plane with $x \geq 0$ and other boundaries at infinity. The domain and the boundary conditions and initial conditions are shown in Fig. 1.

Problem was solved on a 25×20 uniform mesh in a rectangular domain measuring 50 cms in length and 20 cms in width. The porous medium with following arbitrary

transport properties: D_L = 25cm^2/d, D_T = 5cm^2/d and u = 50 cm/d was considered. All concentrations were expressed as dimensionless concentration, C with maximum value of 1 on positive y-axis and 0 on negative y-axis.

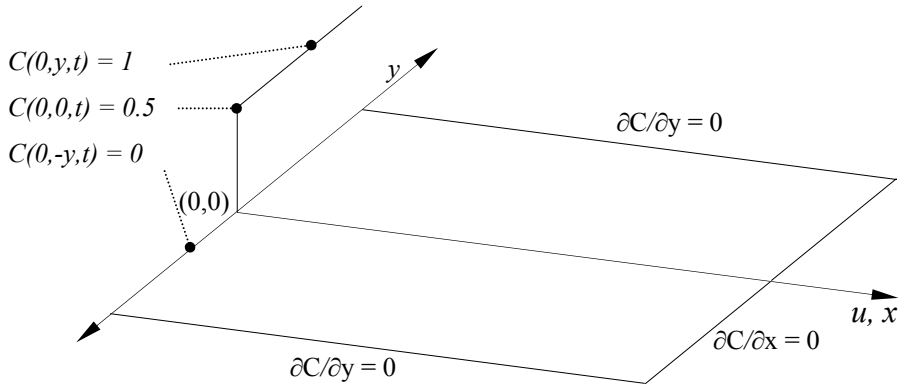

Initial Condition: C(x,y,0) = 0

Fig. 3.1 Domain of advection-diffusion of solute in a half plane

3.4.1.2 Double Glazing Problem

Second problem is a simple model of finding temperature distribution inside a cavity with recirculating wind and with one of the walls hot. The wind recirculating inside is given by $\vec{V}=\left(2y\left(1-x^2\right),-2x\left(1-y^2\right)\right)$. The problem taken from [37], is solved inside a square domain with side 2 units with 50×50 clustered mesh. The problem was also solved using standard Galerkin method and results were compared. The coefficient of thermal conductivity k = 1/200 was used.

3.4.1 Mathematical Formulation

3.4.2.1 Transient Solute Transport Problem

Equation (3.4.1), after θ-discretization can be written as

$$\frac{C^{n+1}}{\Delta t}+u\theta\frac{\partial C^{n+1}}{\partial x}-\theta\left(D_L\frac{\partial^2 C^{n+1}}{\partial x^2}+D_T\frac{\partial^2 C^{n+1}}{\partial y^2}\right)$$
$$=\frac{C^{n}}{\Delta t}-u(1-\theta)\frac{\partial C^{n}}{\partial x}+(1-\theta)\left(D_L\frac{\partial^2 C^{n}}{\partial x^2}+D_T\frac{\partial^2 C^{n}}{\partial y^2}\right) \tag{3.4.2}$$

Let us take the advection part (first order terms) only:

$$\frac{C^{n+1}}{\Delta t}+u\theta\frac{\partial C^{n+1}}{\partial x}=\frac{C^{n}}{\Delta t}-u(1-\theta)\frac{\partial C^{n}}{\partial x} \tag{3.4.3}$$

The least-squares treatment to it gives:

$$\int_\Omega\left(\frac{\{N\}}{\Delta t}+u\theta\frac{\partial\{N\}}{\partial x}\right)\left(\frac{\{N\}}{\Delta t}+u\theta\frac{\partial\{N\}}{\partial x}\right)d\Omega\{C^{n+1}\}$$
$$=\int_\Omega\left(\frac{\{N\}}{\Delta t}+u\theta\frac{\partial\{N\}}{\partial x}\right)\left(\frac{\{N\}}{\Delta t}-u(1-\theta)\frac{\partial\{N\}}{\partial x}\right)d\Omega\{C^{n}\} \tag{3.4.4}$$

resulting in following variational form of Euler-Lagrange equation

$$\int_\Omega\left(\frac{\{N\}\{N\}^T}{\Delta t^2}+\theta u\frac{\{N\}}{\Delta t}\frac{\partial\{N\}^T}{\partial x}+\theta u\frac{\partial\{N\}}{\partial x}\frac{\{N\}^T}{\Delta t}+\theta^2u^2\frac{\partial\{N\}}{\partial x}\frac{\partial\{N\}^T}{\partial x}\right)d\Omega\{C^{n+1}\}$$
$$=\int_\Omega\left(\frac{\{N\}\{N\}^T}{\Delta t^2}-(1-\theta)u\frac{\{N\}}{\Delta t}\frac{\partial\{N\}^T}{\partial x}+\theta u\frac{\partial\{N\}}{\partial x}\frac{\{N\}^T}{\Delta t}-\theta(1-\theta)u^2\frac{\partial\{N\}}{\partial x}\frac{\partial\{N\}^T}{\partial x}\right)d\Omega\{C^{n}\} \tag{3.4.5}$$

which has following equivalent Galerkin formulation

$$\int_\Omega\frac{\{N\}}{\Delta t}\left(\frac{\{N\}^T}{\Delta t}+\theta u\frac{\partial\{N\}^T}{\partial x}+\theta u\frac{\partial\{N\}}{\partial x}-\theta^2u^2\Delta t\frac{\partial^2\{N\}}{\partial x^2}\right)d\Omega\{C^{n+1}\}$$
$$=\int_\Omega\frac{\{N\}}{\Delta t}\left(\frac{\{N\}^T}{\Delta t}-(1-\theta)u\frac{\partial\{N\}^T}{\partial x}+\theta u\frac{\partial\{N\}}{\partial x}+\theta(1-\theta)u^2\Delta t\frac{\partial^2\{N\}}{\partial x^2}\right)d\Omega\{C^{n}\} \tag{3.4.6}$$

Now we simply add the left out second order terms of (3.4.2) in equation (3.4.6)

$$\int_{\Omega}\frac{\{N\}}{\Delta t}\left(\frac{\{N\}^T}{\Delta t}+\theta u\frac{\partial\{N\}^T}{\partial x}+\theta u\frac{\partial\{N\}}{\partial x}-\theta^2u^2\Delta t\frac{\partial^2\{N\}}{\partial x^2}-\theta D_L\frac{\partial^2\{N\}}{\partial x^2}-\theta D_T\frac{\partial^2\{N\}}{\partial y^2}\right)d\Omega\{C^{n+1}\}$$
$$=\int_{\Omega}\frac{\{N\}}{\Delta t}\left(\frac{\{N\}^T}{\Delta t}-(1-\theta)u\frac{\partial\{N\}^T}{\partial x}+\theta u\frac{\partial\{N\}}{\partial x}+\theta(1-\theta)u^2\Delta t\frac{\partial^2\{N\}}{\partial x^2}\right.$$
$$\left.+(1-\theta)D_L\frac{\partial^2\{N\}}{\partial x^2}+(1-\theta)D_T\frac{\partial^2\{N\}}{\partial y^2}\right)d\Omega\{C^n\} \qquad (3.4.7)$$

Effectively now GFEM is being applied to a modified equation which is stabilized after least-squares treatment to the first order terms. After applying integration by parts, we get the matrix form of the equation system

$$\begin{aligned}&\left([M]+\theta u\Delta t\left([M_x]+[M_x]^T\right)+\left(\theta^2u^2\Delta t^2+\theta\Delta tD_L\right)[K_x]+\theta\Delta tD_T[K_y]\right)\{C^{n+1}\}\\&=\left([M]-(1-\theta)u\Delta t[M_x]+\theta u\Delta t[M_x]^T-\theta(1-\theta)u^2\Delta t^2[K_x]-(1-\theta)\Delta tD_L[K_x]\right.\\&\qquad\left.-(1-\theta)\Delta tD_T[K_y]\right)\{C^n\}\end{aligned} \qquad (3.4.8)$$

3.4.2.2 Double Glazing Problem

This problem was solved using LSGSFEM and GFEM. The model equation to solve is standard convection diffusion equation

$$\frac{\partial T}{\partial t}+\vec{V}\cdot\nabla T-k\nabla^2T=0 \qquad (3.4.9)$$

LSGS formulation of this problem, on the lines similar to that in previous section leads to following matrix system of equations for backward Euler method ($\theta = 1$)

$$\left([M]+\Delta t\left([C]+[C]^T\right)+\Delta tk\,[K_D]+\Delta t^2[K_{UP}]\right)\{T^{n+1}\}=\left([M]+\Delta t[C]^T\right)\{T^n\} \qquad (3.4.10)$$

Since the problem was also solved using Galerkin method, the Galerkin formulation for backward Euler method ($\theta = 1$) is

$$\left([M]+\Delta t[C]+\Delta tk\,[K_D]\right)\{T^{n+1}\}=[M]\{T^n\} \qquad (3.4.11)$$

3.4.2 Results and Discussion

3.4.3.1 Transient Solute Transport Problem

The LSGS scheme was run for t = 0.25 d, 0.50 d, 0.75 d, 1 d, 1.25 d and all the way to steady state. Steady state was considered when l^2-norm of residual reached a tolerance level of 1E6. Time step of Δt = 0.001 d was used. Results are presented in Fig. 3.2 and 3.3. Transient solutions at the times stated above are shown in Fig. 3.2. The invasion of solute into the medium at $y > 0$ and the subsequent flattening of the solute front in both directions can be observed. The dimensionless concentration at the end of the domain (x = 50 cm) was recorded at t = 0.75 d, 1 d, 1.25 d and steady state. These profiles along with the analytical solution profiles are compared in Fig. 3.3. Analytical solution profiles were digitally scanned from reference [36].

3.4.3.2 Double Glazing Problem

Steady state results for this benchmark were obtained using LSGS and Galerkin method. In both the cases time step size, Δt = 0.001 was used. Results from this benchmark are shown in Fig. 3.4. Three dimensional surface plots, contour plots and temperature profiles along sections through x = 0.5 and y = 0.5 and the clustered mesh used are presented in Fig. 3.4. Excellent agreement between LSGS results and Galerkin results can be seen.

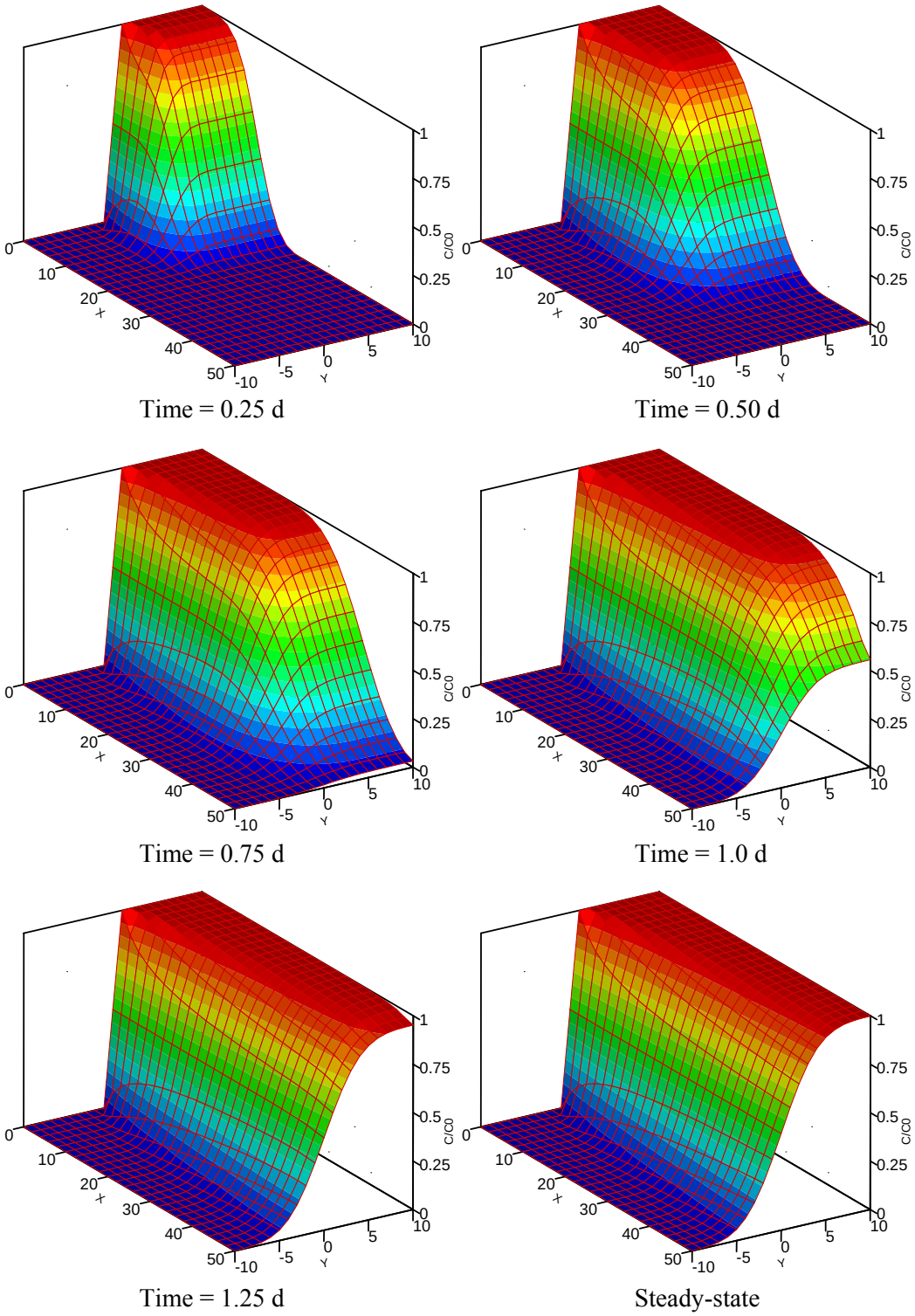

Fig. 3.2 Dimensionless concentration distribution of the solute using LSGS method at various times.

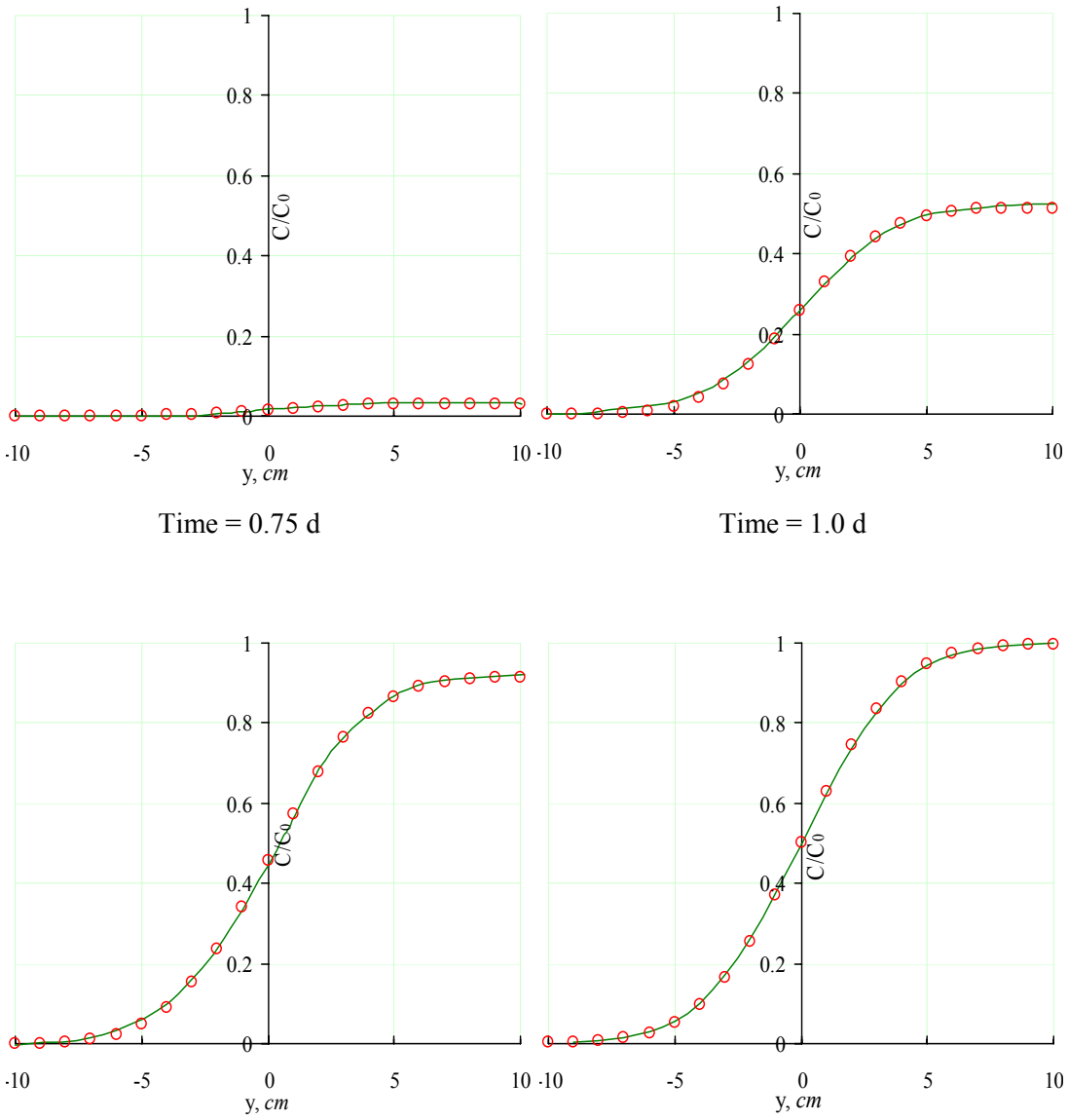

Fig. 3.3 Comparison of dimensionless concentration distribution computed using LSGS method with analytical solution at x = 50 cm. (○ LSGS, — analytical [36])

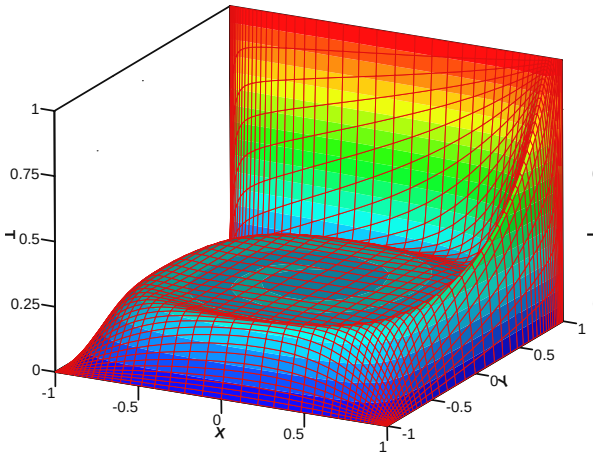

Surface plot LSGS

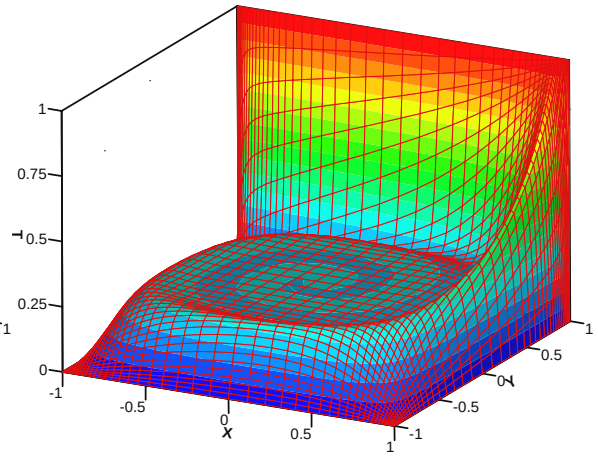

Surface plot GFEM

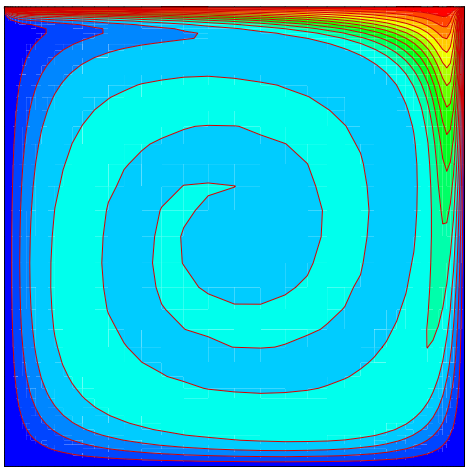

Contour plot LSGS

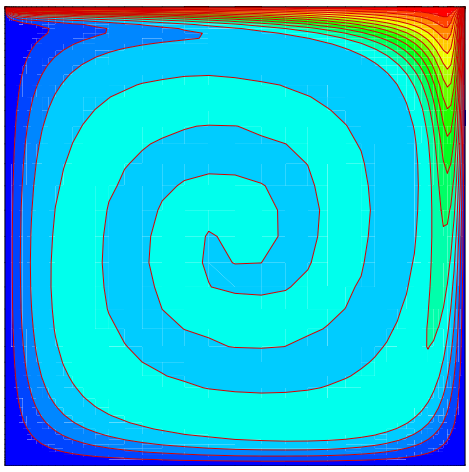

Contour plot GFEM

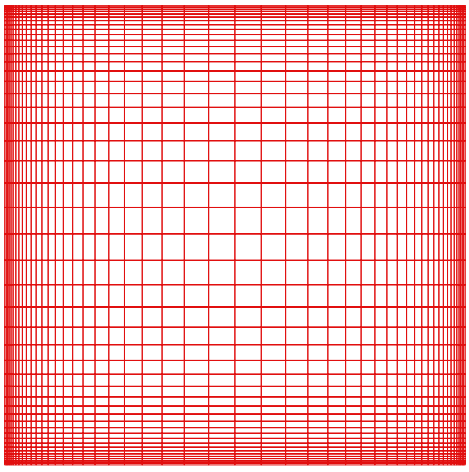

50×50 non-uniform Mesh

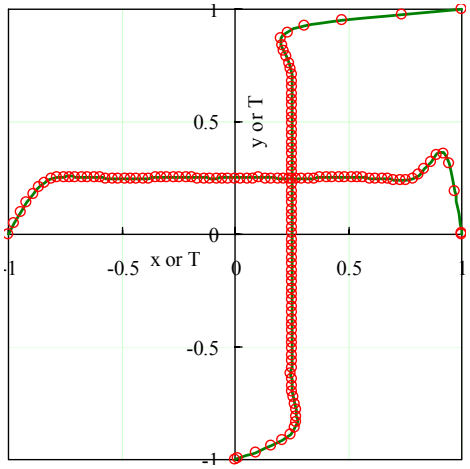

T-profiles across sections thru center

Fig. 3.4 Results from double glazing benchmark (○ LSGSFEM, — Galerkin FEM)

CHAPTER 4

LEAST-SQUARES/GALERKIN SPLIT FINITE ELEMENT METHOD FOR INCOMPRESSIBLE FLOWS

4.1 Introduction

Most of the finite element methods developed for incompressible viscous flows over the past few decades are based on the velocity-pressure formulation due to its simpler boundary conditions and ease of extension to three dimensions. Detailed discussions about these can be found in references [37-39]. The velocity-pressure formulation is implemented mainly through the segregated method, the penalty method, and the mixed Galerkin method.

In the segregated method [23, 24], a SIMPLE-type finite difference algorithm decouples velocity and pressure iterations and achieves considerable computational efficiency, however the computed pressure is often inaccurate due to lack of proper pressure boundary conditions for the pressure correction equation.

In penalty method, the continuity equation is penalized in order to pre-eliminate pressure which is then recovered by using the perturbed conservation of mass equation. However the pressure recovered exhibits oscillations due to ill-conditioning of the pressure matrix. Also, the penalty method is inaccurate for small values of penalty parameter and for very large values it sometimes may not converge at all due to ill-conditioning of the system matrix.

In the mixed Galerkin method, different basis functions are used to interpolate the velocity and pressure in order to satisfy the restrictive Ladyzhenskaya-Babuska-Brezzi (LBB) condition for the existence of the solution [21, 22]. The basis function pairs that satisfy the LBB condition can be difficult to determine and implement. Also the system matrices turn out to be asymmetric and indefinite, which rules out the use of PCG-type iterative methods to directly solve the system of equations.

Recently, an alternate approached based on the least-squares finite element method has been gaining popularity [25-27]. This approach has many attractive advantages over the Galerkin finite element method (GFEM) and its variants and has established itself as a better approach for non-self adjoint systems, such as those governing fluid mechanics.

The least-squares finite element formulation doesn't need to satisfy the difficult LBB condition and always results in a symmetric positive system of algebraic equations unlike GFEM. However, as the method does not employ integration by parts, high-order terms may be present in the weak statement. Thus the continuity requirements for second-order terms in the governing equations force the introduction of additional unknowns by use of an equivalent first-order system of equations or the use of C^1 continuous basis functions. These additional unknowns lead to increased memory and computing time requirements that have limited the application of LSFEM to large-scale practical problems, such as three-dimensional compressible viscous flows.

The least-squares/Galerkin split finite element method proposed here is both simple and effective for solving the incompressible Navier-Stokes equations. The method proposed here employs a least-squares method for first-order derivatives and a Galerkin method for second order derivatives, thereby avoiding the need for additional unknowns required by a pure LSFEM approach. Only the primitive variables *u, v* and *p* need to be solved for, in the two dimensional problems using the proposed method whereas LSFEM needs one additional unknown that is introduced in order to get the equivalent first order system [25-27]. In three dimensions LSFEM would require three additional unknowns whereas the proposed method still requires only the primitive variables. This is one of the attractive features of the proposed method.

When the unsteady form of the governing equations is used, a streamline upwinding term is introduced naturally by the least-squares method. The method is stable for convection-dominated flows and allows for equal-order basis functions for both pressure and velocity. In addition, the resulting system of equations **is always symmetric** and is solved using the conjugate gradient method with standard pre-conditioners. Non-linear terms are treated effectively by linearization in time. The stability and accuracy of the method have been demonstrated with preliminary results of few benchmark convection-diffusion and incompressible flow problems solved using low-order C^0 continuous elements [28, 29].

4.2 LSGS Formulation for Incompressible Navier-Stokes Equations

Incompressible laminar fluid flow is governed by Navier-Stokes equation, which in non-dimensional unsteady form in two dimensions is given as:

$$\begin{aligned}
&\frac{\partial u}{\partial x}+\frac{\partial v}{\partial y}=0\\
&\frac{\partial u}{\partial t}+\vec{V}\cdot\nabla u+\frac{\partial p}{\partial x}-\frac{1}{Re}\nabla^2 u=0\\
&\frac{\partial v}{\partial t}+\vec{V}\cdot\nabla v+\frac{\partial p}{\partial y}-\frac{1}{Re}\nabla^2 v=0
\end{aligned} \tag{4.1}$$

Here first equation is the continuity and other two are momentum equations. $\vec{V}$ is the velocity field with u and v as its x and y components respectively, p the pressure and Re is the Reynolds number. By discretizing spatial derivative using θ-method and the unsteady terms using Euler backward differences

$$\frac{\partial u}{\partial t}\approx\frac{u^{n+1}-u^{n}}{\Delta t}\quad\text{and}\quad\frac{\partial v}{\partial t}\approx\frac{v^{n+1}-v^{n}}{\Delta t} \tag{4.2}$$

and linearization in time gives matrix form of the system

$$\mathscr{L}\,U^{n+1}=f \tag{4.3}$$

where $U = (u, v, p)^T$ is the vector of unknowns, the operator $\mathscr{L}$ is given as

$$\mathscr{L}=\begin{bmatrix}
\dfrac{\partial}{\partial x} & \dfrac{\partial}{\partial y} & 0\\
I+\theta\Delta t\vec{V}^{n}\cdot\nabla-\dfrac{\theta\Delta t}{Re}\nabla^2 & 0 & \theta\Delta t\dfrac{\partial}{\partial x}\\
0 & I+\theta\Delta t\vec{V}^{n}\cdot\nabla-\dfrac{\theta\Delta t}{Re}\nabla^2 & \theta\Delta t\dfrac{\partial}{\partial y}
\end{bmatrix} \tag{4.4}$$

and the right hand side vector f is given as

$$f=\begin{Bmatrix}
0\\
u^{n}-(1-\theta)\Delta t\vec{V}^{n}\cdot\nabla u^{n}+\dfrac{(1-\theta)\Delta t}{Re}\nabla^2 u^{n}-(1-\theta)\Delta t\dfrac{\partial p^{n}}{\partial x}\\
v^{n}-(1-\theta)\Delta t\vec{V}^{n}\cdot\nabla v^{n}+\dfrac{(1-\theta)\Delta t}{Re}\nabla^2 v^{n}-(1-\theta)\Delta t\dfrac{\partial p^{n}}{\partial y}
\end{Bmatrix} \tag{4.5}$$

Where $\vec{V}^n$ is the velocity field vector at previous time step and I, an $m \times m$ identity matrix, m being number of nodes per element. The residual vector is given as

$$\mathscr{R} = \mathscr{S} U^{n+1} - f \tag{4.6}$$

The residual is minimized using a suitable weighting operator that comes from LSFEM applied to Euler's equations. As explained in chapter 3, section 3.4, we first apply LSFEM to first order terms and get the variational form of Euler-Lagrange equation. This E-L form has an equivalent Galerkin form. Once we find the Galerkin form, we simply add the left out second order terms of the NS equations and apply Galerkin method to complete modified equation. For linear elements it is equivalent as treating the weighted residual of (4.6) with weighting operator $\mathscr{S}$ as

$$\int_\Omega (\mathscr{S} N)^T (\mathscr{S} U^{n+1} - f) d\Omega = 0 \tag{4.7}$$

Where $\mathscr{S}$ is obtained from taking first order terms of governing equations i.e. Euler equation part given by

$$\mathscr{S} = \begin{bmatrix} \dfrac{\partial}{\partial x} & \dfrac{\partial}{\partial y} & 0 \\ I + \theta \Delta t \vec{V}^n \cdot \nabla & 0 & \theta \Delta t \dfrac{\partial}{\partial x} \\ 0 & I + \theta \Delta t \vec{V}^n \cdot \nabla & \theta \Delta t \dfrac{\partial}{\partial y} \end{bmatrix} \tag{4.8}$$

Introducing the finite element approximation

$$U^{n+1} \approx U_h^{n+1} = \sum_i^m N_i U_i^{n+1} \tag{4.9}$$

where m is the number of nodes per element and N_i is the element shape function associated with i^{th} node. Substituting the approximation into the weak formulation in (4.7) leads to linear algebraic equations

$$[K]\{U^{n+1}\} = \{F\} \tag{4.10}$$

where global stiffness matrix $[K]$ and the vector $\{F\}$ result from assembling the element stiffness matrices and vectors respectively given by

$ke = \int_{\Omega_e} (\mathscr{S} N_i)^T (\mathscr{L} N_j)\, d\Omega;$ $\quad fe = \int_{\Omega_e} (\mathscr{S} N_i)^T f\, d\Omega.$ Full form of ke and fe is given in Appendix B. Weighting operator $\mathscr{S}$ ensures split treatment to first order terms and second order terms in the governing equation. Thus, the first order term are treated like LSFEM and the second order viscous terms get treated similar to GFEM. Integrals containing second order terms are resolved the Galerkin way through integration by parts. Subsequent terms containing second order derivatives are dropped, as is the standard practice [35] to ignore computationally expensive higher order derivatives for linear elements.

4.3 Benchmark Problems

The LSGS method described above has been tested by solving few steady flow benchmarks (θ = 1) and an unsteady time accurate problem (θ = 1/2). Steady flow problems include plane Poiseuille flow and classical benchmark problems of the driven cavity flow and the backward-facing step flow. The plane Poiseuille flow for which analytical solution is available has been included in order to study convergence as well. Transient flow past rectangular cylinder was solved as unsteady benchmark.

4.3.1 Plane-Poiseuille Flow

A plane-Poiseuille flow is a flow between two parallel plates in the presence of pressure gradient. The plates can be stationary or moving. All three cases: plates fixed

and $\frac{dp}{dx}<0$, top plate moving with $U_0 \neq 0$ and $\frac{dp}{dx}$ being either <0 or >0 were simulated. A uniform 20×20 mesh with bilinear elements was used inside a unit square domain. A quick convergence study was carried out by running the code on coarse uniform meshes comprising of 4, 6, 8 and 10 elements along the side of the square domain.

The boundary conditions: $u = 0, v = 0$ on bottom surface, $v = 0, p = p_{out}$ at the outlet, $u = 0$ or $U_0, v = 0$ on the top surface and $v = 0, p = p_{in}$ at the inlet were applied. Analytical solution for plane Poiseuille flow with stationary plates and with upper plate moving with velocity U_0 is given by $u(y) = -\frac{y}{\mu}\frac{dp}{dx}\left(b - \frac{y}{2}\right)$ and $u(y) = \frac{yU_0}{2b} - \frac{y}{\mu}\frac{dp}{dx}\left(b - \frac{y}{2}\right)$ respectively. Here $2b$ is the gap between the plates and U_0 is the velocity of the upper surface. Problem was solved for $Re = \frac{2bU_0}{v} = 100$.

4.3.2 Lid-Driven Cavity Flow

The classical lid-driven cavity flow problem continues being investigated since some pioneering works providing accurate benchmark solutions were published decades ago [41, 42]. More recent work by Bruneau and Saad [43] is particularly noteworthy, where he provided comprehensive results for the driven cavity problem upto Re = 10000 and accurately localized the first Hopf-bifurcation. The domain is a unit square with three surfaces stationary and top surface moving. The mesh used comprised of

50×50 non-uniform bilinear elements (Fig. 4.1a) with the smallest element, a square with side = 0.002 at four corners similar to ref. [25].

The boundary conditions are as follows: $u = v = 0$ on sides and bottom surfaces, $u = 1,\ v = 0$ on top-lid and $p = 0$ at the center of the bottom surface. Computations were carried out for Reynolds numbers ranging from 100 to 10000.

4.3.3 Backward Facing Step Flow

Flow over a two-dimensional backward-facing step is another standard test problem that has been investigated experimentally and computationally by numerous researchers. Experimental work by Armaly et al [44], computational work by Sohn [45] and Gartling [46] are among the few important ones. The configuration chosen here is similar to one used by Gartling. The aspect ratio of the step (h) to the overall cross-sectional width in present study is 1:2 and the total length in the horizontal direction is 60h. A fully developed parallel flow with parabolic profile given by $u(y) = 24y\ (0.5-y)$ is specified at the inlet $0 \leq y \leq 0.5$. This produces a maximum inflow velocity, $u_{max} = 1.5$ and an average inflow velocity, $u_{avg} = 1.0$. The outflow boundary condition assumed a parallel flow, i.e. $v = 0$ and $p = 0$. The boundary conditions at outlet come actually from the hybrid boundary condition applied in his benchmark by Gartling, which is $v = 0$ and $-p + \frac{2}{Re}\frac{\partial u}{\partial x} = 0$. Since outlet at $x = 60h$ from the step is far enough to assume a parallel uniform flow with fully developed parabolic profile that allows us to have $p = 0$ at the outlet. After getting the solution, pressure field was adjusted such that the pressure was zero at the step corner. For non-dimensional form of Navier-Stokes equations and fixed

geometry, *Re* is the only non-dimensional parameter of interest and it is defined by $u_{avg}2h/\nu$. Simulation was carried out for Reynolds numbers of 200, 300, 400, 500, 600, 700 and 800.

Flow simulation especially at *Re* = 800 is very interesting since some researchers like Kaiksis [47], Runchal [48] and others argued that flow at this *Re* was unsteady and exhibited chaotic behavior. Later studies by Gartling [46] and Torczynski [49] proved that flow at this *Re* was steady. Torczynski found out that Kaiksis et al got unsteady and chaotic results since the flow was under-resolved with the grid they used.

In the present study a 32×252 non-uniform bilinear mesh was used. Mesh details and the boundary conditions are shown in Fig. 4.1b and 4.1c. The mesh was clustered in vertical direction near upper and lower surfaces and at the centerline. In horizontal direction 100 elements were used before $x = 5$ and clustered towards the step in such a way that worst element aspect ratios occurring on the upper and the lower walls ranged from 1.3 to 16.8. Uniform mesh comprising of 102 elements were used thereafter from 5 to 20 such that the worst element aspect ration was kept close to 16.8. Thereafter uniform mesh with the aspect ratio of around 24 was used with 50 elements.

4.3.4 Unsteady Flow past Rectangular Cylinder

Two-dimensional unsteady flow past rectangular cylinder is a popular benchmark problem. We considered a cylinder with an aspect ratio (length/width) of two. For this geometry, previous researchers [50, 51] have found that the Strouhal number (*St*), which is non-dimensional frequency of vortex shedding, monotonically increases in the range $60 < Re < 400$ from ≈ 0.10 to ≈ 0.17.

Computational domain was a rectangular box of size 10 × 27 (Fig. 4.1d). An unstructured mesh having 4074 quadrilateral elements (4190 nodes) was used. Mesh was constructed very fine on the cylinder and in the wake behind in order to capture the boundary layer and subsequent vortex shedding. Simulation was carried out for Reynolds numbers of 80, 150 and 300 using time step sizes of 0.0004 and 0.001.

4.4 Results and Discussion

Steady state results were reached by time marching. Non-linear terms were linearized in time using simple successive substitution. Resulting linear system of equations was solved using pre-conditioned conjugate gradient (pcg) method using diagonal pre-conditioner and sparse matrix storage. A pcg-tolerance of 10^{-7} or maximum pcg iterations of 8000 was used inside each time step and an overall tolerance of 10^{-6} for l^2-norm of residual was used as convergence criterion throughout. Driven cavity flow at Re = 100, 400 and 1000 was solved using Δt = 0.01 all starting from zero initialization in order to study the variation of pcg-iterations as the solution progressed towards convergence (Fig 4.2a). The pcg iterations required at each time step quickly declined as the solution progressed towards convergence. The total number of pcg iterations can be greatly reduced by using more sophisticated pre-conditioner like block pre-conditioner and faster convergence can be achieved. Reduced integration using one point Gaussian quadrature was used to evaluate the element matrices.

4.4.1 Plane-Poiseuille Flow

Three cases of plane Poiseuille flow: flow driven by favorable pressure gradient between two stationary surfaces, flow driven by moving upper surface in the presence

of favorable/adverse pressure gradient were simulated at Re = 100. Coarse meshes as described in the previous section were used to study convergence. Convergence plots for horizontal velocity and pressure are shown in Fig 4.2b. The horizontal velocity shows a quadratic convergence whereas pressure converges with a slope of ≈ 1.5. Fully developed velocity profiles for the three cases of plane-Poiseuille flow are compared with the analytical results in Fig. 2c. The velocity profiles from the study match the analytical solutions very well.

4.4.2 Lid-Driven Cavity Flow

Computations for this benchmark were carried out at Reynolds numbers of 100, 400, 1000, 3200, 5000, 7500 and 10000. The initial conditions used for Re = 100 are $u(x,y,0) = v(x,y,0) = 0$. Converged solution from this case was used as the initial input for next Reynolds number and so on. The results are presented in Figs. 4.3 to 4.10. Plots for streamlines, pressure contours, vorticity contours and velocity vectors are displayed. The streamlines, vorticity contours and vortex locations and dimensions for all Reynolds numbers compare well with those of Ghia et al [41] except the vortex at lower right corner at Re = 10,000 which compares favorably rather with that of Jiang [25]. The pressure contours compare well with those of Jiang [25] and Sohn et al [45]. Horizontal and vertical velocity profiles through the geometric center of the cavity are shown in Fig. 4.10. These profiles agree well with the published results.

4.4.3 Backward Facing Step Flow

Computations were carried out for Re = 200, 300, 400, 500, 600, 700 and 800 for this benchmark. Initial guess of $u = v = 0$ is used for Re = 200, the converged

solution for Re = 200 is used as initialization for Re = 300 and so on. Results have also been compared with the experimental results from Armaly's work although he used slightly different dimensions. Computed results (streamlines, pressure and vorticity contours) are presented in Figs. 4.11 and 4.12. Since few phenomena of interest occur downstream of x = 10, plots only show contours up to this location. The results compare well with that by Gartling [46]. The reattachment length of the recirculation zone behind the step and the location of separation and reattachment of recirculation zone on the upper wall are compared with published experimental and computational results in Fig. 4.12. The cited published results were optically scanned from the literature available [25, 44]. Here x_1 is the reattachment location of the main vortex behind the step, x_4 is the separation location and x_5 is the reattachment location of the recirculating zone on the upper wall. The length of the main recirculating zone behind the step matches well with both experimental [44] as well as computational results [25] for smaller Re. At higher Reynolds numbers it agrees more with computational and less with the experimental results. The lengths for the recirculating zone on the upper wall match well with the experimental results for smaller Reynolds numbers and computational results at higher Reynolds numbers. The differences with the experimental results at higher Reynolds number cases may be attributed to three-dimensional effects of the experiments.

4.4.4 Unsteady Flow past Rectangular Cylinder

Computations were carried out for Re = 80, 150 and 300. Reynolds number was effectively $1/\nu$ as reference velocity and length both were unity. Boundary conditions

were as follows: $u = U_\infty$, $v = 0$ on top and bottom surfaces of the domain, $p = 0$ at the mid-point of the exit, $u = U_\infty$, $v = 0$ at the inlet and no slip condition on the cylinder surface. Different values of time step size, $\Delta t = 0.001$ and 0.0004, with under-relaxation parameter of 0.9 for pressure were used. Results from the study are listed in table 4.1 and Figs 4.13-4.15. Pressure contours, streamlines and variation of the vertical velocity recorded at a downstream location in $1.5 < x < 2.0$ are shown for $\Delta t = 0.0004$. The streamline patterns show vortex shedding downstream of the cylinder. The vortex shedding frequency is sensitive to time step size. In the case of $Re = 80$, it is hard to get sustained vortex shedding as the flow settles to a steady solution for relatively bigger values of Δt. The Strouhal number, St, which is non-dimensional frequency of vortex shedding, was computed from the period of vortex shedding T. Table 4.1 shows computed St compared with published results.

4.5 Conclusions

The proposed least-squares/Galerkin split finite element method has been successfully applied to incompressible flow benchmark problems. Both steady and transient benchmarks have been solved using C^0-continuous elements and results compare very well with the standard published literature.

Table 4.1 Strouhal Numbers for Unsteady Flow past Rectangular Cylinder

Re	Present Study	Computations [51]	Experiments [50]
80	0.1263	0.113	0.10 – 0.12
150	0.1322 – 0.1643	0.122 – 0.126	0.13 – 0.15
300	0.1577 – 0.1732	0.126 – 0.137	0.15 – 0.17

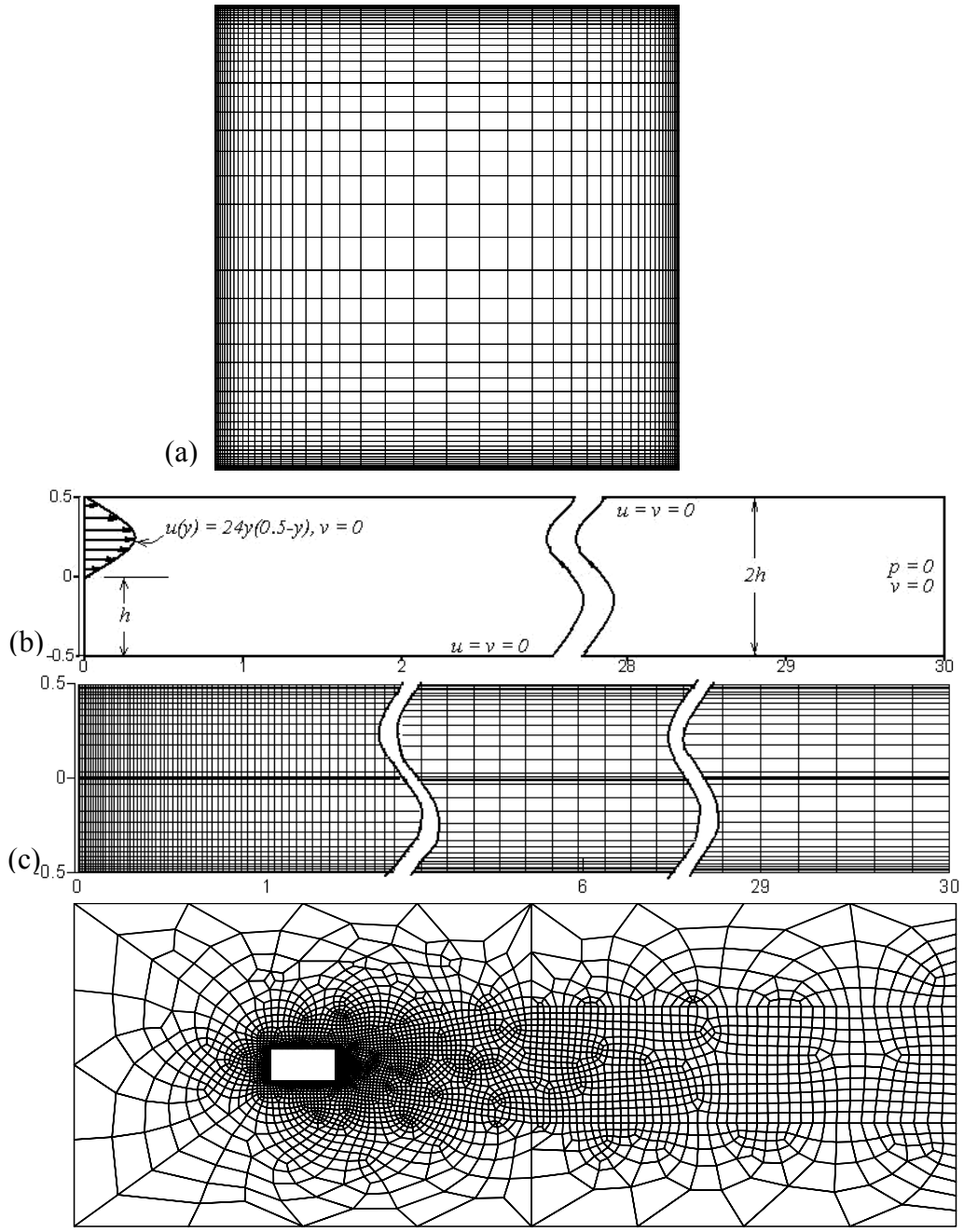

Fig. 4.1 Meshes and the boundary conditions for the incompressible flow benchmarks: (a) Mesh for driven cavity flow, 50×50 bilinear elements; (b) Boundary conditions for the backward-facing step flow; (c) Mesh for the backward-facing step flow, 32×252 bilinear elements; (d) Unstructured mesh for flow over rectangular cylinder, 4074 elements.

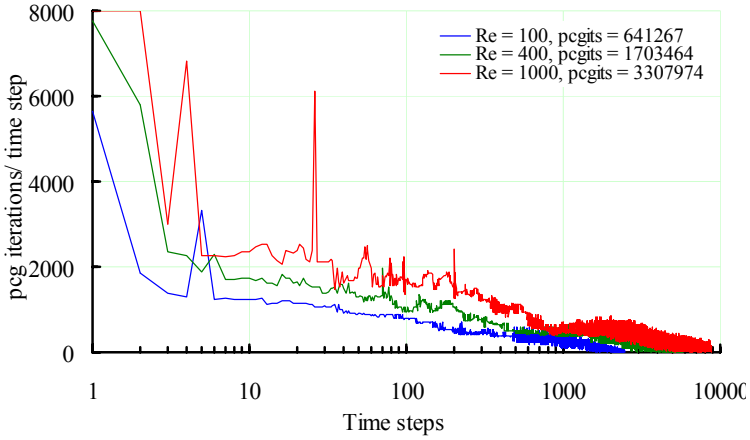

Fig. 4.2 Variation of pcg iterations with time (driven cavity flow)

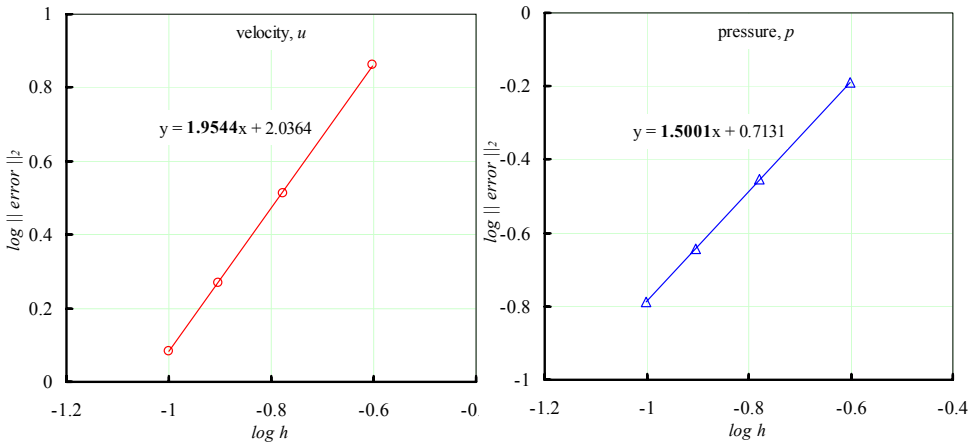

Fig. 4.3 Convergence plots for velocity and pressure (Poiseuille flow)

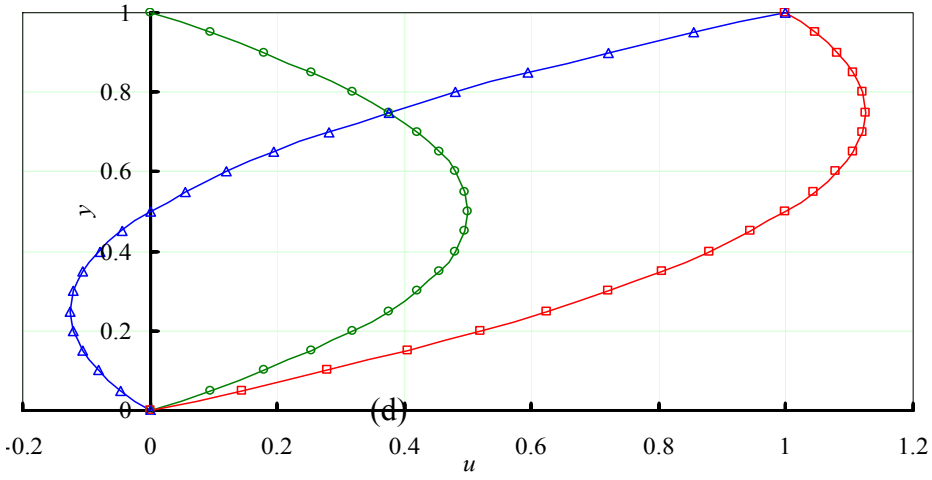

Fig. 4.4 Velocity profiles for plane-Poiseuille flow: (—Analytical, Δ,O,□ LSGSFEM) Δ: Flow with $U_{top} = 1$, $U_{bot} = 0$ and $dp/dx > 0$, O: Flow with $U_{top} = U_{bot} = 0$ and $dp/dx<0$, □: Flow with $U_{top} = 1$, $U_{bot} = 0$ and $dp/dx<0$.

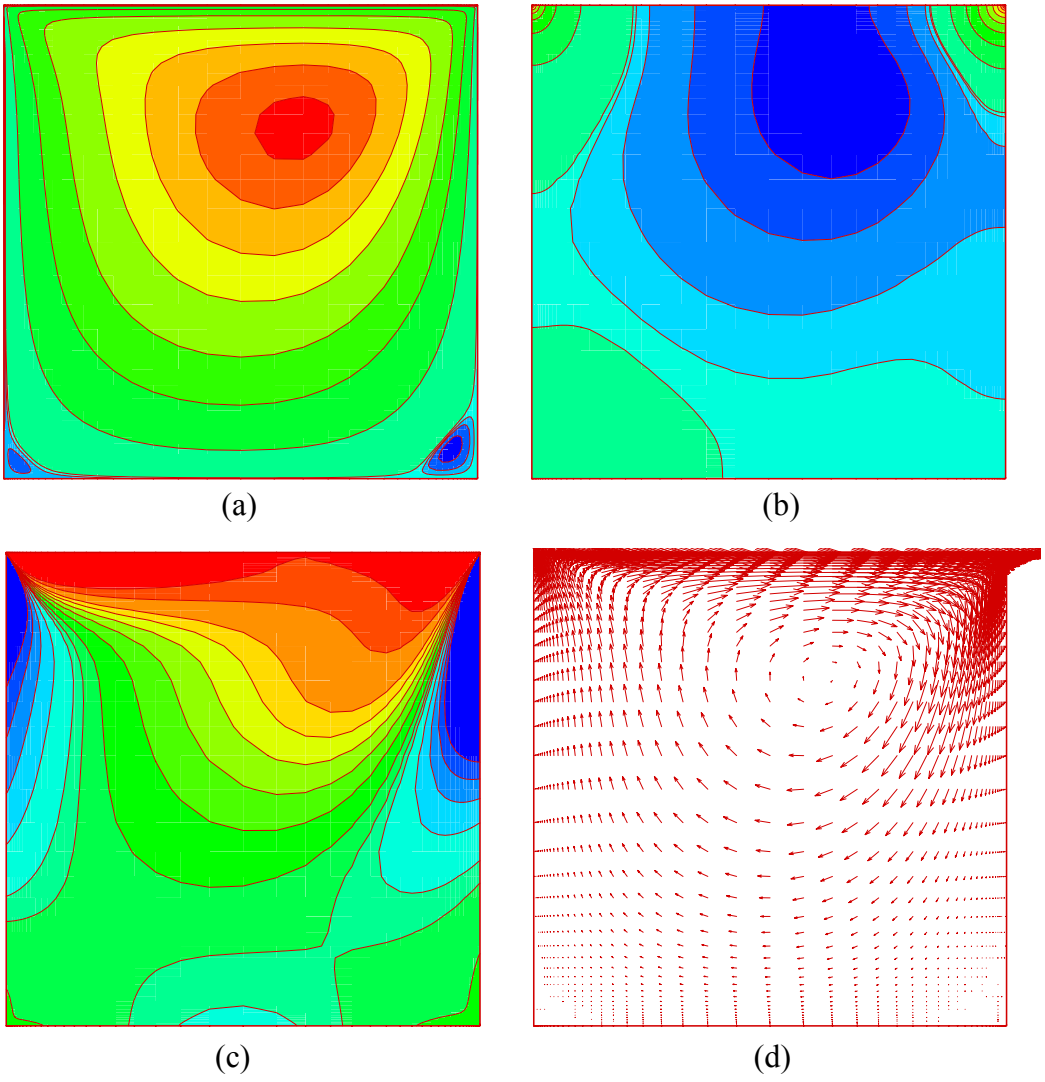

Fig. 4.5 Driven cavity flow results using LSGSFEM at *Re* = 100:
(a) Streamlines, (b) Pressure contours, (c) Vorticity contours, (d) Velocity vectors

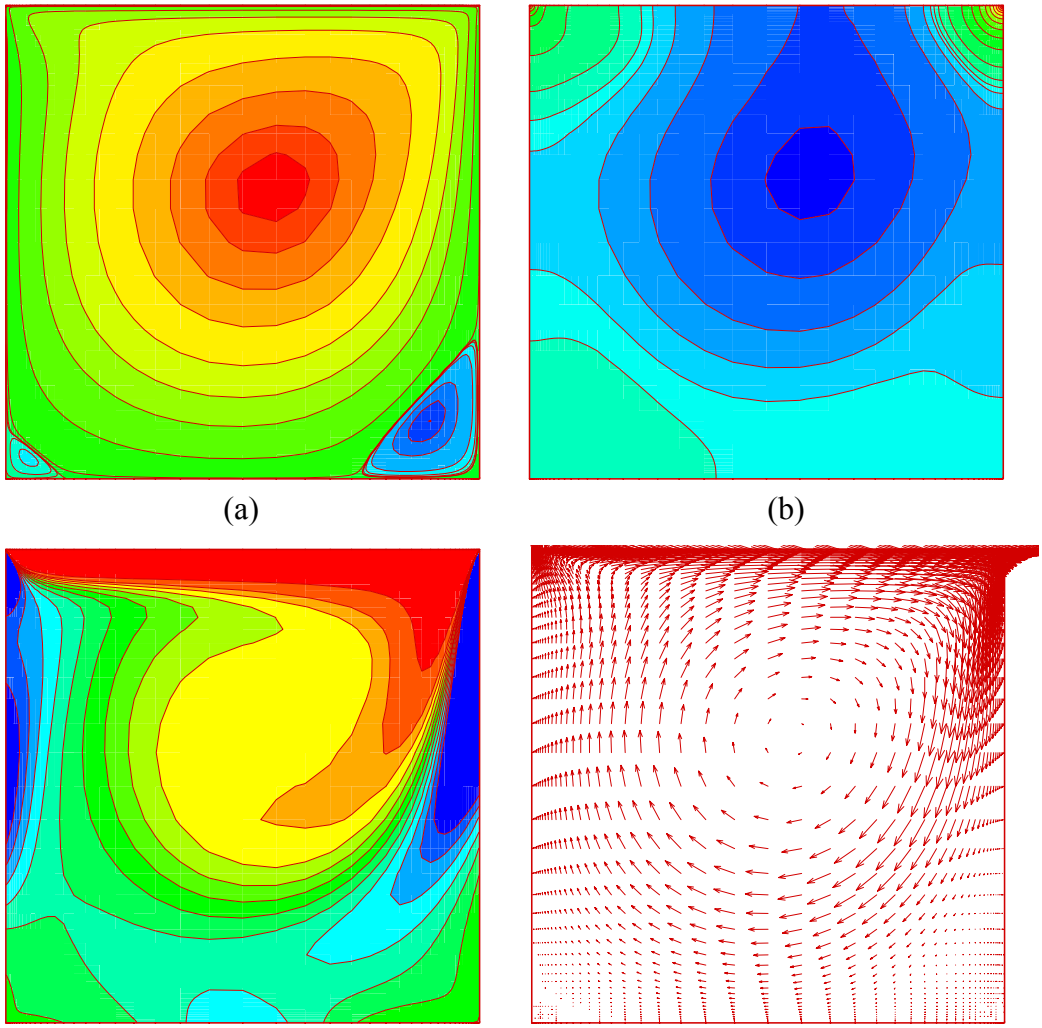

Fig. 4.6 Driven cavity flow results using LSGSFEM at *Re* = 400:
(a) Streamlines, (b) Pressure contours, (c) Vorticity contours, (d) Velocity vectors

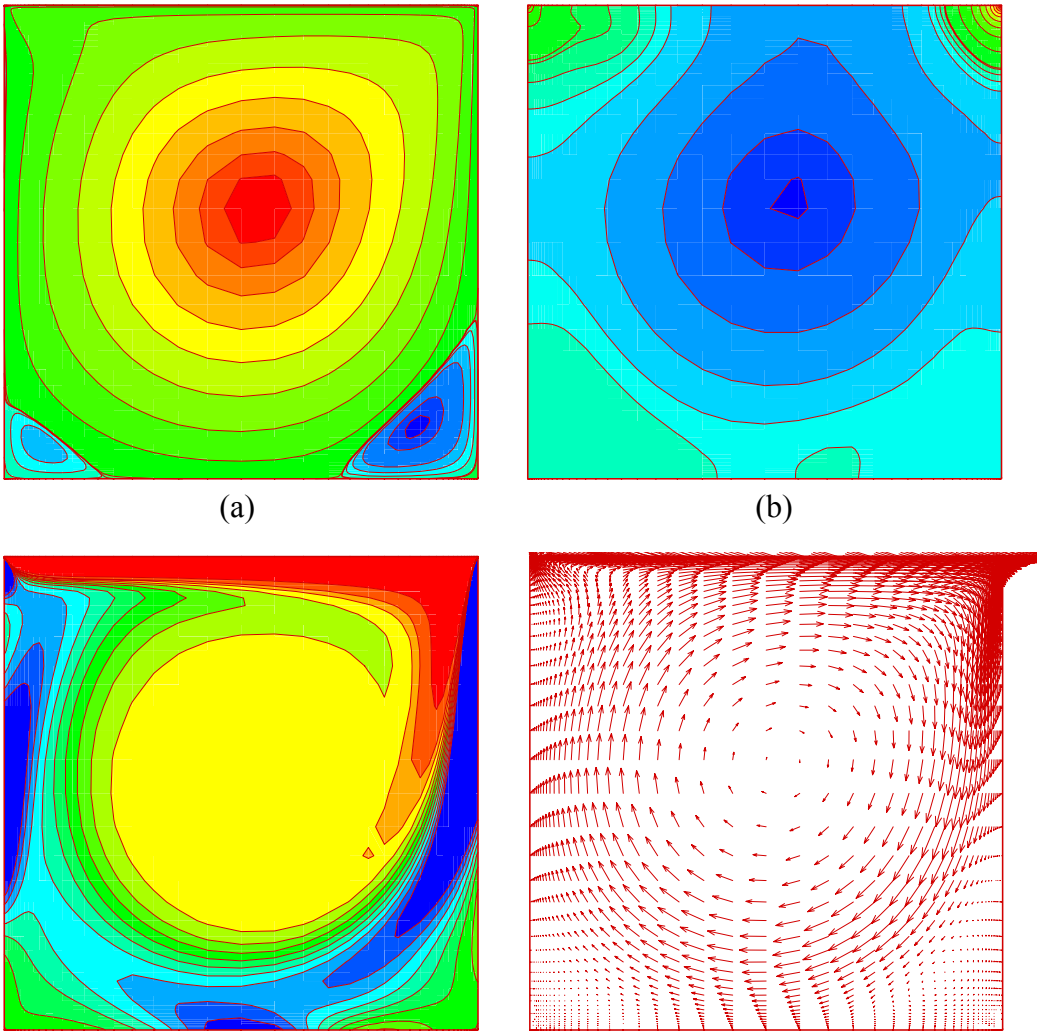

(a) (b)

(c) (d)

Fig. 4.7 Driven cavity flow results using LSGSFEM at *Re* = 1000:
(a) Streamlines, (b) Pressure contours, (c) Vorticity contours, (d) Velocity vectors

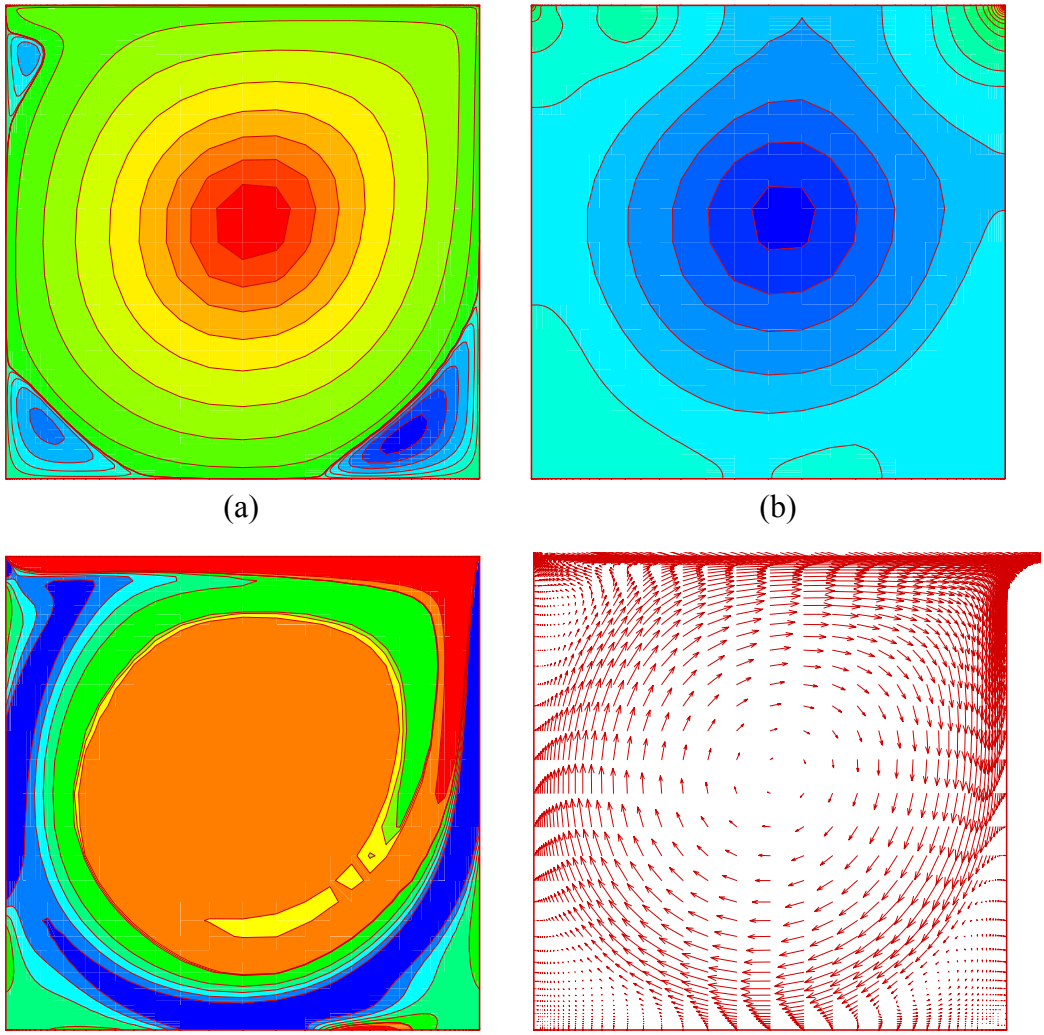

(a) (b)

(c) (d)

Fig. 4.8 Driven cavity flow results using LSGSFEM at *Re* = 3200:
(a) Streamlines, (b) Pressure contours, (c) Vorticity contours, (d) Velocity vectors

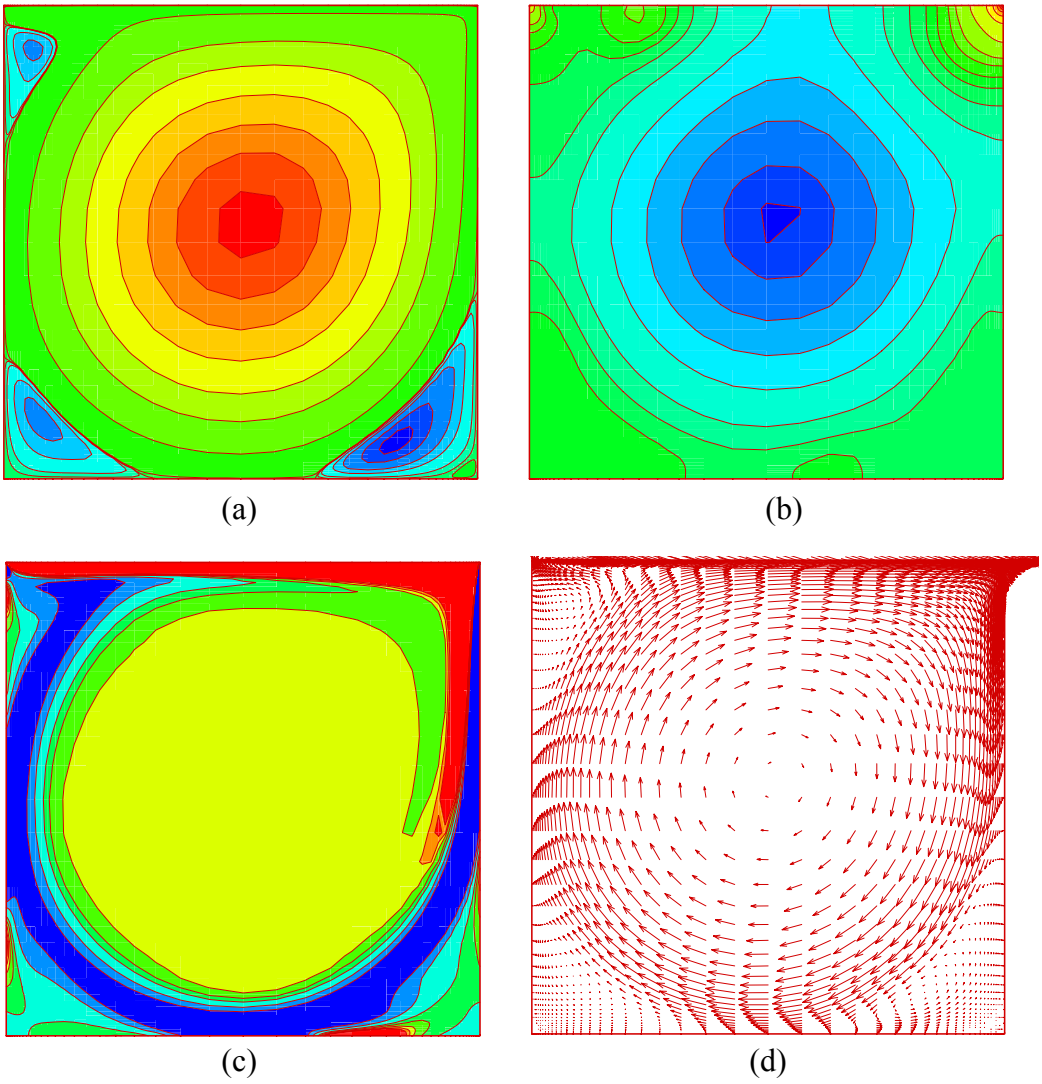

Fig. 4.9 Driven cavity flow results using LSGSFEM at *Re* = 5000:
(a) Streamlines, (b) Pressure contours, (c) Vorticity contours, (d) Velocity vectors

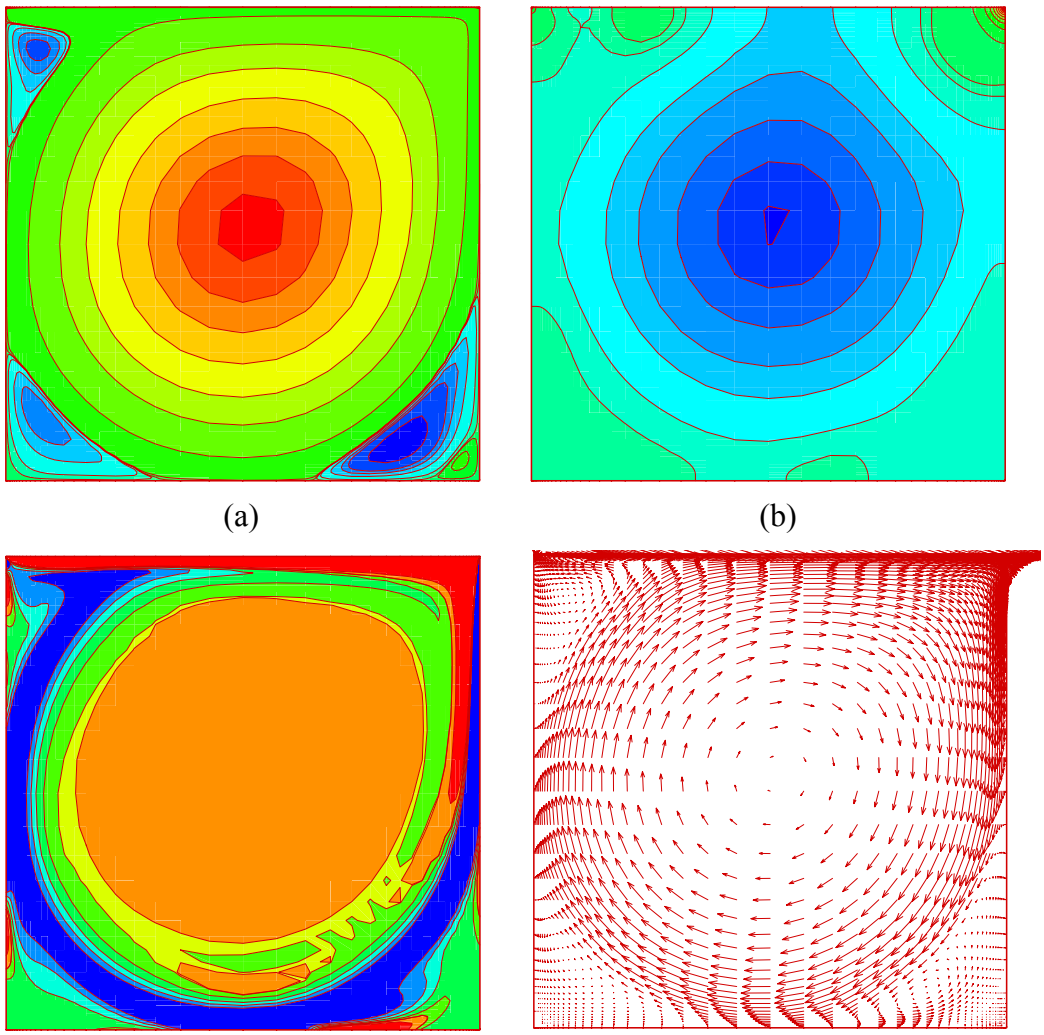

Fig. 4.10 Driven cavity flow results using LSGSFEM at *Re* = 7500:
(a) Streamlines, (b) Pressure contours, (c) Vorticity contours, (d) Velocity vectors

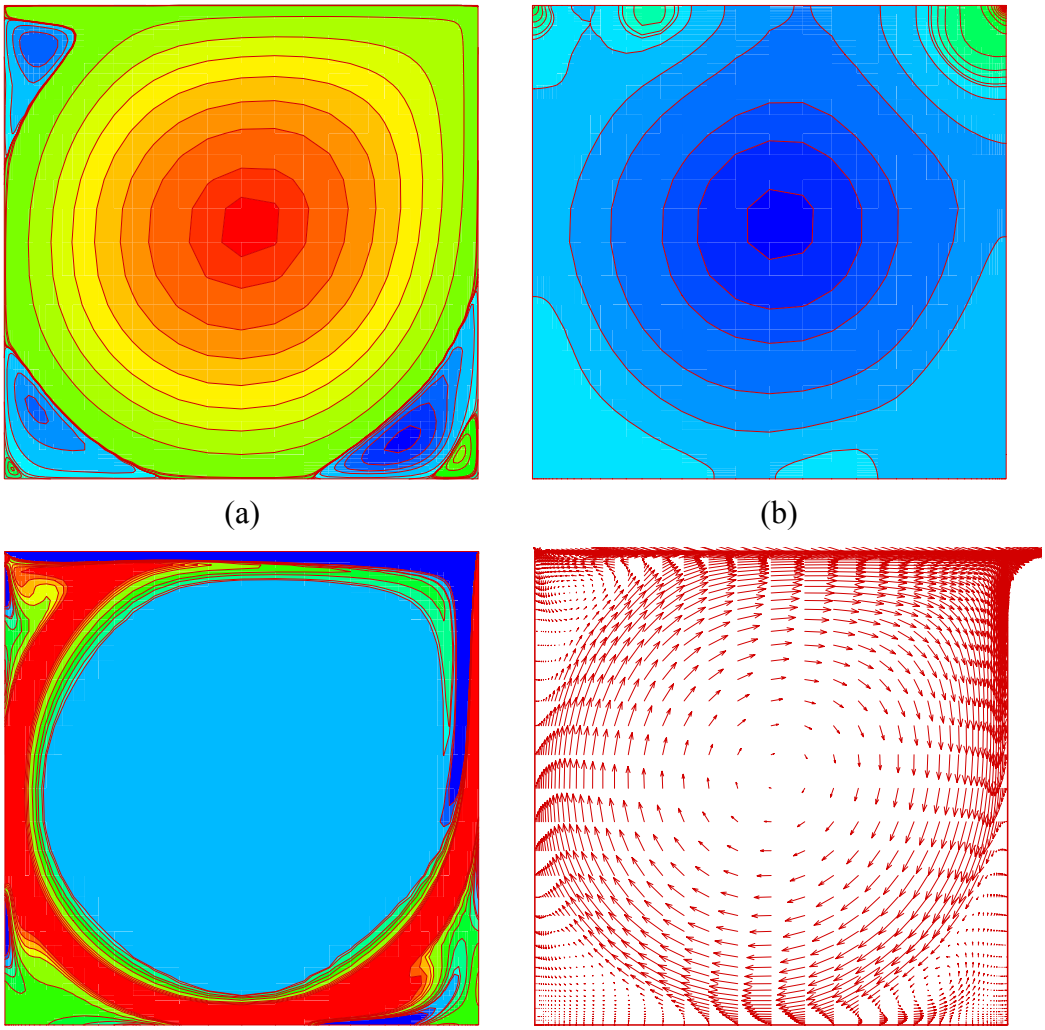

Fig. 4.11 Driven cavity flow results using LSGSFEM at *Re* = 10000:
(a) Streamlines, (b) Pressure contours, (c) Vorticity contours, (d) Velocity vectors

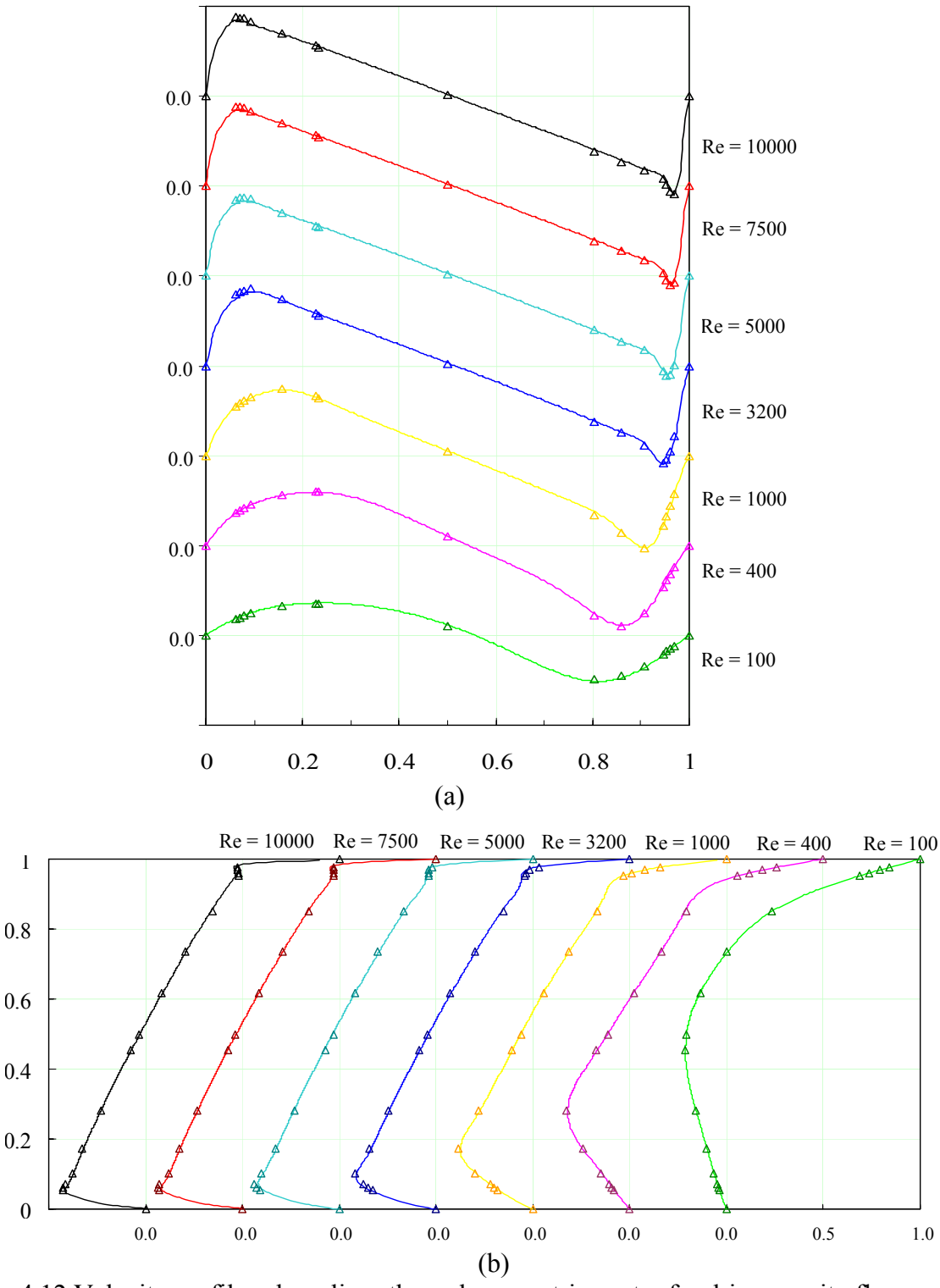

Fig. 4.12 Velocity profiles along lines through geometric center for driven cavity flow (a) *y*-velocity profiles, (b) *x*-velocity profiles (—LSGSFEM, Δ Ghia et al [41])

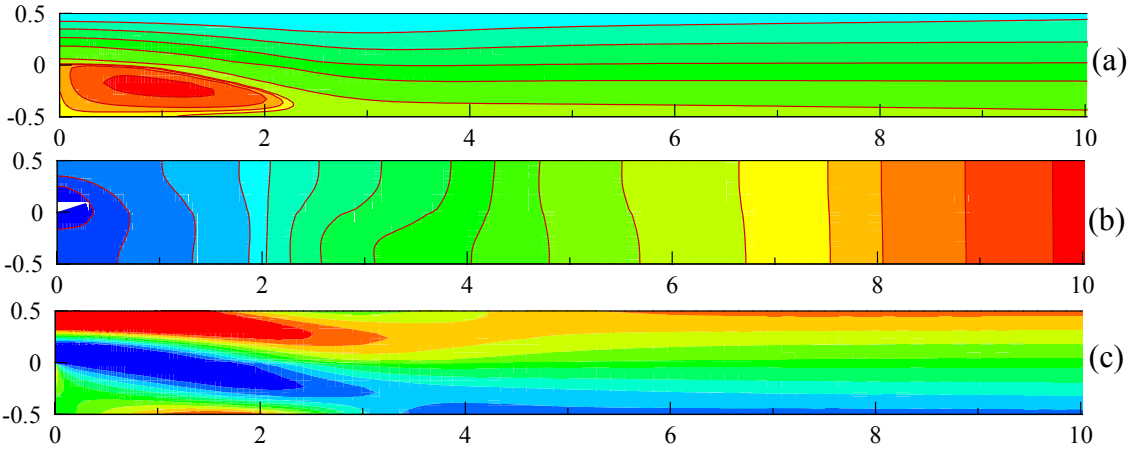

Fig. 4.13 Contour plots for backward-facing step flow using LSGSFEM at Re = 200: (a) Streamlines, (b) Pressure contours and (c) Vorticity contours

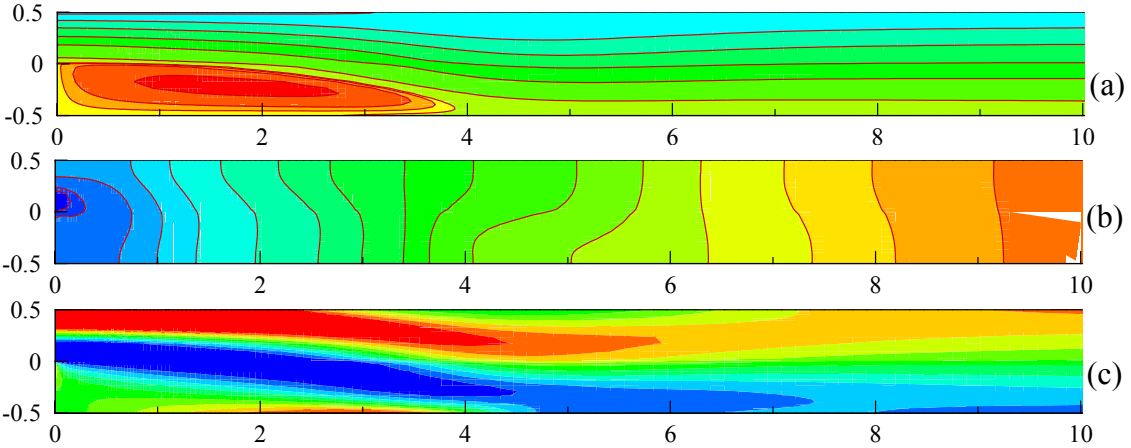

Fig. 4.14 Contour plots for backward-facing step flow using LSGSFEM at Re = 400: (a) Streamlines, (b) Pressure contours and (c) Vorticity contours

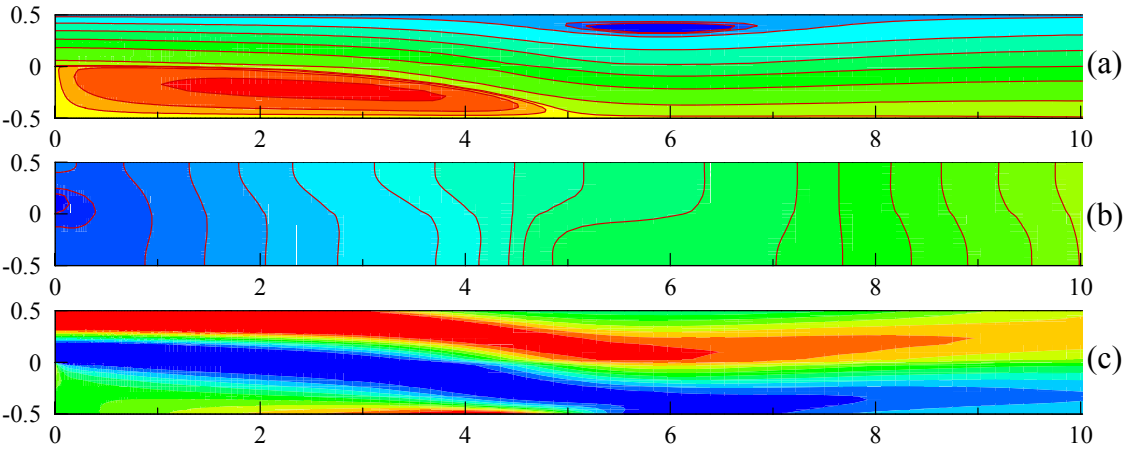

Fig. 4.15 Contour plots for backward-facing step flow using LSGSFEM at Re = 600: (a) Streamlines, (b) Pressure contours and (c) Vorticity contours

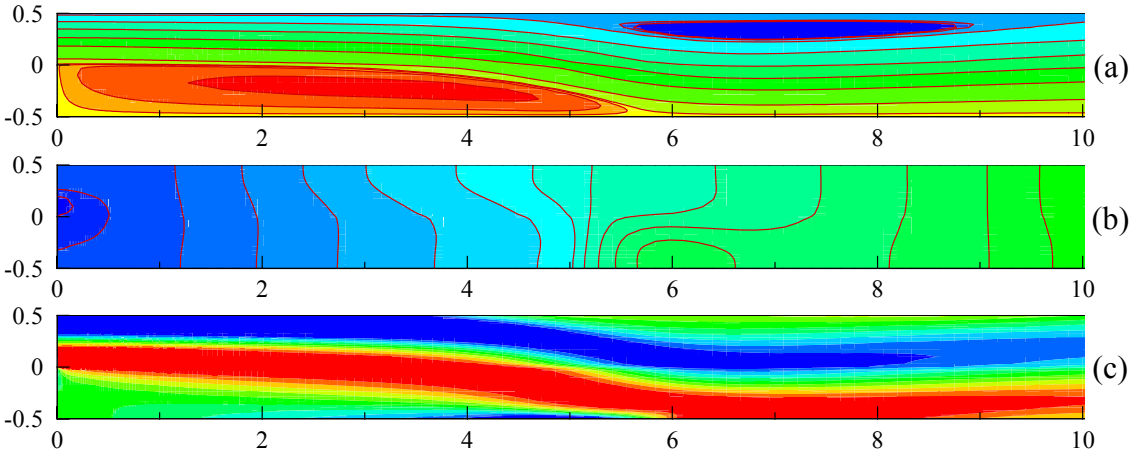

Fig. 4.16 Contour plots for backward-facing step flow using LSGSFEM at *Re* = 800: (a): Streamlines, (b): Pressure contours and (c): Vorticity contours

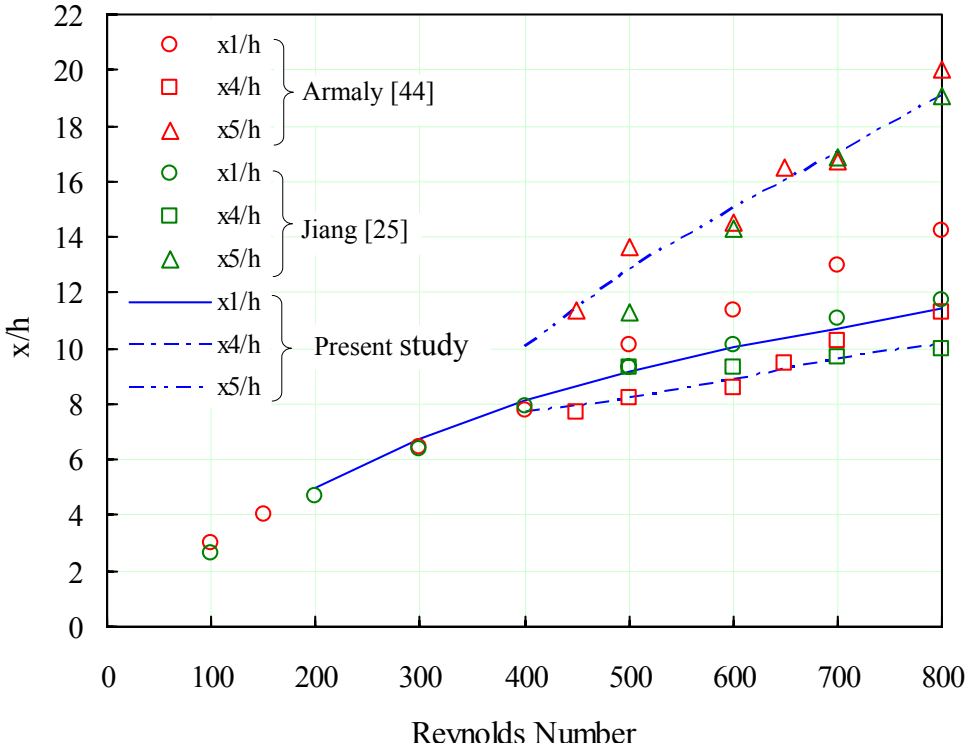

Fig. 4.17 Computed reattachment/separation length Vs Reynolds number for backward facing step flow: Comparison with published results

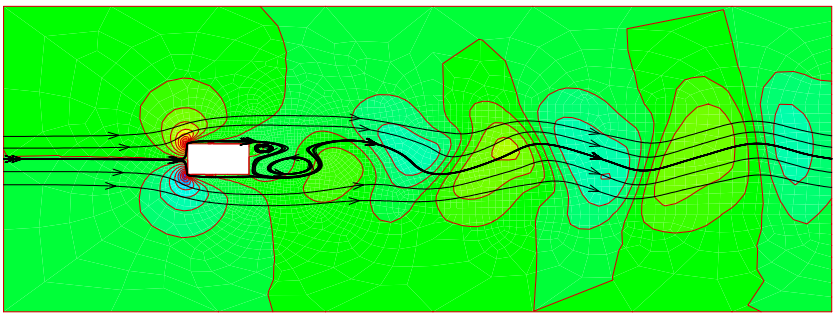

(a)

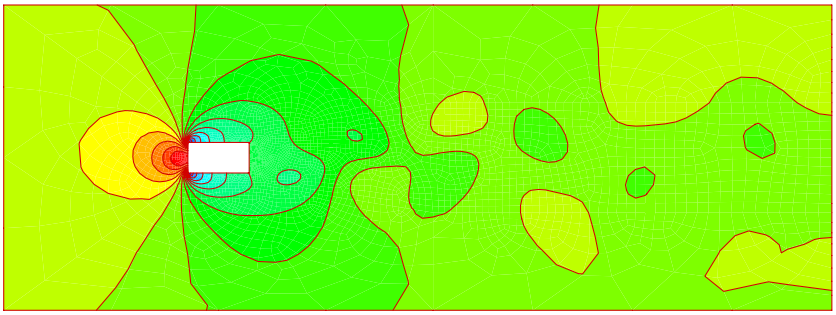

(b)

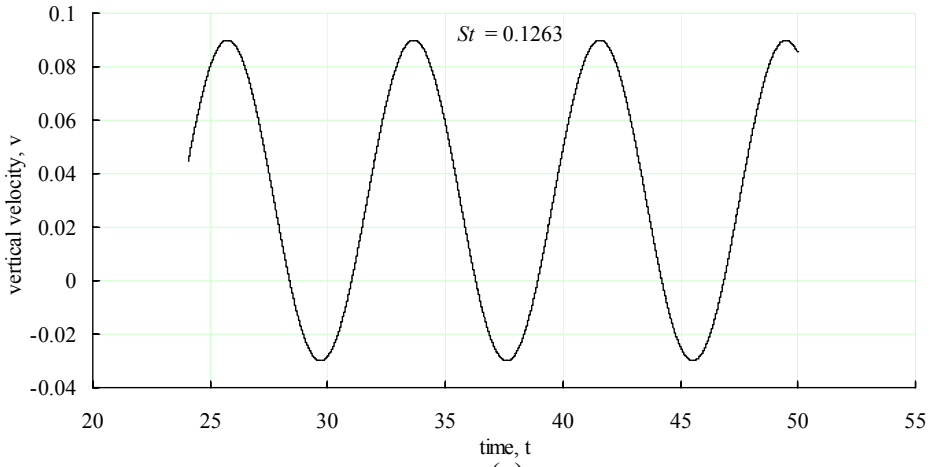

(c)

Fig. 4.18 Results for unsteady flow past rectangular cylinder at $Re = 80$:
(a) Instantaneous streamlines and vertical velocity contours, (b) Pressure contours,
(c) Variation of vertical velocity at $x/L \cong 1.5$ from trailing edge

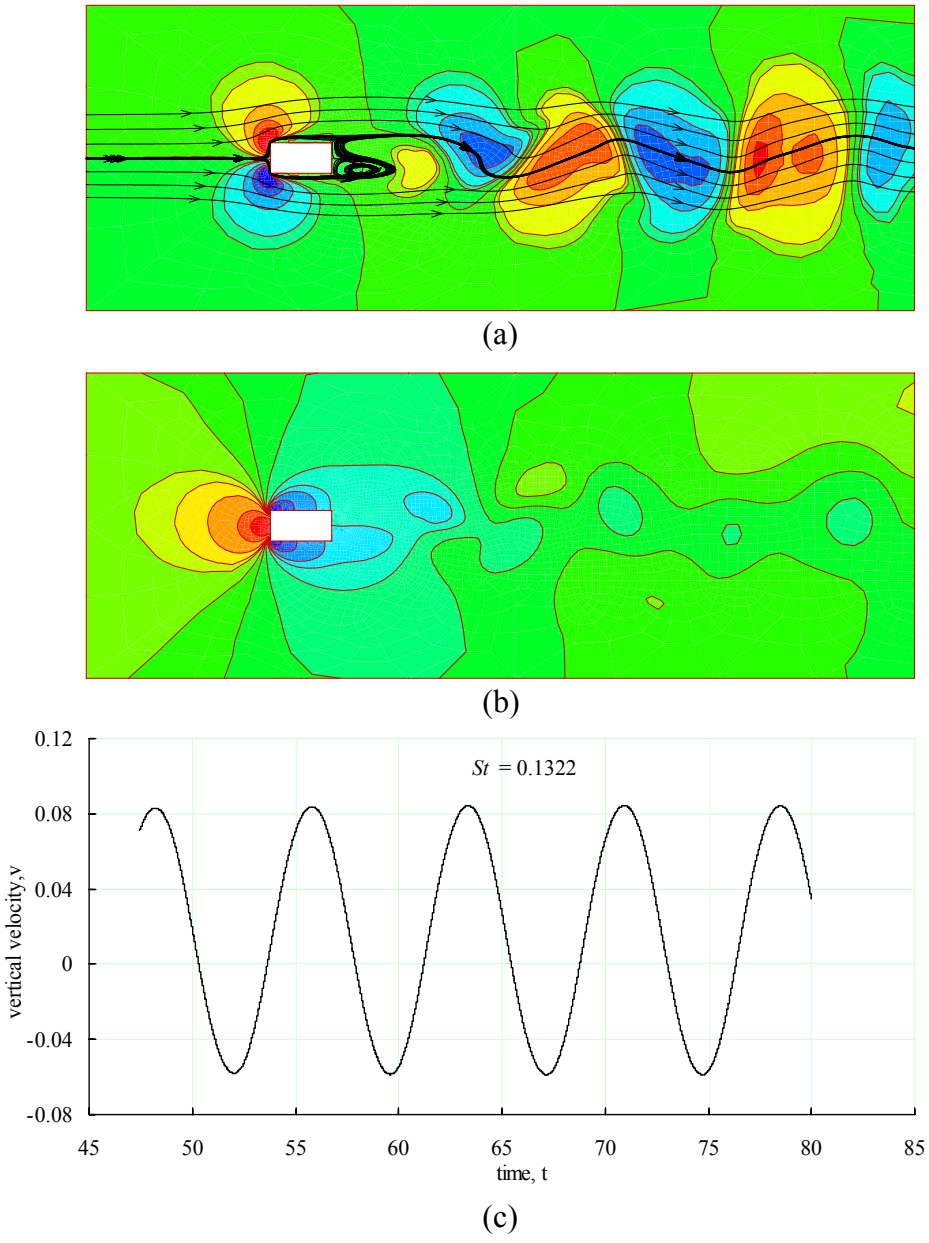

Fig. 4.19 Results for unsteady flow past rectangular cylinder at $Re = 150$:
(a) Instantaneous streamlines and vertical velocity contours, (b) Pressure contours,
(c) Variation of vertical velocity at $x/L \cong 1.5$ from trailing edge

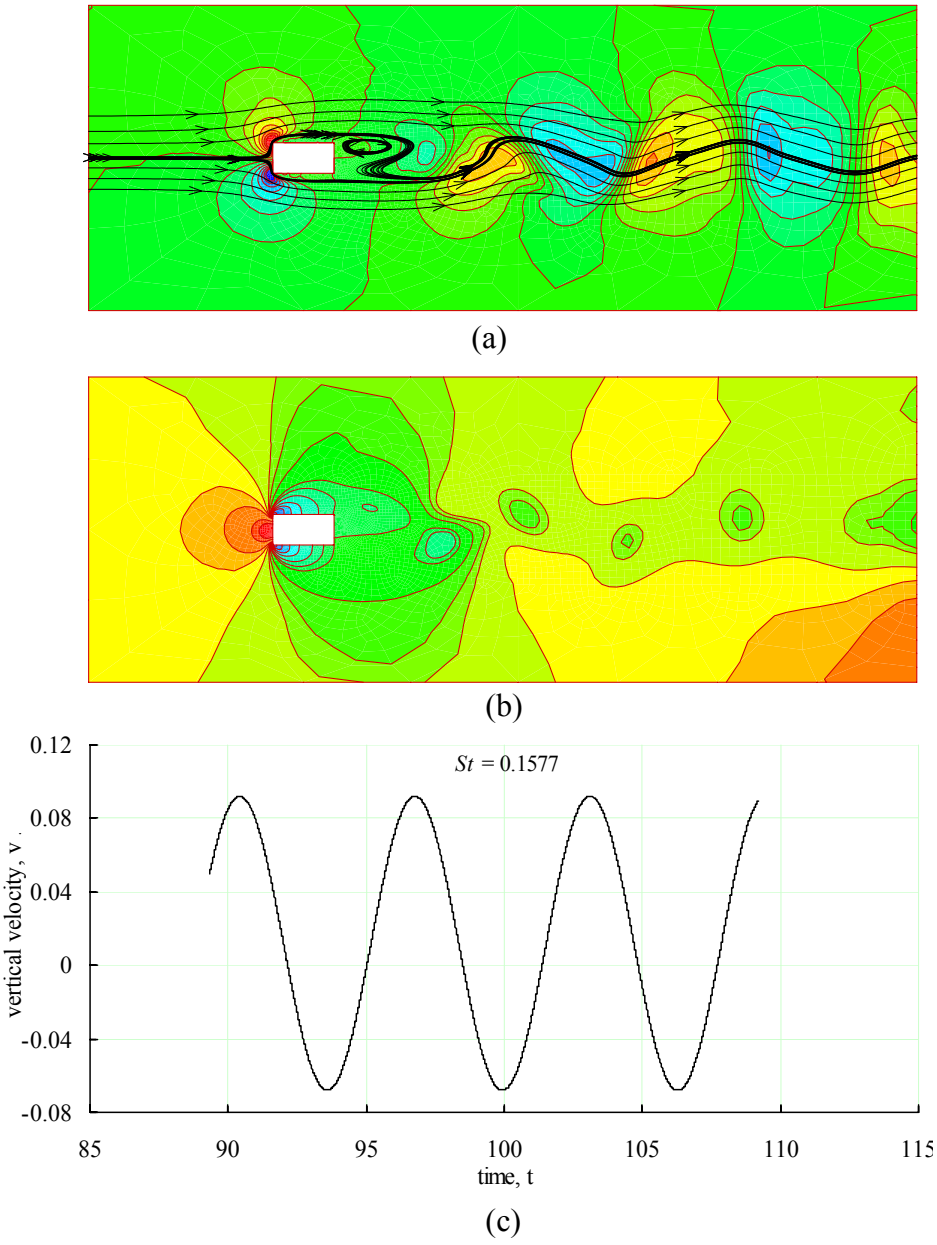

Fig. 4.20 Results for unsteady flow past rectangular cylinder at $Re = 300$:
(a) Instantaneous streamlines and vertical velocity contours, (b) Pressure contours,
(c) Variation of vertical velocity at $x/L \cong 1.5$ from trailing edge

CHAPTER 5

LEAST-SQUARES/GALERKIN SPLIT FINITE ELEMENT METHOD APPLIED TO BUOYANCY-DRIVEN INCOMPRESSIBLE FLOWS

5.1 Introduction

The buoyancy-driven flow in a square cavity with differentially heated walls is one of the least pursued areas in finite element methods, although it has been an extensively explored area in finite difference methods. Physics involved in the buoyancy-driven flow inside a square domain has relevance to a variety of practical problems such as nuclear reactor insulation, ventilation of rooms, solar energy collection, crystal growth in liquids and convective heat transfer associated with boilers and electronics etc. Buoyancy-driven flows have added complexity in form of coupling between transport properties of the flow and the thermal fields. Internal flow problems like one being discussed are more complex compared to external flows due to the fact that unlike the external flows where flow outside the boundary layer can be considered unaffected by boundary layer, over here the flow outside the boundary layer forms a core surrounded by boundary layers on the four walls. The confined core and surrounding boundary layer interact and this interaction causes added complexity especially at higher Rayleigh numbers (*Ra*) and larger temperature differences [51-53]. Davis [55] used a false transient approach based on a stream function-vorticity finite difference method employing forward difference and second order central difference for

time and space derivatives respectively to solve natural convection in a square cavity within the Boussinesq approximation.

Chenoweth and Paolucci [56] investigated the steady state flow in rectangular cavities with large temperature differences between vertical isothermal walls of rectangular cavities. They used transient form of the flow equations, simplified for low Mach numbers.

Vierendeels et al [57] solved full Navier-Stokes equations for low speed compressible flows to simulate buoyancy-driven flow inside a square domain without resorting to Boussinesq approximation or low Mach number approximation. The low Mach number stiffness was tackled by appropriate discretization and local pre-conditioning. Their study employing multigrid provides benchmark solutions for the thermally driven flows in a square cavity.

Recently lattice Boltzmann method which is based on discrete lattice kinetic theory has gained tremendous popularity as an alternative to traditional numerical methods like finite difference, finite elements and finite volume methods for solving the fluids problems. Some of the noteworthy works relevant to present study are those of Chen et al [58], Eggels and Somers [59] and more recently by Dixit and Babu [60] to name a few.

Li Q Tang [61] solved time dependent Navier-Stokes equations for an incompressible constant property fluid in Boussinesq approximation using least-squares based *V-p-ω-T-q* formulation. He obtained results for buoyancy-driven flow in a square cavity in *Ra*-range of 10^3-10^6. The solution vector had seven variables. In three

dimensional problems it would have been a vector of eleven unknowns. This is the main reason that limited the application of the LSFEM in practical fluid dynamics problems.

In the LSGS formulation used here, only the primitive variables of velocity, pressure and temperature are solved for and an equal-order basis function is used for all of them meaning no LBB condition to be satisfied. Resulting system matrix is symmetric and positive definite and can be solved by iterative solvers like pre-conditioned conjugate gradient (pcg) method. The intent of this part of study is to test and validate the proposed LSGSFEM by simulating the complex buoyancy-driven flow inside a square domain with differentially heated vertical sides.

5.2 Mathematical Formulation

5.2.1 Governing Equations

This study assumes a Newtonian fluid with constant properties except density in body force term of the momentum equation. We considered time-dependent incompressible flow with thermal convection. The Boussinesq-approximation relates the density changes to the temperature changes and thereby couples temperature-field with the flow-field. The governing equations for the thermal convection flow using conservation of mass, momentum and energy can be written as:

$$\begin{aligned}
&\frac{\partial u}{\partial x}+\frac{\partial v}{\partial y}=0\\
&\frac{\partial u}{\partial t}+u\frac{\partial u}{\partial x}+v\frac{\partial u}{\partial y}=-\frac{1}{\rho}\frac{\partial p}{\partial x}+\nu\left(\frac{\partial^2 u}{\partial x^2}+\frac{\partial^2 u}{\partial y^2}\right)\\
&\frac{\partial v}{\partial t}+u\frac{\partial v}{\partial x}+v\frac{\partial v}{\partial y}=-\frac{1}{\rho}\frac{\partial p}{\partial y}+\nu\left(\frac{\partial^2 v}{\partial x^2}+\frac{\partial^2 v}{\partial y^2}\right)+g\beta\left(T-T_c\right)\\
&\frac{\partial T}{\partial t}+u\frac{\partial T}{\partial x}+v\frac{\partial T}{\partial y}=\alpha\left(\frac{\partial^2 T}{\partial x^2}+\frac{\partial^2 T}{\partial y^2}\right)
\end{aligned} \tag{5.1}$$

with boundary conditions:

no slip condition on the walls. $T(0,y)=T_H$, $T(L,y)=T_C$ and $\frac{\partial T}{\partial y}=0$ on top and bottom walls (Fig. 5.1). Here u and v are the velocity components in x and y directions respectively. The density is denoted by ρ, pressure by p and T is the temperature. Symbols v and α are for the kinematic viscosity and the thermal diffusivity respectively. T_H and T_C are temperatures at the hot and the cold walls respectively, L the length of the square domain and β the coefficient of thermal expansion. The equations were non-dimensionalized as follows:

$$x' = \frac{x}{L},\ y' = \frac{y}{L},\ u' = \frac{u\,L}{\alpha},\ \ v' = \frac{v\,L}{\alpha},\ T' = \frac{T - T_C}{T_H - T_C} \text{ and } p' = \frac{p L^2}{\rho \alpha^2}$$

where variables with x', y' and u' *etc.* are the non-dimensionalized variables. With these non-dimensional variables we get the following non dimensional form of the governing equations where $'$ has been dropped for the sake of clarity.

$$\begin{aligned}
&\frac{\partial u}{\partial x} + \frac{\partial v}{\partial y} = 0 \\
&\frac{\partial u}{\partial t} + u\frac{\partial u}{\partial x} + v\frac{\partial u}{\partial y} = -\frac{\partial p}{\partial x} + Pr\left(\frac{\partial^2 u}{\partial x^2} + \frac{\partial^2 u}{\partial y^2}\right) \\
&\frac{\partial v}{\partial t} + u\frac{\partial v}{\partial x} + v\frac{\partial v}{\partial y} = -\frac{\partial p}{\partial y} + Pr\left(\frac{\partial^2 v}{\partial x^2} + \frac{\partial^2 v}{\partial y^2}\right) + Ra\,Pr\,T \\
&\frac{\partial T}{\partial t} + u\frac{\partial T}{\partial x} + v\frac{\partial T}{\partial y} = \left(\frac{\partial^2 T}{\partial x^2} + \frac{\partial^2 T}{\partial y^2}\right)
\end{aligned} \tag{5.2}$$

And the boundary conditions are:

$u = v = 0$ on all four walls. $T(0,y)=T_H$, $T(1,y)=T_C$ and $\frac{\partial T}{\partial y}=0$ on top and bottom walls. Here *Pr* and *Ra* are the dimensionless numbers called Prandtl number and Rayleigh number respectively. These are given as: $Pr=\frac{v}{\alpha}$ and $Ra=\frac{g\beta(T_H-T_C)L^3Pr}{v^2}$ respectively.

5.2.2 Least-Squares/Galerkin Split Formulation for Buoyancy-Driven Flow

LSGS method is based on time-dependent formulation of Navier Stokes equations. Time derivatives are discretized using Euler backward differences as:

$$\frac{\partial u}{\partial t} \approx \frac{u^{n+1}-u^{n}}{\Delta t} \quad \text{and} \quad \frac{\partial v}{\partial t} \approx \frac{v^{n+1}-v^{n}}{\Delta t} \tag{5.3}$$

and non-linear terms are linearized in time to get the matrix form of the system

$$\mathscr{L} U^{n+1} = f \tag{5.4}$$

where $U = (u, v, p, T)^T$ is the vector of unknowns, the operator $\mathscr{L}$ is given as

$$\mathscr{L} = \begin{bmatrix} \frac{\partial}{\partial x} & \frac{\partial}{\partial y} & 0 & 0 \\ I + \Delta t \vec{V}^n \cdot \nabla - \Delta t\, Pr \nabla^2 & 0 & \Delta t \frac{\partial}{\partial x} & 0 \\ 0 & I + \Delta t \vec{V}^n \cdot \nabla - \Delta t\, Pr \nabla^2 & \Delta t \frac{\partial}{\partial y} & 0 \\ 0 & 0 & 0 & I + \Delta t \vec{V}^n \cdot \nabla - \Delta t \nabla^2 \end{bmatrix} \tag{5.5}$$

and the vector *f* is given as

$$f = \begin{Bmatrix} 0 \\ u^n \\ v^n + \Delta t RaPrT^n \\ T^n \end{Bmatrix} \tag{5.6}$$

here $\vec{V}^n$ is the velocity vector at the previous time level and I is an $m \times m$ identity matrix, m being the number of nodes per element. The residual vector is given as

$$\mathscr{R} = \mathscr{L} U^{n+1} - f \tag{5.7}$$

The residual is minimized using a suitable weighting operator that comes from LSFEM applied to the first order terms in the governing equations. LSFEM gives a symmetric system of equations and the inherent streamline upwinding term provides stability. The weighting operator for LSGS method, $\mathscr{S}$, therefore is taken from LSFEM applied to inviscid part of governing equations as

$$\mathscr{S} = \begin{bmatrix} \frac{\partial}{\partial x} & \frac{\partial}{\partial y} & 0 & 0 \\ I + \Delta t \vec{V}^n \cdot \nabla & 0 & \Delta t \frac{\partial}{\partial x} & 0 \\ 0 & I + \Delta t \vec{V}^n \cdot \nabla & \Delta t \frac{\partial}{\partial y} & 0 \\ 0 & 0 & 0 & I + \Delta t \vec{V}^n \cdot \nabla \end{bmatrix} \tag{5.8}$$

Hence minimizing of the residual in (5.7) using the weighting operator in (5.8) leads to following weak form for LSGSFEM

$$\int_\Omega (\mathscr{S} N)^T (\mathscr{L} U^{n+1} - f) \, d\Omega = 0 \tag{5.9}$$

Introducing the finite element approximation

$$U^{n+1} \approx U_h^{n+1} = \sum_i^m N_i U_i^{n+1} \tag{5.10}$$

where m is the number of nodes per element and N_i is the element shape function associated with i^{th} node. Substituting the approximation into the weak formulation in (5.9) leads to linear algebraic equations

$$[K]\{U^{n+1}\} = \{F\} \tag{5.11}$$

Global stiffness matrix [K] and the vector $\{F\}$ result from assembling the element stiffness matrices and vectors respectively given by

$$ke = \int_{\Omega_e} (\mathscr{S} N_i)^T (\mathscr{L} N_j)\, d\Omega; \qquad fe = \int_{\Omega_e} (\mathscr{S} N_i)^T f\, d\Omega. \tag{5.12}$$

The element stiffness matrix, *ke* and the element load vector, *fe* are given in full form in Appendix C. Integrals are evaluated using Gaussian quadrature. The weighting operator $\mathscr{S}$ ensures split treatment to first order terms and second order terms in the governing equation. Thus, the first order term are treated like LSFEM and the second order viscous terms get treated similar to GFEM. Integrals containing second order terms are resolved the Galerkin way through integration by parts. Subsequently, terms containing second order derivatives are dropped, as explained in previous chapter.

5.3 Computation of Derived Variables

Variables like vorticity, stream function and Nusselt number are computed from the solution as post-processing products. The method of obtaining these quantities is described in this section.

5.3.1 Vorticity, ω_z

Vorticity at each node was computed by using the definition of vorticity, $\omega = \nabla \times V$. For two dimensional cases it becomes

$$\omega_z = \frac{\partial v}{\partial x} - \frac{\partial u}{\partial y} \tag{5.13}$$

A variable X can be expanded using the basis set $\{N\}$ as $X = \sum_i^n N_i X_i$, where n is the number of nodes per element and N_i and X_i are the element shape function and the value of variable X respectively associated with i^{th} node. We can write (5.13) as

$$N_i \omega_{zi} = \frac{\partial N_i v_i}{\partial x} - \frac{\partial N_i u_i}{\partial y} \tag{5.14}$$

Applying Galerkin method to (5.14) gives the system of equations

$$\int_{\Omega} \{N_i\}\{N_j\}^T d\Omega\{\omega_{zi}\} = \int_{\Omega} \{N_i\}\left\{\frac{\partial N_j}{\partial x}\right\}^T d\Omega\{v_i\} - \int_{\Omega} \{N_i\}\left\{\frac{\partial N_j}{\partial y}\right\}^T d\Omega\{u_i\} \tag{5.15}$$

Which is solved to get values of vorticity at each node. No boundary condition is specified.

5.3.2 Stream Function, ψ

Stream function was computed from the relation

$$\nabla^2 \psi = \frac{\partial^2 \psi}{\partial x^2} + \frac{\partial^2 \psi}{\partial y^2} = \frac{\partial u}{\partial y} - \frac{\partial v}{\partial x} \tag{5.16}$$

where anticlockwise circulation is taken as positive ψ and clockwise circulation as negative ψ. Finite element expansion with the help of basis set $\{N\}$ for the variables ψ, u and v similar to that in previous section and application of Galerkin method gives the system of equations

$$\int_{\Omega} \{N_i\}\{\nabla^2 N_j\}^T d\Omega\{\psi_i\} = \int_{\Omega} \{N_i\}\left\{\frac{\partial N_j}{\partial y}\right\}^T d\Omega\{u_i\} - \int_{\Omega} \{N_i\}\left\{\frac{\partial N_j}{\partial x}\right\}^T d\Omega\{v_i\} \tag{5.17}$$

Integral involving second order term is treated by Green's theorem and the resulting boundary term is ignored because of no slip condition on all the four walls. The system of equations resulting, that needs to be solved in order to get nodal values of ψ is

$$\int_{\Omega} \{\nabla N_i\}\{\nabla N_j\}^T d\Omega\{\psi_i\} = \int_{\Omega} \{N_i\}\left\{\frac{\partial N_j}{\partial x}\right\}^T d\Omega\{v_i\} - \int_{\Omega} \{N_i\}\left\{\frac{\partial N_j}{\partial y}\right\}^T d\Omega\{u_i\} \tag{5.18}$$

5.3.3 Nusselt Number, Nu

Nusselt number, *Nu* is the ratio of convection heat transfer to fluid conduction heat transfer under the same conditions. Davis [55] in his paper computed average *Nu* throughout the cavity, on the vertical midplane and on the vertical hot wall on the right side. On the hot wall he also computed maximum and minimum Nusselt numbers along with their locations. Component of *Nu* in x-direction averaged over a vertical plane is

$$Nu_x = \int_0^1 q_x(x,y)\,dy = \int_0^1 \left(uT - \frac{\partial T}{\partial x} \right) dy \tag{5.19}$$

The component of heat flux in *x*-direction, $q_x(x,y)$ was computed in a similar way using relation $q_x(x,y) = uT - \frac{\partial T}{\partial x}$ and Galerkin treatment to it as before, gives

$$\int_\Omega \{N_i\}\{N_j\}^T d\Omega \{q_{xi}\} = \int_\Omega u_0 \{N_i\}\{N_j\}^T d\Omega \{T_i\} - \int_\Omega \{N_i\} \left\{ \frac{\partial N_j}{\partial y} \right\}^T d\Omega \{T_i\} \tag{5.20}$$

Once Nu_x is computed, overall average Nusselt number, $\overline{Nu}$ is computed as

$$\overline{Nu} = \int_0^1 Nu_x\,dx \tag{5.21}$$

Similarly other values of Nusselt numbers can be computed. Integrals in (5.19) and (5.21) were computed using Simpson's method. To get more accurate values, the nodal values of integrand were first interpolated to finer resolution using cubic spline method.

5.4 Results and Discussion

Computations were carried out in the Rayleigh number range of $10^3 - 10^6$ and value of Prandtl number, *Pr* was taken as 0.71 which is the value for air at room temperature. Davis [55] used uniform meshes with 10, 20 and 40 element per side for

$Ra = 10^3$ and 10^4 and 10, 20, 40, 60 and 80 element-meshes for $Ra = 10^5$ and 10^6. He also used Richardson extrapolation in order to get the exact solution. Uniform meshes with 10, 20 and 40 elements per side for $Ra = 10^3$; 20, 30, 40 and 60 element-meshes for $Ra = 10^4$; 20, 30, 40, 60 and 80 element-meshes for $Ra = 10^5$ and 40, 50, 60, 80 and 100 element-meshes for $Ra = 10^6$ were used in present study. Gaussian quadrature with one-point reduced integration was used to compute the integrals. A time step size, Δt = 0.001 was used for $Ra = 10^3 - 10^5$, whereas for highly nonlinear case of $Ra = 10^6$, time step Δt = 0.0005 with under relaxation factor of 0.6 was used. For all the cases a tolerance of 10^{-9} or maximum of 8000 iterations were used for pcg-iterations at each time step. An external tolerance of 10^{-6} for l^2-norm of residual was used as stopping criterion. Results in form of tables and contours have been compared with the benchmark results by Davis [55]. Contour plots for stream function, horizontal and vertical velocity components, temperature and vorticity are presented in Figs 5.2-5.6. Contours match well with those by Davis [55]. The streamline contours are fully anti-symmetric with respect to the center of the cavity and for lower Rayleigh numbers maximum value of stream function occurs at the center of the cavity. For higher Rayleigh numbers there are two maxima on both sides of the center. Various other parameters computed similar to those computed by Davis are listed in Tables I-IV. These values are compared with those obtained by Davis on uniform 40×40 and 80×80 meshes. It should be noted that Davis used a finite difference method that was first order in time and second order in space. The definition and nomenclature for the quantities compared in the table are same as those by Davis [55], which are:

$|\psi|_{mid}$ Magnitude of the stream function at the center of the cavity

$|\psi|_{\max}$ Magnitude of the maximum value of stream function (also its location)

u_{max} Maximum horizontal velocity on vertical mid-plane (also its y-location)

v_{max} Maximum vertical velocity on horizontal mid-plane (also its x-location)

$\overline{Nu}$ The average Nusselt number throughout the cavity

$Nu_{1/2}$ The average Nusselt number on the vertical mid-plane of the cavity

Nu_0 The average Nusselt number on the vertical hot surface of the cavity

Nu_{max} The maximum value of local Nusselt number on the vertical hot surface

Nu_{min} The minimum value of local Nusselt number on the vertical hot surface

To obtain more accurate values for these quantities and their locations, the node point data were first interpolated using a cubic-spline interpolation to a finer resolution. The values thus computed were further refined using Richardson extrapolation:

$$f_{extpn} = f_h - Ch^{\alpha}$$

where

$$\alpha = ln\left(\frac{f_h - f_{h'}}{f_{h/2} - f_{h'/2}}\right)/ln(2) \qquad (5.22)$$

and $$C = \frac{f_h - f_{h/2}}{h^{\alpha}(1 - 2^{-\alpha})}$$

Here h is given by $1/N$, and N is the number of elements in one direction in the finest mesh and h' is the value for next finest mesh used for a particular Rayleigh number case (see tables 5.1-5.4). The computed value of α gives roughly the order of convergence. Convergence plots for u_{max} and v_{max} are shown in Fig. 5.7. The slopes of the plots average around 2, which is expected as u_{max} and v_{max} are the primary solution

variables. Convergence rates for derived variables like stream function and Nusselt numbers are less than quadratic. The pcg iterations required at each time step quickly declined as the solution progressed towards convergence. The variation of pcg iterations for the Ra-range tested was recorded for 40×40 mesh run at $\Delta t = 0.001$. A typical plot is shown in Fig. 5.8. The figure also shows the total number of pcg-iterations to reach the converged solutions. The results listed in tables 5.1-5.4 show the correct trend and the extrapolated values are close to benchmarks values by Davis [55].

5.5 Conclusions

Complex buoyancy-driven flow in a square cavity with differentially heated vertical walls and Boussinesq approximation has been solved using least-squares/Galerkin split finite element method (LSGSFEM) that employs a least-squares method for first-order derivatives and a Galerkin method for second order derivatives, thereby avoiding the need for additional unknowns required by pure a LSFEM approach. This method has inherent streamline upwinding term and allows for equal-order basis functions for velocity, pressure and temperature thereby avoids LBB condition. Non-linear terms are treated by linearization in time. Results were obtained using low-order C^0 continuous elements and compare well with the standard published results.

Table 5.1 Comparison of Results for Buoyancy-Driven Flow at $Ra = 10^3$

	Mesh size	$\lvert\psi\rvert_{mid}$	$\lvert\psi\rvert_{max}$ x, y	u_{max} z	v_{max} x	$\overline{Nu}$	$Nu_{1/2}$	Nu_0	Nu_{max}	Nu_{min}
	0.1	1.1866	-	3.884 0.822	3.949 0.171	1.1095	1.1152	1.1137	1.4965 0.128	0.6898 0.999
LSGS Method	$h' = 0.05^*$	1.1764	-	3.697 0.814	3.748 0.178	1.1131	1.1135	1.1175	1.5033 0.091	0.6930 0.999
	$h = 0.025^*$	1.1739	-	3.657 0.813	3.706 0.178	1.1139	1.1129	1.1184	1.5052 0.09	0.6937 0.999
Extrapolated solns		1.173	-	3.646 0.813	3.695 0.178	1.114	1.113	1.118	1.506 0.09	0.6939 0.999
Benchmark solutions Davis [55]		**1.174**	**-**	**3.649 0.813**	**3.697 0.178**	**1.118**	**1.118**	**1.117**	**1.505 0.092**	**0.692 1**

*see extrapolation equation (5.22)

Table 5.2 Comparison of Results for Buoyancy-Driven Flow at $Ra = 10^4$

	Mesh Size	$\lvert\psi\rvert_{mid}$	$\lvert\psi\rvert_{max}$ x, y	u_{max} z	v_{max} x	$\overline{Nu}$	$Nu_{1/2}$	Nu_0	Nu_{max}	Nu_{min}
	0.1	5.1953	-	16.863 0.825	20.178 0.119	2.2026	2.2223	2.2266	3.4471 0.0161	0.6020 0.999
LSGS Method	$h' = 0.05^*$	5.1479	-	16.588 0.825	19.856 0.118	2.2029	2.2148	2.2300	3.4521 0.157	0.6043 0.999
	$h = 0.025^*$	5.1316	-	16.495 0.825	19.724 0.118	2.2028	2.2114	2.2311	3.4532 0.155	0.6050 0.999
		5.1200	-	16.429 0.825	19.634 0.118	2.2027	2.2090	2.2318	3.4540 0.153	0.6052 0.999
Extrapolated solns		5.1162	-	16.408 0.825	19.598 0.118	2.2026	2.2064	2.2319	3.4543 0.152	0.6054 0.999
Benchmark solutions Davis [55]		**5.071**	**-**	**16.178 0.823**	**19.617 0.119**	**2.243**	**2.243**	**2.238**	**3.528 0.143**	**0.586 1**

*see extrapolation equation (5.22)

Table 5.3 Comparison of Results for Buoyancy-Driven Flow at $Ra = 10^5$

	Mesh Size	$\lvert\psi\rvert_{mid}$	$\lvert\psi\rvert_{max}$ x, y	u_{max} z	v_{max} x	$\overline{Nu}$	$Nu_{1/2}$	Nu_0	Nu_{max}	Nu_{min}
LSGS Method	0.05	9.6258	10.2281 0.3, 0.65	40.665 0.857	75.259 0.067	4.244	4.310	4.295	6.817 0.14	0.794 0.967
	0.03$\dot{3}$	9.4705	10.0099 0.3, 0.644	39.039 0.860	70.264 0.064	4.275	4.332	4.341	6.847 0.106	0.840 0.982
	0.025	9.4183	9.9319 0.3, 0.625	38.480 0.86	68.846 0.064	4.281	4.337	4.361	6.873 0.105	0.847 0.999
	$h' =$ 0.01$\dot{6}$*	9.3817	9.8743 0.3, 0.617	38.088 0.86	68.071 0.064	4.287	4.341	4.376	6.916 0.103	0.850 0.999
	$h =$ 0.0125*	9.3690	9.854 0.300, 0.615	37.953 0.861	67.761 0.064	4.289	4.343	4.381	6.926 0.101	0.851 0.999
Extrapolated solns		9.353	9.8268 289, 0.614	36.783 0.86	67.458 0.64	4.291	4.344	4.386	6.960 0.098	0.852 1
Benchmark solutions Davis [55]		**9.111**	**9.612 0.285, 0.601**	**34.73 0.855**	**68.59 0.066**	**4.519**	**4.519**	**4.509**	**7.717 0.081**	**0.729 1**

*see extrapolation equation (5.22)

Table 5.4 Comparison of Results for Buoyancy-Driven Flow at $Ra = 10^6$

	Mesh size	$\lvert\psi\rvert_{mid}$	$\lvert\psi\rvert_{max}$ x, y	u_{max} z	v_{max} x	$\overline{Nu}$	$Nu_{1/2}$	Nu_0	Nu_{max}	Nu_{min}
LSGS Method	0.025	16.845	17.3750 0.15, 0.55	69.063 0.842	238.535 0.038	8.655	8.673	8.619	16.464 0.068	0.905 0.98
	0.02	16.728	17.1730 0.16, 0.55	68.303 0.845	230.296 0.038	8.673	8.705	8.664	16.613 0.057	0.973 0.999
	0.01$\dot{6}$	16.663	17.1005 0.15, 0.55	67.892 0.847	226.419 0.038	8.682	8.713	8.684	16.603 0.05	1.031 0.991
	$h' =$ 0.0125*	16.598	17.0051 0.15, 55	67.488 0.848	223.870 0.038	8.691	8.726	8.705	16.588 0.047	1.042 0.999
	$h = 0.01$*	16.568	16.962 0.15, 0.540	67.303 0.849	222.465 0.038	8.695	8.732	8.715	16.621 0.046	1.045 0.999
Extrapolated solns		16.511	16.9046 0.150, 0.539	66.982	220.86	8.702	8.737	8.729	16.809 0.044	1.047 0.999
Benchmark solutions Davis [55]		**16.32**	**16.75 0.151, 0.547**	**64.63 0.850**	**219.36 0.0379**	**8.800**	**8.799**	**8.817**	**17.925 0.0378**	**0.989 1**

*see extrapolation equation (5.22)

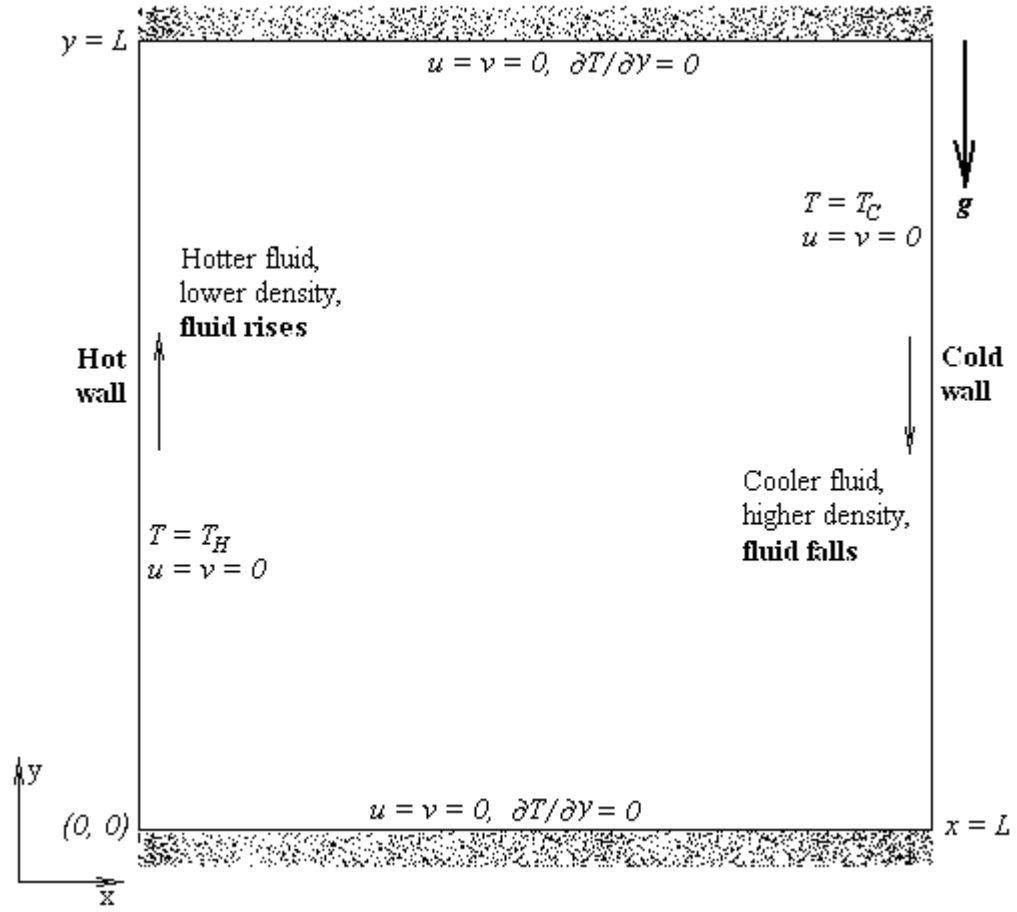

Fig. 5.1 Computational domain and the boundary conditions for buoyancy-driven flow

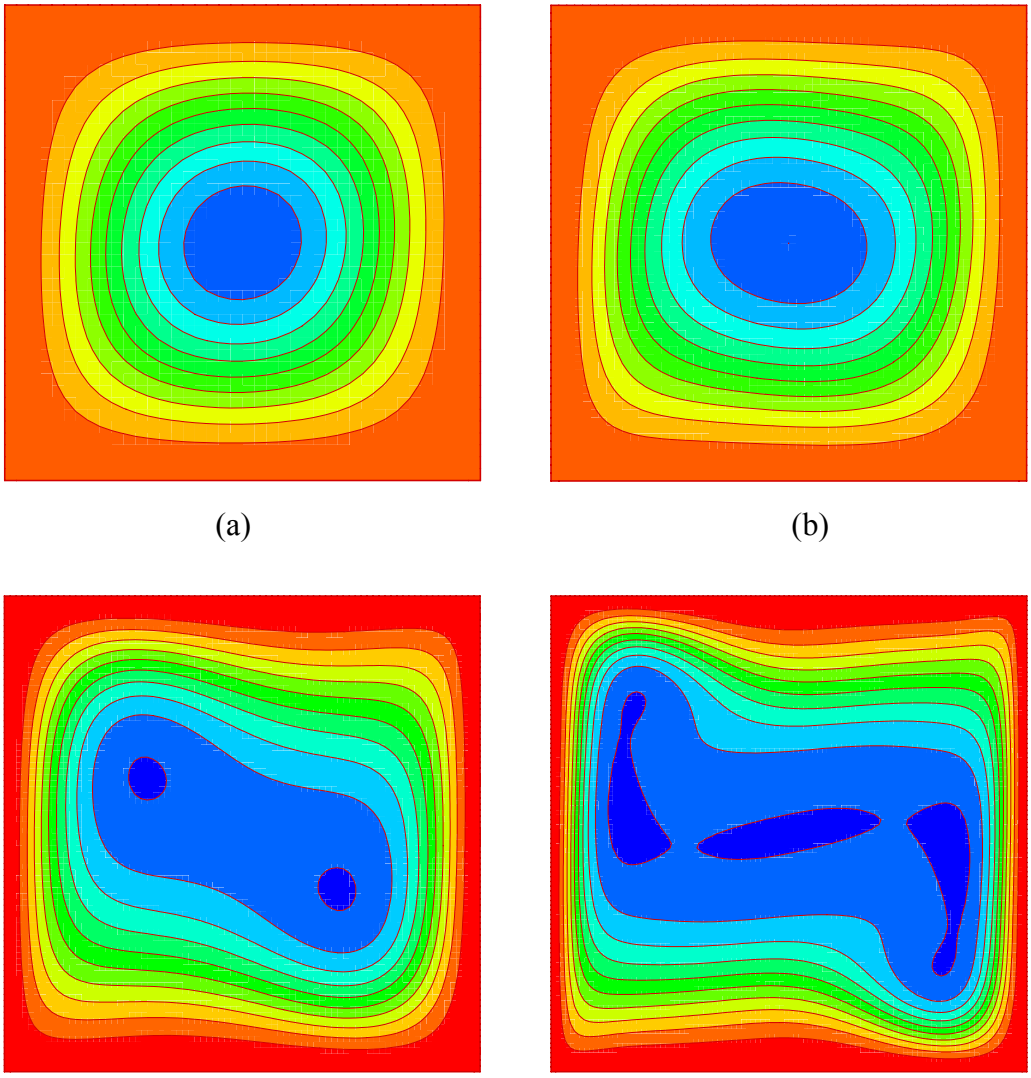

(a) (b)

(c) (d)

Fig. 5.2 Contour maps of stream function ψ : (a) $Ra = 10^3$; contours at -1.1739 (0.1174) 0, (b) $Ra = 10^4$; contours at -5.1199 (0.5112) 0, (c) $Ra = 10^5$; contours at -9.7780, -8.80 (0.9778) 0, (d) $Ra = 10^6$; contours at -16.49, -14.84 (1.649) 0

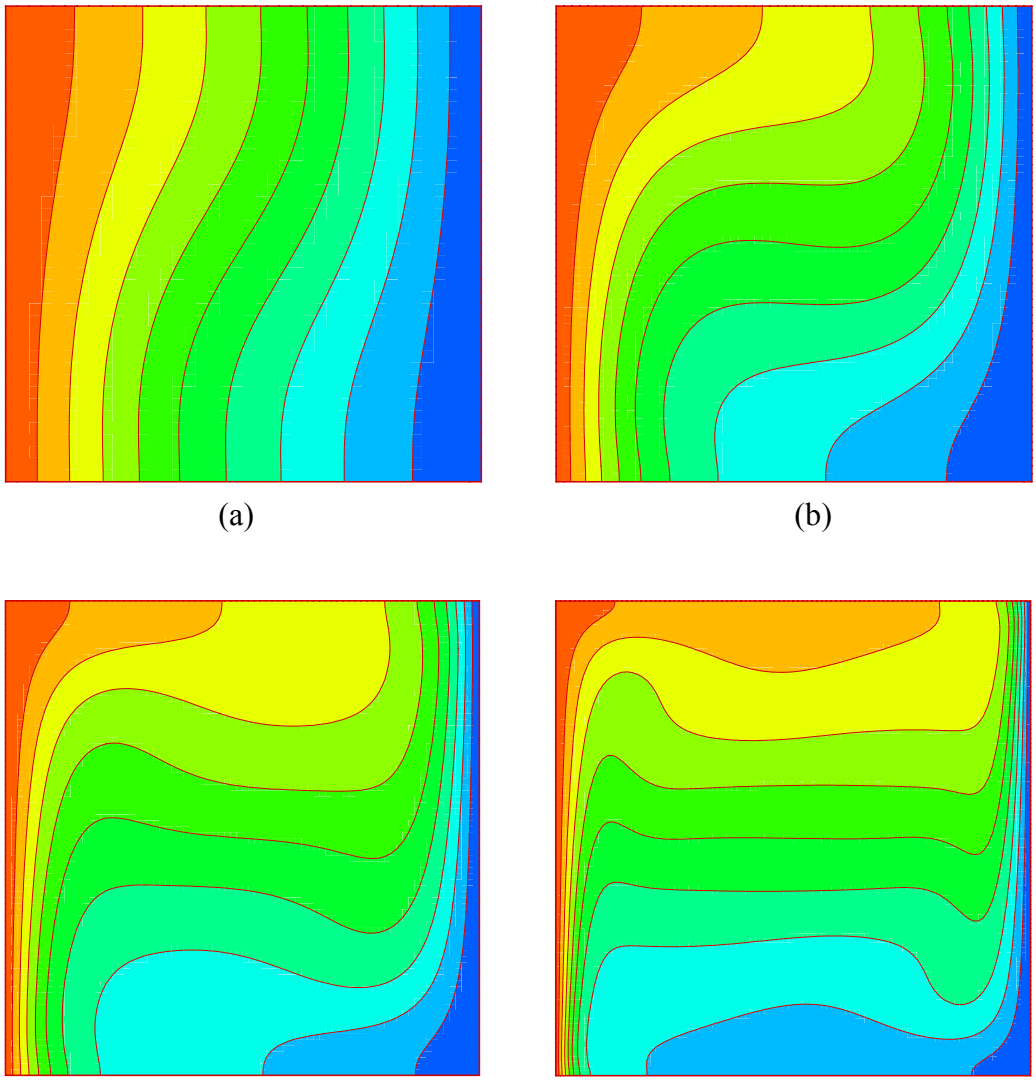

Fig. 5.3 Contour maps of temperature T: (a) $Ra = 10^3$, (b) $Ra = 10^4$, (c) $Ra = 10^5$, (d) $Ra = 10^6$ contours at 0.0 (0.1) 1.0 for all.

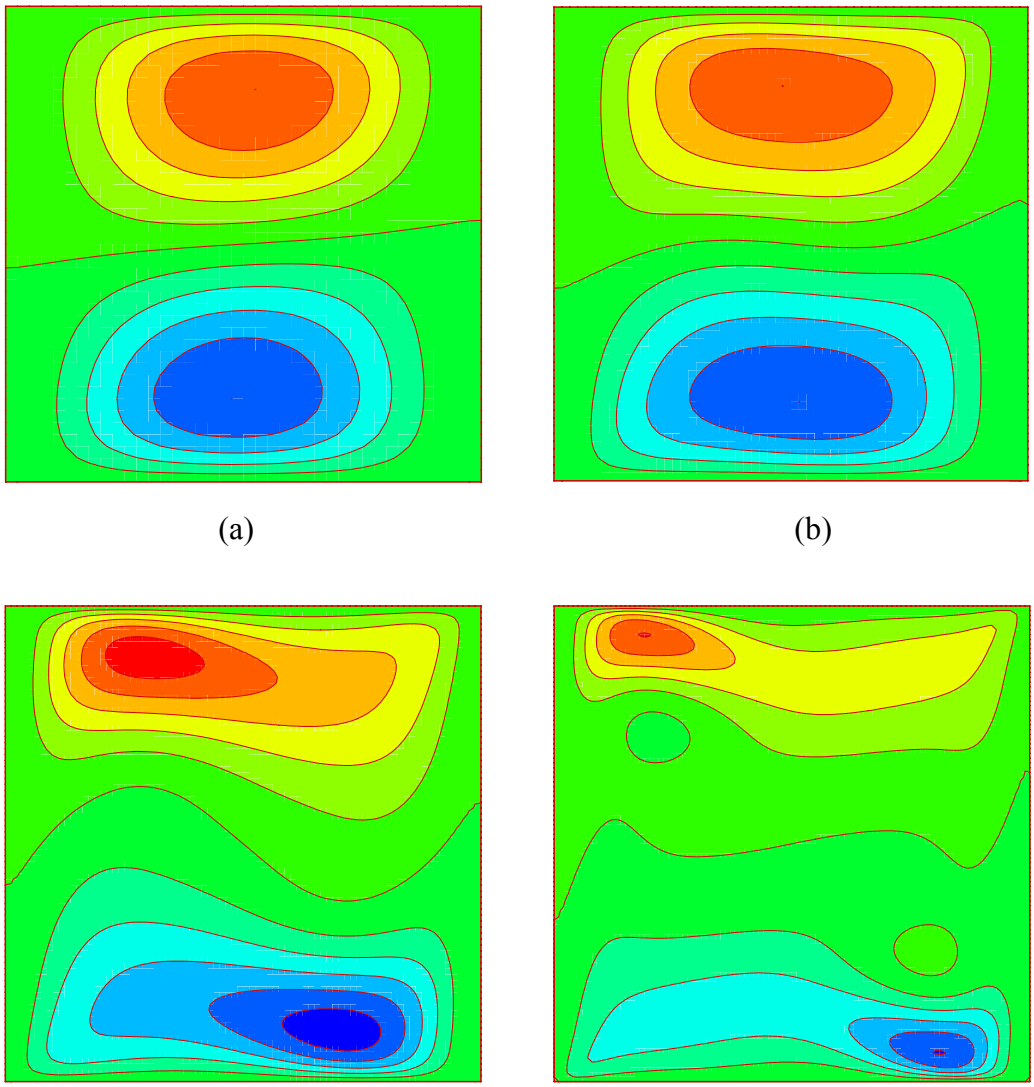

(a) (b)

(c) (d)

Fig. 5.4 Contour maps of horizontal velocity u: (a) $Ra = 10^3$; contours at -3.6478 (0.72956) 3.6478, (b) $Ra = 10^4$; contours at -16.440 (3.2880) 16.440, (c) $Ra = 10^5$; contours at -43.0 (8.6) 43.0, (d) $Ra = 10^6$; contours at -135.756 (27.151) 135.756

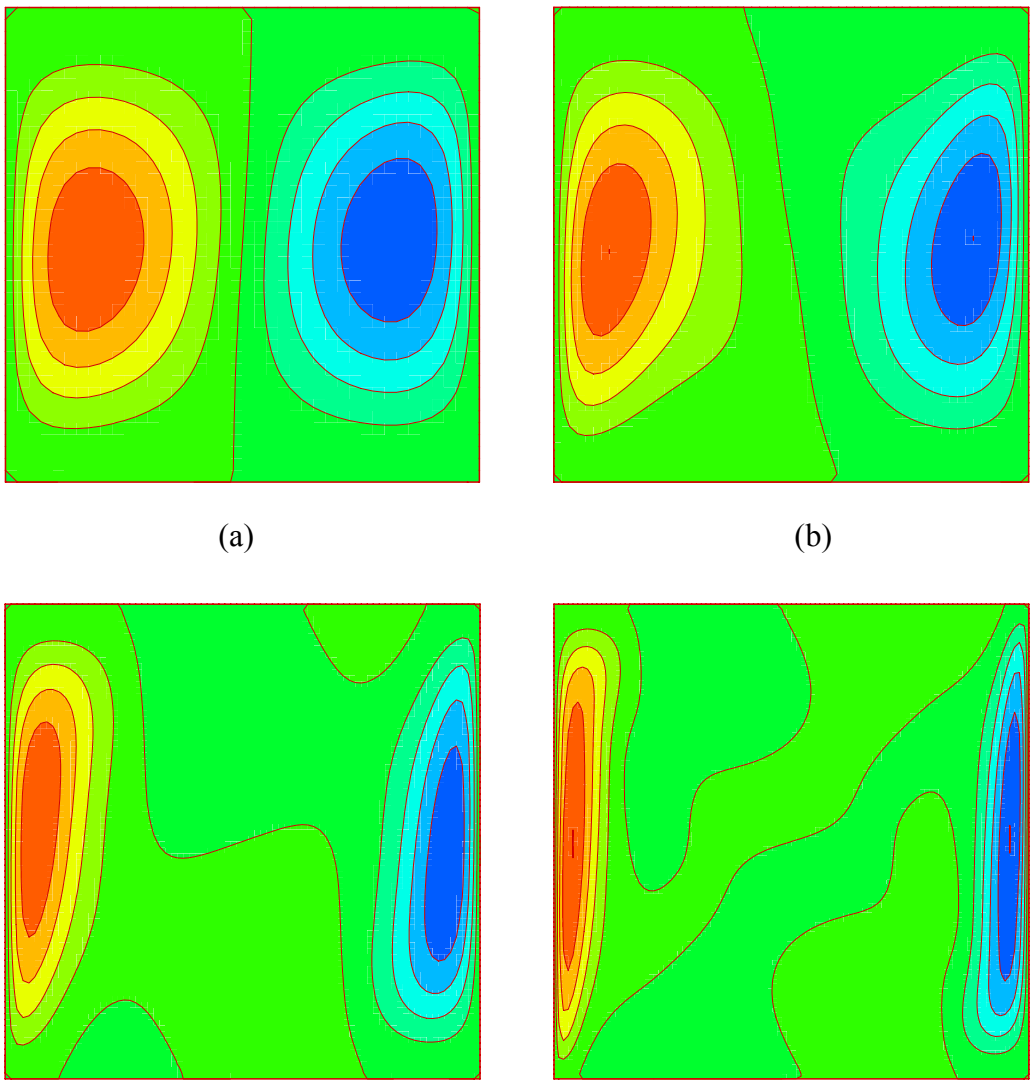

(a) (b)

(c) (d)

Fig. 5.5 Contour maps of vertical velocity *v*: (a) $Ra = 10^3$; contours at -3.7058 (0.74116) 3.7058, (b) $Ra = 10^4$; contours at -19.640 (3.928) 19.640, (c) $Ra = 10^5$; contours at -68.2 (13.64) 68.2, *(d)* Ra = 10^6; contours at -221.31 (44.262) 221.31

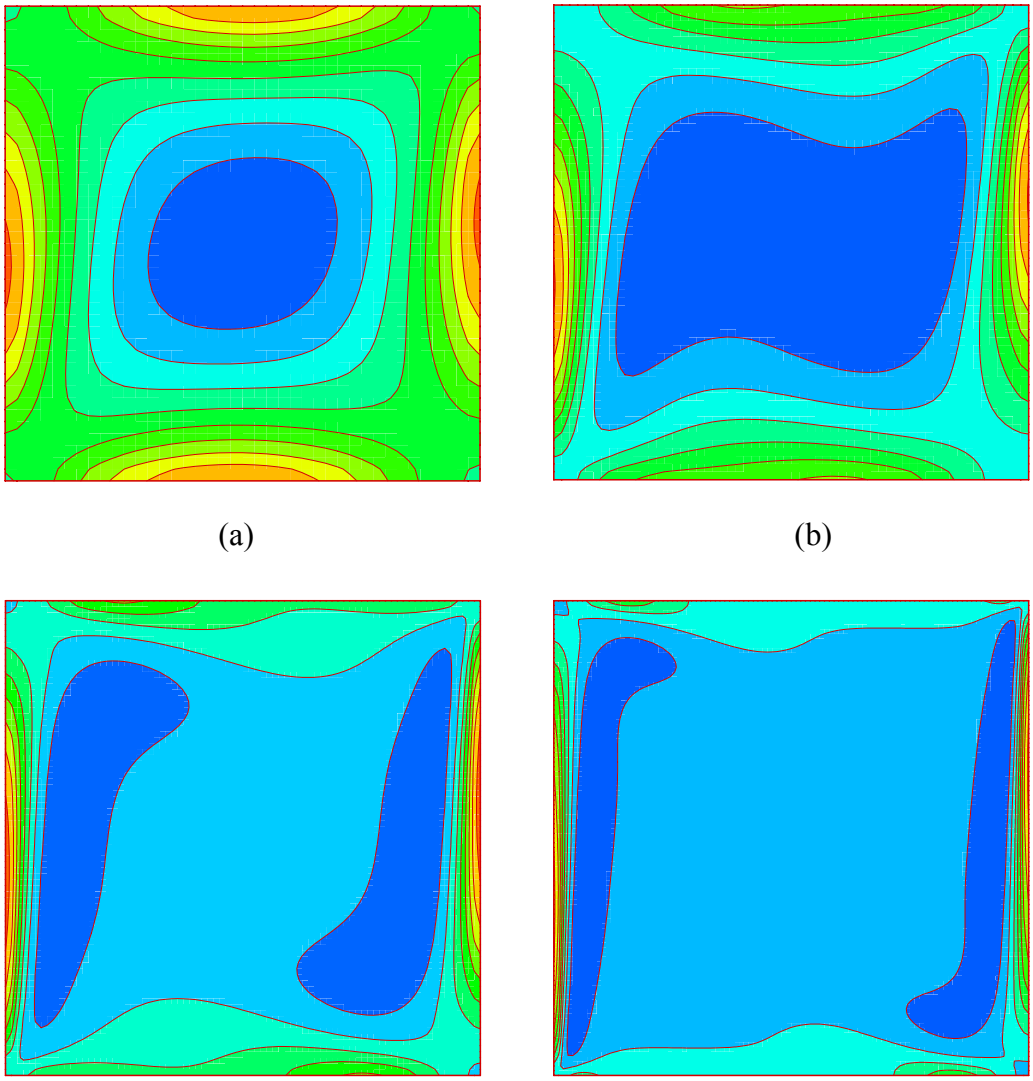

(a) (b)

(c) (d)

Fig. 5.6 Contour maps of vorticity ω: (a) $Ra = 10^3$; contours at -32.352 (8.354) 51.19, (b) $Ra = 10^4$; contours at -124.10 (54.84) 424.3, (c) $Ra = 10^5$; contours at -600 (322.0) 2600, (d) $Ra = 10^6$; contours at -3165.8 (1827.14) 15105.6

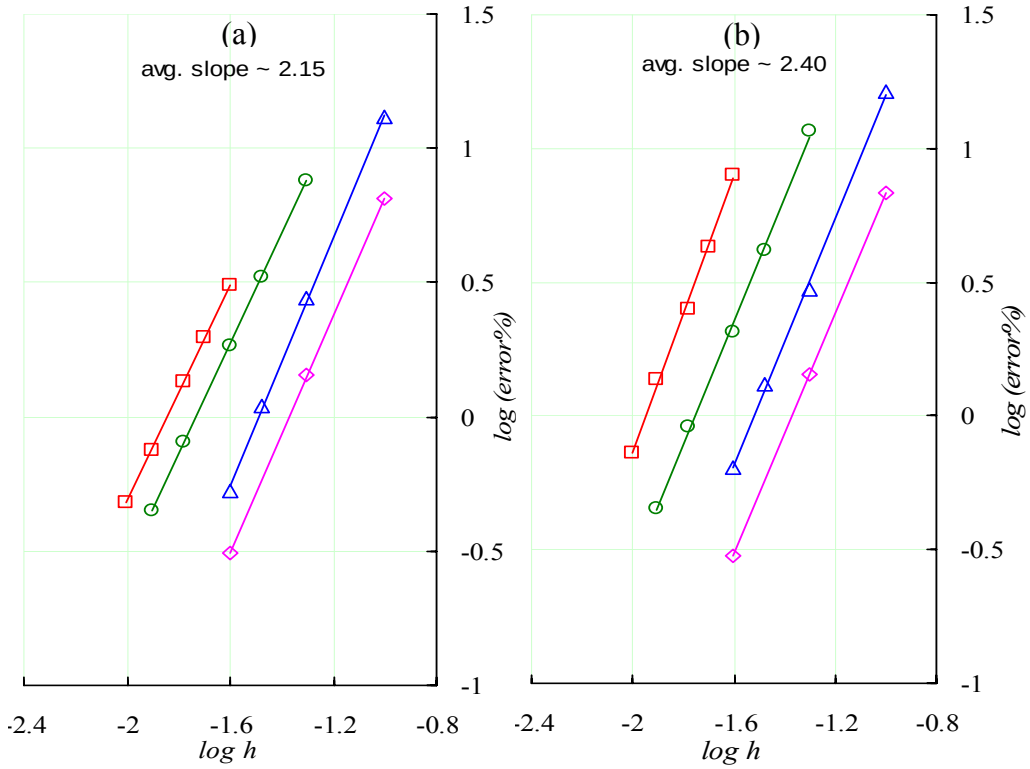

Fig. 5.7 Convergence-rate plots: (a) u_{max} (b) v_{max}
◇ $Ra = 10^3$, Δ $Ra = 10^4$, ○ $Ra = 10^5$ and □ $Ra = 10^6$

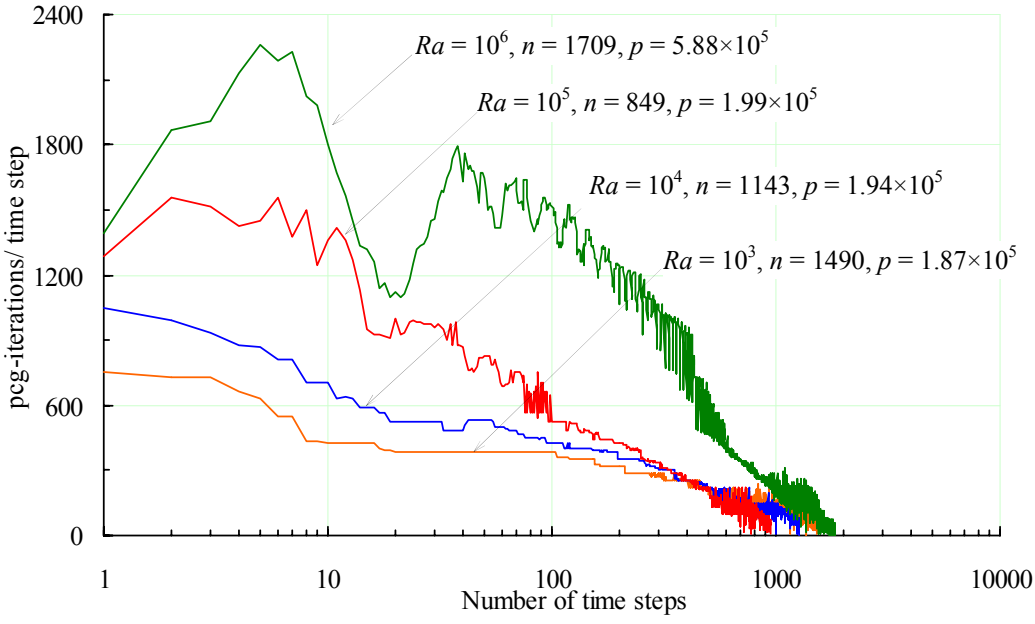

Fig. 5.8 A typical convergence plot using 40×40 mesh (l^2-*norm of residual* → 10^{-6})
n : number of time steps, p : number of pcg-iterations

CHAPTER 6

LEAST-SQUARES/GALERKIN SPLIT FINITE ELEMENT METHOD FOR COMPRESSIBLE FLOWS

6.1 Introduction

The search for stabilized methods for compressible flows started in 1970s and first significant contribution in that direction came from Brooks and Hughes [12], though applied to convection-diffusion and incompressible Navier-Stokes equations, was called SUPG (Streamline Upwind Petrov-Galerkin) method. The SUPG method is a residual based upwinding technique (hence variationally consistent), aimed at stabilizing Galerkin finite element methods based on equal order interpolations. The effect of the SUPG terms on the equation is to transform the original Galerkin method into a physics-adaptive Petrov-Galerkin formulation. Later Tezduyar and Hughes [62, 63] developed the first finite element compressible flow formulation based on conserved variables. A more robust formulation was needed to capture shock waves in compressible flows. Michel Mallet along with Hughes and Mizukami [64] developed shock capturing operators. Le Beau [65] revisited the original SUPG formulation for compressible flows and developed shock capturing operators in conserved variables.

Shakib in his thesis published in [66, 67] gave second stabilized method to achieved popularity, namely, Galerkin/least-squares or GLS method. Ken Jansen [68-70] developed entropy consistent formulation and was first to apply GLS to turbulent

compressible flows. This idea was extended to k-∈ turbulence model by Guillermo Hauke [71]. He generalized stabilized compressible flow methods to an arbitrary set of variables. He also used physical variables in transonic flows with shocks and thereby dispelled myths from the finite difference literature that only conserved variables were appropriate for capturing the shocks.

Over the years, significant progress has been made in the field of compressible flows. These include time-accurate local time-stepping techniques [72], large scale parallel 3D computations [73-75], unified formulation for compressible and incompressible flows [76] and shock capturing with multi-scale spatial discretization [77] etc. to name a few.

The LSGS formulation described in previous chapters has inherent streamline upwinding term. In this section LSGS formulation based on primitive variables of $(\rho, u, v, T)^T$ has been used to solve a couple of benchmark problems in supersonic and transonic flow.

6.2 Mathematical Formulation

6.2.1 Governing Equations

The complete Navier-Stokes equations governing an unsteady, compressible, viscous laminar flow are given as:

$$\begin{aligned}
&\frac{\partial \rho}{\partial t} + \vec{V}.\nabla\rho + \rho\nabla\cdot\vec{V} = 0 \\
&\rho\frac{\partial \vec{V}}{\partial t} + \rho\left(\vec{V}\cdot\nabla\right)\vec{V} + \nabla p = \mu\left[\Delta\vec{V} + \frac{1}{3}\nabla\left(\nabla\cdot\vec{V}\right)\right] + \rho f \\
&\rho\frac{\partial h}{\partial t} + \rho\vec{V}\cdot\nabla h = \frac{\partial p}{\partial t} + \vec{V}\cdot\nabla p + \nabla\cdot\left(k\nabla T\right) + \Phi
\end{aligned} \tag{6.1}$$

where $\Phi = \frac{4}{3}\mu\left[\left(\frac{\partial u}{\partial x}\right)^2 + \left(\frac{\partial v}{\partial y}\right)^2 - \frac{\partial u}{\partial x}\frac{\partial v}{\partial y}\right] + \mu\left(\frac{\partial u}{\partial y} + \frac{\partial v}{\partial x}\right)^2$ is the viscous dissipation term.

Since the governing equations above are in $(\rho, u, v, p)^T$ form, we need to reformulate above equations and get non-dimensionalized equations in $(\rho, u, v, T)^T$ form. Using the following non-dimensionalization parameters:

$$\begin{aligned}
&\rho' = \frac{\rho}{\rho_\infty}, \quad u' = \frac{u}{U_\infty}, \quad v' = \frac{v}{U_\infty} \\
&x' = \frac{x}{L}, \quad y' = \frac{y}{L}, \quad t' = \frac{t}{\tau} \ \ where\ \tau = \frac{L}{U_\infty} \\
&p' = \frac{p}{\rho_\infty U_\infty^2}, \quad u' = \frac{u}{U_\infty}, \quad v' = \frac{v}{U_\infty} \\
&and\ T' = \frac{T}{T_\infty} \quad where\ T_\infty = \frac{|U_\infty|^2}{c_V}
\end{aligned} \tag{6.2}$$

Here variables with $'$ on top are non-dimensional variables. After non-dimensionalizing and reformulating the governing equations in $(\rho, u, v, T)^T$ can be written similar to Bristeau [78] as:

$$\begin{aligned}
&\frac{\partial \rho}{\partial t} + u\frac{\partial \rho}{\partial x} + v\frac{\partial \rho}{\partial y} + \rho\left(\frac{\partial u}{\partial x} + \frac{\partial v}{\partial y}\right) = 0 \\
&\frac{\partial u}{\partial t} + u\frac{\partial u}{\partial x} + v\frac{\partial u}{\partial y} + (\gamma - 1)\frac{T}{\rho}\frac{\partial \rho}{\partial x} + (\gamma - 1)\frac{\partial T}{\partial x} = \frac{1}{\rho Re}\left[\frac{\partial^2 u}{\partial x^2} + \frac{\partial^2 u}{\partial y^2} + \frac{1}{3}\frac{\partial}{\partial x}\left(\frac{\partial u}{\partial x} + \frac{\partial v}{\partial y}\right)\right] + f_x \\
&\frac{\partial v}{\partial t} + u\frac{\partial v}{\partial x} + v\frac{\partial v}{\partial y} + (\gamma - 1)\frac{T}{\rho}\frac{\partial \rho}{\partial y} + (\gamma - 1)\frac{\partial T}{\partial y} = \frac{1}{\rho Re}\left[\frac{\partial^2 v}{\partial x^2} + \frac{\partial^2 v}{\partial y^2} + \frac{1}{3}\frac{\partial}{\partial y}\left(\frac{\partial u}{\partial x} + \frac{\partial v}{\partial y}\right)\right] + f_y \\
&\frac{\partial T}{\partial t} + u\frac{\partial T}{\partial x} + v\frac{\partial T}{\partial y} + (\gamma - 1)T\left(\frac{\partial u}{\partial x} + \frac{\partial v}{\partial y}\right) = \frac{\gamma}{\rho RePr}\left(\frac{\partial^2 T}{\partial x^2} + \frac{\partial^2 T}{\partial y^2}\right) + \frac{1}{\rho Re}F(\nabla V)
\end{aligned} \tag{6.3}$$

For convenience the $'$ symbol atop non-dimensional variables has been dropped from the governing equations. In the equations above *Re* and *Pr* are the similarity parameters

the Reynolds number and the Prandtl number given as $\frac{\rho_\infty U_\infty L}{\mu}$ and $\frac{\mu C_p}{k}$ respectively. Here k is the thermal conductivity, μ the viscosity and C_p the specific heat at constant pressure, for the fluid. $F(\nabla V)$ is the non-dimensional energy dissipation term given by:

$$F(\nabla V)=\frac{4}{3}\left[\left(\frac{\partial u}{\partial x}\right)^2+\left(\frac{\partial v}{\partial y}\right)^2-\frac{\partial u}{\partial x}\frac{\partial v}{\partial y}\right]+\left(\frac{\partial u}{\partial y}+\frac{\partial v}{\partial x}\right)^2 \tag{6.4}$$

6.2.2 Least-Squares/Galerkin Split Formulation for Compressible Flows

LSGS method is based on time-dependent formulation of Navier Stokes equations. Using Euler backward differences for time derivatives as

$$\frac{\partial u}{\partial t}\approx\frac{u^{n+1}-u^n}{\Delta t} \quad \text{and} \quad \frac{\partial v}{\partial t}\approx\frac{v^{n+1}-v^n}{\Delta t} \tag{6.5}$$

The energy-dissipation term, $F(\nabla V)$ in the equation (6.3) was linearized in time as

$$\begin{aligned} F(\nabla V)&=\frac{4}{3}\left[\left(\frac{\partial u}{\partial x}\right)^2+\left(\frac{\partial v}{\partial y}\right)^2-\frac{\partial u}{\partial x}\frac{\partial v}{\partial y}\right]+\left(\frac{\partial u}{\partial y}+\frac{\partial v}{\partial x}\right)^2 \\ &=\frac{4}{3}\left[\left|\frac{\partial u}{\partial x}\right|^n\frac{\partial u}{\partial x}+\left|\frac{\partial v}{\partial y}\right|^n\frac{\partial v}{\partial y}-\frac{1}{2}\left(\left|\frac{\partial u}{\partial x}\right|^n\frac{\partial v}{\partial y}+\left|\frac{\partial v}{\partial y}\right|^n\frac{\partial u}{\partial x}\right)\right]+\left|\frac{\partial u}{\partial y}+\frac{\partial v}{\partial x}\right|^n\left(\frac{\partial u}{\partial y}+\frac{\partial v}{\partial x}\right) \end{aligned} \tag{6.6}$$

where terms with $|^n$ are evaluated at the previous time level. Now with *Euler*-backward discretization for spatial derivative and linearizing rest of non-linear terms in time we get the matrix form of the system

$$\mathscr{L}\,U^{n+1}=f \tag{6.7}$$

where $U=(\rho, u, v, T)^T$ is the vector of unknowns, the operator $\mathscr{L}$ is given as

$$\mathscr{L}=\begin{bmatrix} I+\Delta t\vec{V}^{n}\cdot\nabla & \Delta t\rho\dfrac{\partial}{\partial x} \\ \Delta t(\gamma-1)\dfrac{T}{\rho}\dfrac{\partial}{\partial x} & I+\Delta t\vec{V}^{n}\cdot\nabla-\dfrac{\Delta t}{\rho Re}\nabla^{2}-\dfrac{\Delta t}{3\rho\,\mathrm{Re}}\dfrac{\partial^{2}}{\partial x^{2}} \\ \Delta t(\gamma-1)\dfrac{T}{\rho}\dfrac{\partial}{\partial y} & -\dfrac{\Delta t}{3\rho\,\mathrm{Re}}\dfrac{\partial^{2}}{\partial y\partial x} \\ 0 & \Delta t(\gamma-1)T\dfrac{\partial}{\partial x}-\dfrac{4a\Delta t}{3\rho\,\mathrm{Re}}\dfrac{\partial}{\partial x}-\dfrac{c\Delta t}{\rho Re}\dfrac{\partial}{\partial y} \end{bmatrix}$$

$$\begin{bmatrix} \Delta t\rho\dfrac{\partial}{\partial y} & 0 \\ -\dfrac{\Delta t}{3\rho\,\mathrm{Re}}\dfrac{\partial^{2}}{\partial x\partial y} & \Delta t(\gamma-1)\dfrac{\partial}{\partial x} \\ I+\Delta t\vec{V}^{n}\cdot\nabla-\dfrac{\Delta t}{\rho Re}\nabla^{2}-\dfrac{\Delta t}{3\rho\,\mathrm{Re}}\dfrac{\partial^{2}}{\partial y^{2}} & \Delta t(\gamma-1)\dfrac{\partial}{\partial y} \\ \Delta t(\gamma-1)T\dfrac{\partial}{\partial y}-\dfrac{4b\Delta t}{3\rho\,\mathrm{Re}}\dfrac{\partial}{\partial y}-\dfrac{c\Delta t}{\rho Re}\dfrac{\partial}{\partial x} & I+\Delta t\vec{V}^{n}\cdot\nabla \end{bmatrix} \tag{6.8}$$

f the right hand side vector (see Appendix D) and $\vec{V}^{n}$ is the velocity field vector at previous time step, I an $m\times m$ identity matrix, m being number of nodes per element and N is the basis function set. The residual vector is given as

$$\mathscr{R}=\mathscr{L}U^{n+1}-f \tag{6.9}$$

The residual is minimized using a suitable weighting operator that comes from LSFEM applied to first order terms of the governing equations. As explained in section 3.4, we get the equivalent Galerkin form the Euler-Lagrange formulation resulting from application of LSFEM to first order portion of the governing equations. Once we find the Galerkin form, we add the left out second order terms of the NS equations and apply Galerkin method to complete equation. For linear elements it is equivalent as treating the weighted residual of (6.9) with weighting operator $\mathscr{S}$ as

$$\int_{\Omega}(\mathscr{S}N)^{T}(\mathscr{L}U^{n+1}-f)d\Omega=0 \tag{6.10}$$

Where $\mathscr{S}$ is obtained from taking first order terms of governing equations (see Appendix D). Introducing the finite element approximation

$$U^{n+1} \approx U_h^{n+1} = \sum_i^m N_i U_i^{n+1} \tag{6.11}$$

where m is the number of nodes per element and N_i is the element shape function associated with i^{th} node. Substituting the approximation into the weak formulation in (6.10) leads to linear algebraic equations

$$[K]\{U^{n+1}\} = \{F\} \tag{6.12}$$

Global stiffness matrix $[K]$ and the vector $\{F\}$ result from assembling the element stiffness matrices and vectors respectively given by

$$ke = \int_{\Omega_e} (\mathscr{S} N_i)^T (\mathscr{L} N_j)\, d\Omega; \qquad fe = \int_{\Omega_e} (\mathscr{S} N_i)^T f\, d\Omega. \tag{6.13}$$

Detailed derivation of the elements of the matrix *ke* and vector *fe* and the introduced constants *a, b, c and d* is given in Appendix D. Weighting operator $\mathscr{S}$ ensures split treatment to first order terms and second order terms in the governing equation. Thus, the first order term are treated like LSFEM and the second order viscous terms get treated similar to GFEM. Integrals containing second order terms are resolved the Galerkin way through integration by parts. Subsequent terms containing second order derivatives are dropped, as is the standard practice [35] to ignore computationally expensive higher order derivatives for linear elements.

6.3 Compressible Benchmark Problems

Test problems of steady supersonic laminar viscous flow over a flat plate and over NACA0012 airfoil were explored.

6.3.1 Supersonic Viscous Flow over a Flat Plate

This test case originally solved by Carter [79], is extensively used to test the performance of the schemes for a viscous supersonic flow over flat plate. This problem consists of a Mach 3 flow over the plate at a Reynolds number of 1000 based on the length of the plate. The Prandtl number, *Pr* is taken as 0.72. The boundary conditions used are as follows:

ρ = 1.0, u = 1.0, v = 0, $T = T_\infty = \dfrac{1}{\gamma(\gamma-1)M_\infty^2}$ at the inlet and top boundary. On the segment in front of the plate v = 0. On the plate surface $u = v = 0$ and $T = T_s$ was used and no boundary conditions were applied at the exit. The temperature of the plate is assumed constant and equal to

$$T_s = \frac{1}{\gamma(\gamma-1)M_\infty^2}\left(1+\frac{\gamma-1}{2}M_\infty^2\right) \tag{6.14}$$

Fig. 6.2a shows the structured mesh used in the analysis with 7623 nodes with 7448 bilinear quadrilateral elements. This mesh is clustered in such a way as to have enough layers of nodes in the boundary layer.

6.3.2 Flow over NACA 0012 Airfoil

Laminar viscous flow was simulated over a NACA 0012 airfoil in subsonic, transonic and supersonic Mach number regime. In the first case, subsonic flow at M_∞ = 0.5 was simulated at an angle of attack, α of 0° at a *Re* = 2000. In second case transonic flow at M_∞ = 0.8, α = 10° at *Re* = 500 was simulated. In third case flow at M_∞ = 1.2, α = 0° at *Re* = 1000 was tried. An unstructured mesh (Fig. 6.4) consisting of 57191

quadrilateral elements and 57799 nodes was used. Mesh was constructed very fine on the surface in order to capture boundary layer.

6.3.2.1 Boundary Conditions

Transonic and supersonic viscous flows over NACA0012 airfoil are considered. For these flow regimes, the Navier-Stokes equations form a mixed parabolic-hyperbolic set of partial differential equations. The different types of boundary conditions in these cases are discussed below.

6.3.2.1.1 Subsonic Flow

Boundary conditions are normally determined by performing one dimensional characteristic analysis normal to the boundary. The sign of the Eigen values determine what conditions may be specified. Subsonic inflow typically has three Eigen values (wave speeds) directed into the domain and one having negative slope is directed out of the domain. Therefore three variables may be specified and one must be extrapolated.

At the subsonic inflow boundary, the boundary conditions therefore are imposed by specifying the velocity components and the static temperature. Pressure (or density) is generally extrapolated.

At the subsonic outflow boundary (Γ_{∞}^{+}), however, situation is completely reversed. Three wave speeds are directed out of the domain and one is directed into the domain. Three variables therefore must be extrapolated and one be specified. Generally *u, v, w* and *T* are extrapolated and density or pressure is specified.

On the body surface, boundary conditions for viscous flows are much simpler than those for inviscid flows. At the surface the no-slip, isothermal boundary condition

is applied. The no-slip condition is implemented simply by specifying appropriate essential boundary conditions for the momentum components of the equation system. The isothermal boundary condition is implemented as

$$T = T_\infty \left(1 + \frac{(\gamma - 1)}{2} M_\infty^2 \right) \tag{6.15}$$

6.3.2.1.2 Supersonic Flow

A supersonic flow has all four characteristics directed into the flow domain. Therefore all the four state variables need to be specified.

The situation at the supersonic outflow boundary is exactly opposite, where all the characteristics are directed out of domain. Therefore all the state variables must be extrapolated.

At the body-surface the boundary conditions are the same as in subsonic flow.

6.3.2.2 Boundary Conditions for the Test Case

Based on the discussion above, following boundary conditions were applied for the test case of flow over NACA0012 airfoil (see Fig 6.1).

On the inflow boundary (Γ_∞^-)

$$\rho = 1,\ u = 1,\ v = 0 \ \textit{and}\ T = T_\infty = \frac{1}{\gamma(\gamma - 1) M_\infty^2} \qquad \text{(Supersonic flow)}$$

$$u = 1,\ v = 0, T = T_\infty = \frac{1}{\gamma(\gamma - 1) M_\infty^2} \ \textit{and}\ \frac{\partial \rho}{\partial n} = 0 \qquad \text{(Subsonic flow)}$$

On the outflow boundary (Γ_∞^+)

$$\frac{\partial \rho}{\partial n} = \frac{\partial u}{\partial n} = \frac{\partial v}{\partial n} = \frac{\partial T}{\partial n} = 0 \qquad \text{(Supersonic flow)}$$

$$\frac{\partial u}{\partial n}=\frac{\partial v}{\partial n}=\frac{\partial T}{\partial n}=0 \text{ and } \rho=1 \qquad \text{(Subsonic flow)}$$

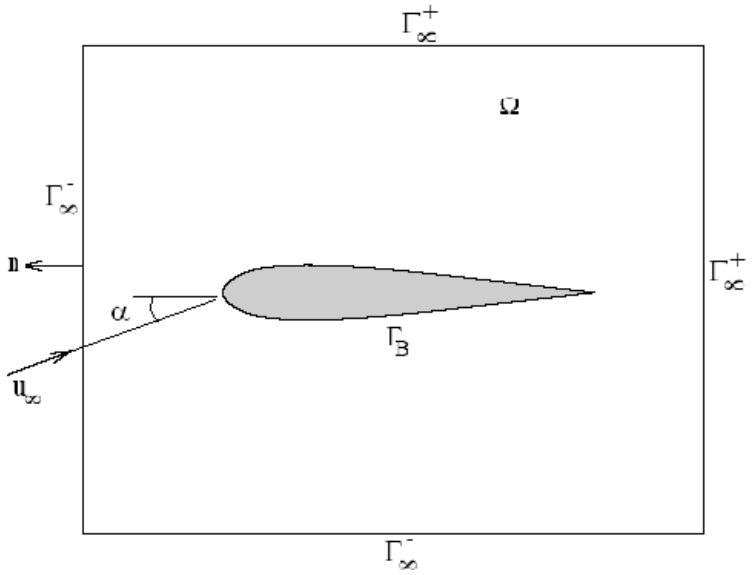

Fig. 6.1 Typical domain and boundaries for flow over an airfoil

On the body surface

$$u=0, v=0, \ \frac{\partial \rho}{\partial n}=0 \text{ and } T_s=T_\infty\left(1+\frac{\gamma-1}{2}M_\infty^2\right) \qquad \text{(Supersonic/subsonic flow)}$$

In finite element methods Neumann boundary conditions are implemented by not specifying any boundary conditions.

6.4 Results and Discussion

6.4.1 Supersonic Viscous Flow over a Flat Plate

Mach 3 viscous flow over a flat plate was simulated. Results are shown in Figs. 6.2 and 6.3. Pressure distribution along the plate is compared with that from Carter [79] in Fig. 6.2b. Mach number and pressure contours are displayed in Figs 6.2c and 6.2d. Variation of the dependent variables at the exit plane is compared with Carters results in Figs 6.3. Carter's results for grid size 0.025 along with the similar solutions

for comparison were digitally scanned from reference [79]. Reasonably good agreement with the published results can be observed.

6.4.2 Flow over NACA 0012 Airfoil

Flow over the airfoil was simulated in subsonic, transonic and supersonic Mach numbers. Fig. 6.5 presents subsonic results at $M_\infty = 0.5$, $\alpha = 0°$ at $Re = 2000$. Mach number and pressure contours followed by C_p-distribution on the airfoil surface are displayed. The pressure distribution compares well with the published results [90] although they are for a $Re = 5000$. Results from transonic flow at $M_\infty = 0.8$, $\alpha = 10°$ at $Re = 500$ are shown in Fig 6.6 in comparison with Tang's results [91]. Reasonably good agreement can be observed. The supersonic results at $M_\infty = 1.2$, $\alpha = 0°$ at $Re = 1000$ from are shown in Fig 6.7. The transonic results do not show clear presence of local normal shock as the highest local Mach number is around a low 1.13. Mach and pressure contours for supersonic case clearly show formation of bow shock upstream of the airfoil.

6.5 Conclusions

Least-squares/Galerkin split finite element method that treats first order terms the least squares way and second order terms the Galerkin way has been successfully applied to compressible flow problems of flow over flat plate and flow over a NACA 0012 airfoil in subsonic, transonic and supersonic Mach number regimes. A density, velocity, temperature formulation in non-conservative form was used. C^0-continuous elements for ρ, u, v and T was used. Reasonably good results have been achieved.

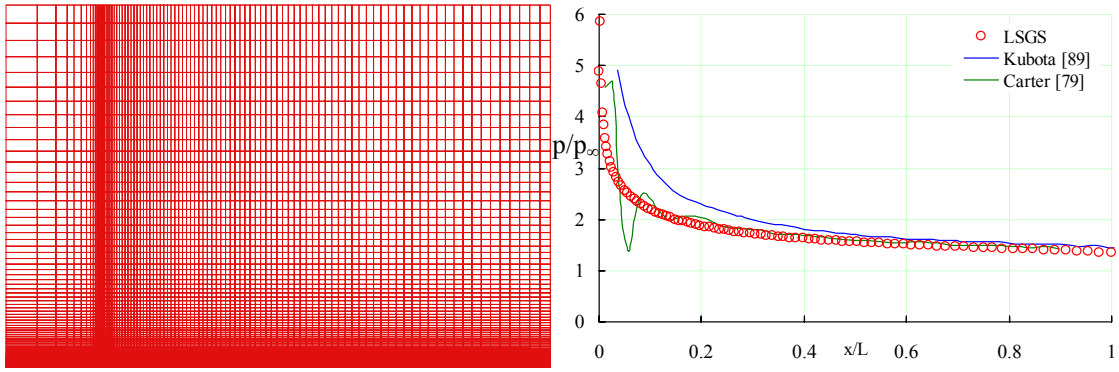

(a) (b)

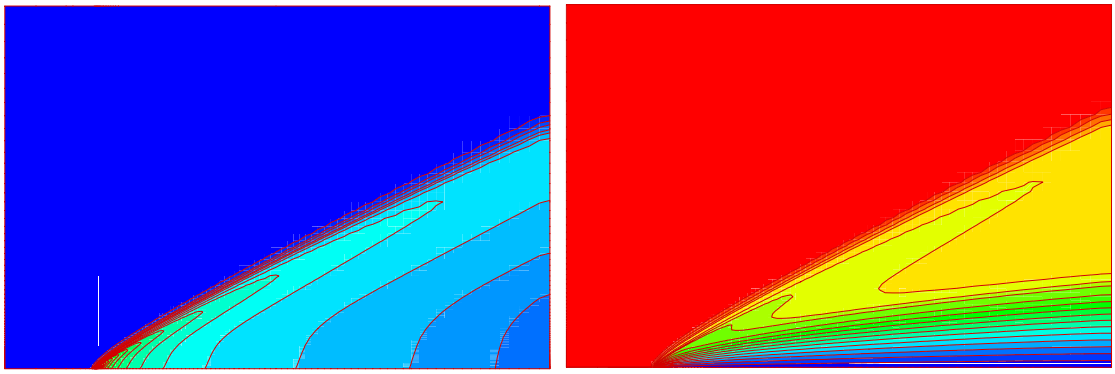

(c) (d)

Fig. 6.2 Results for supersonic laminar viscous flow over a flat plate using LSGS finite element method (M = 3.0, Re = 1000 based on plate length): (a) Mesh used (7623 nodes, 7448 elements), (b) Pressure distribution on the wall, (c) Pressure contours, (d) Mach contours

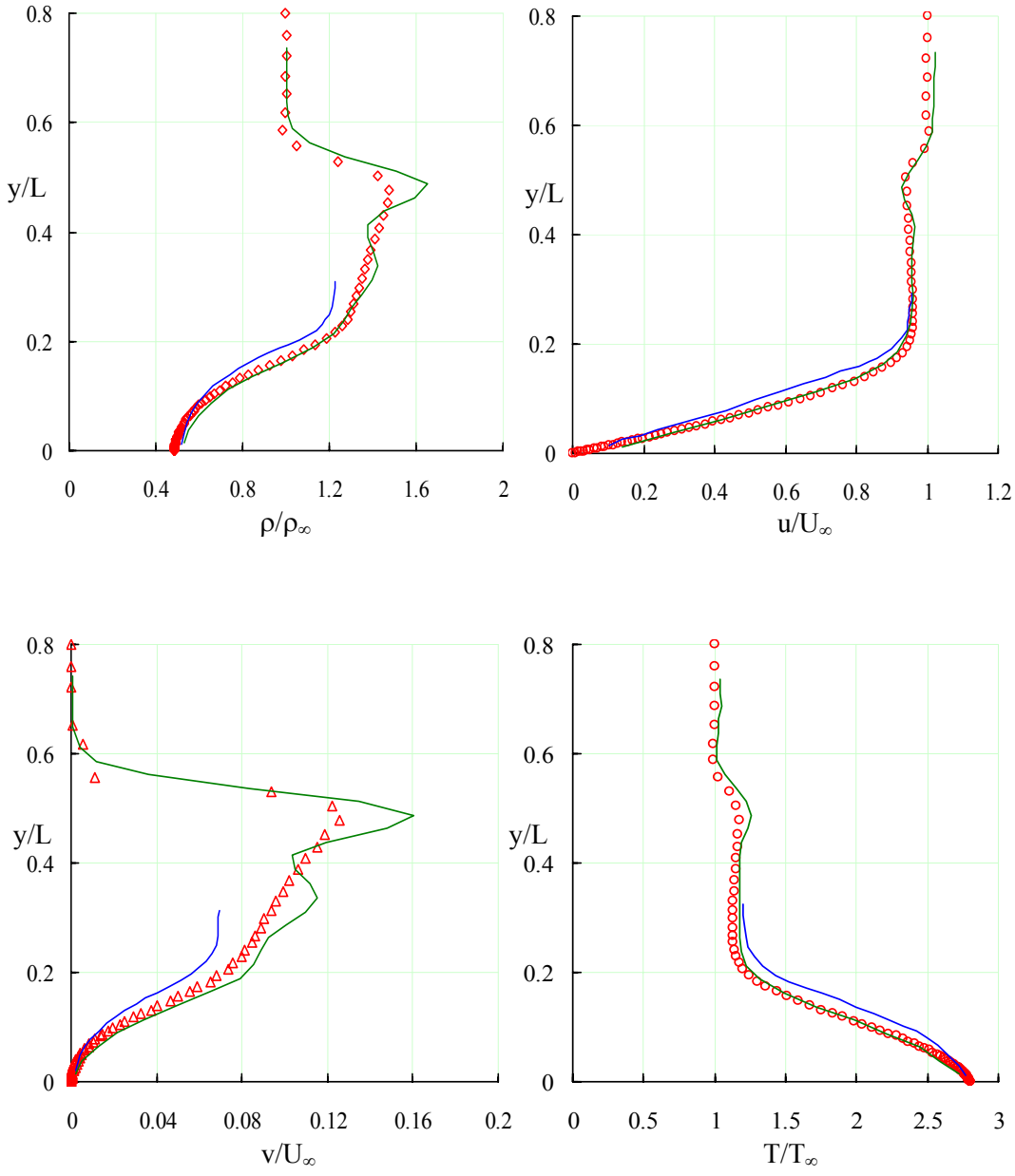

Fig. 6.3 Computed variables at the exit plane, results using LSGS method (— Similar solutions, — Carter [79], symbols LSGS method)

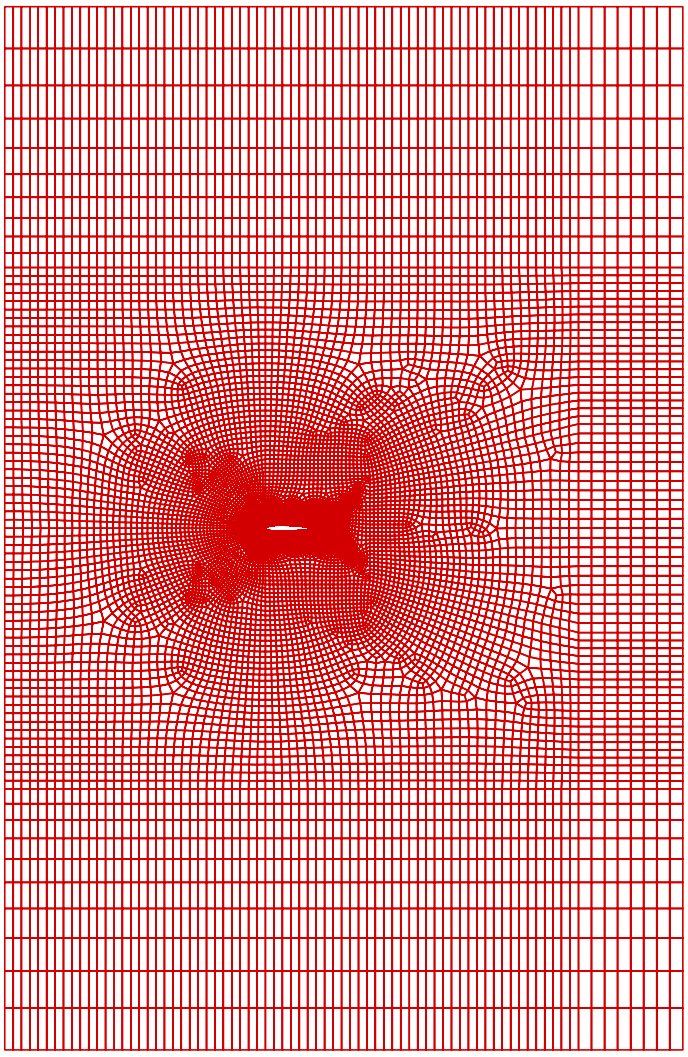

Fig 6.4 Mesh used for Flow over NACA0012 Airfoil
(57191 quadrilateral elements, 57799 nodes)

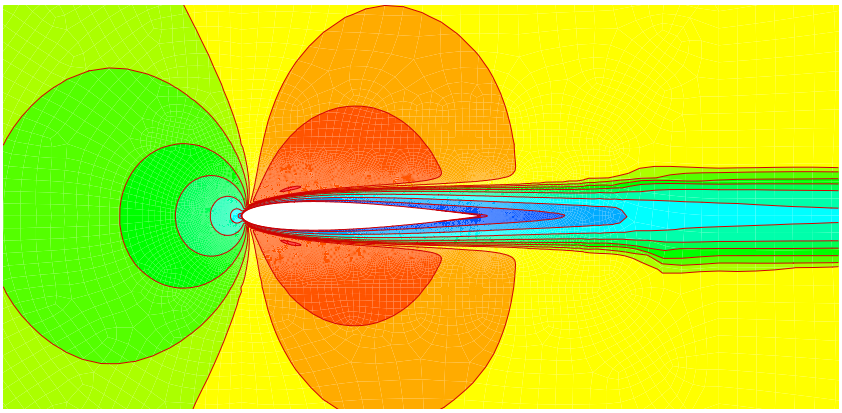

(a)

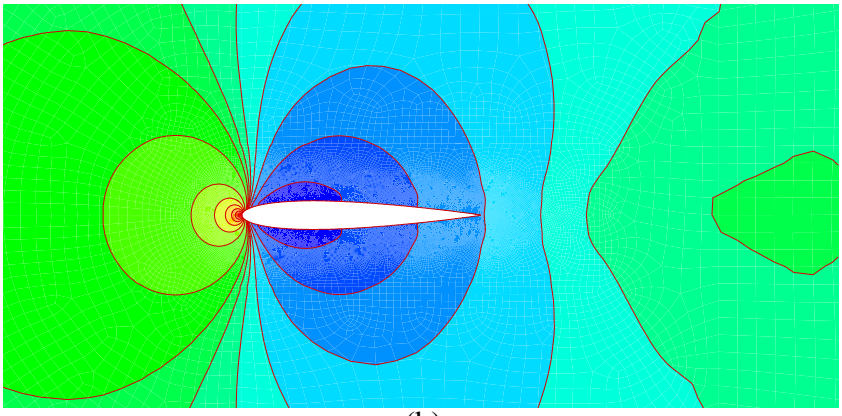

(b)

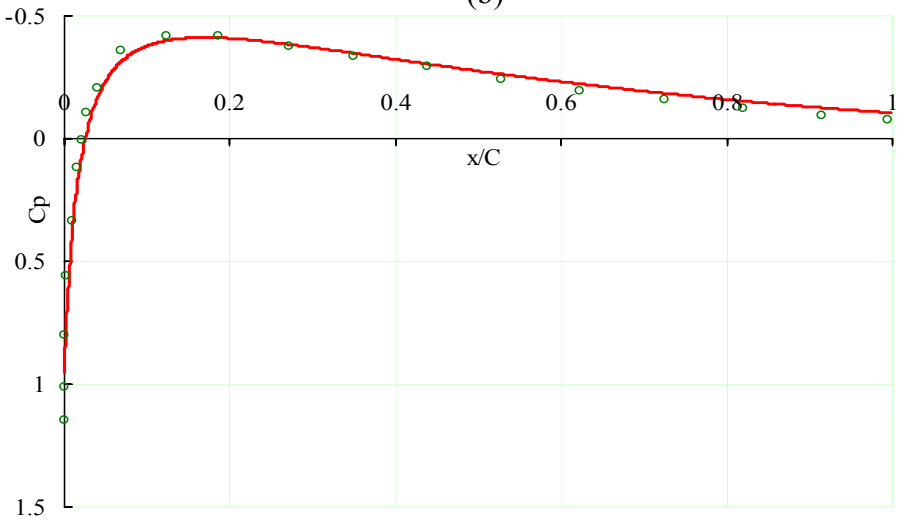

(c)

Fig 6.5 Result plots for subsonic flow over NACA0012 airfoil, (M_∞= 0.5, α = 0º and Re = 2000): (a) Mach number contours, (b) pressure contours, (c) Cp-distribution (— LSGS Method, O Mavriplis [90] at Re = 5000)

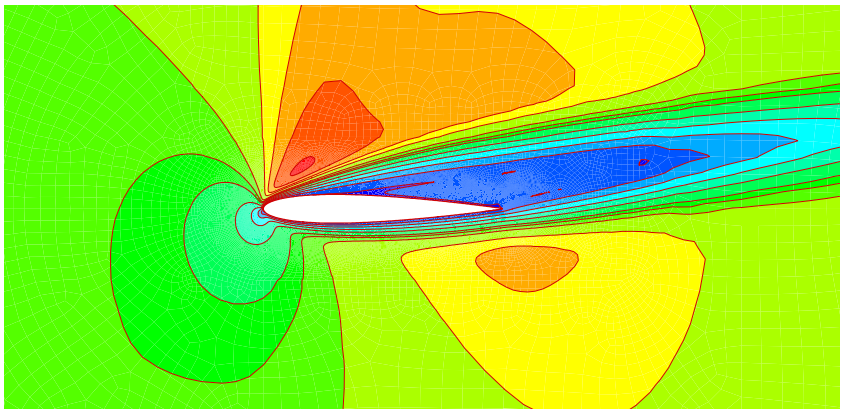

(a)

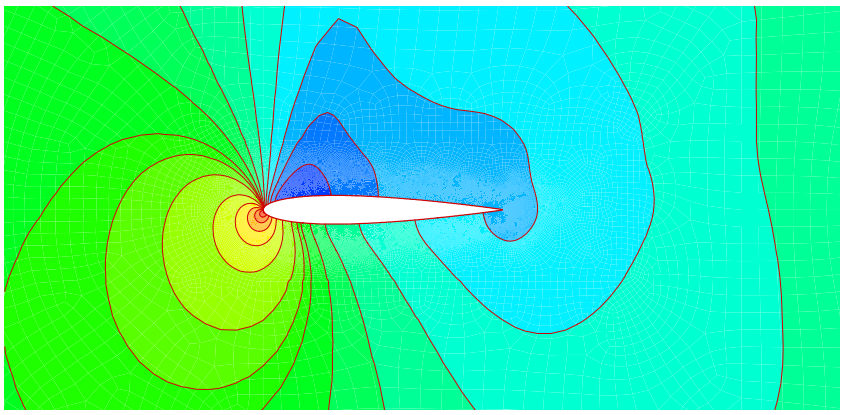

(b)

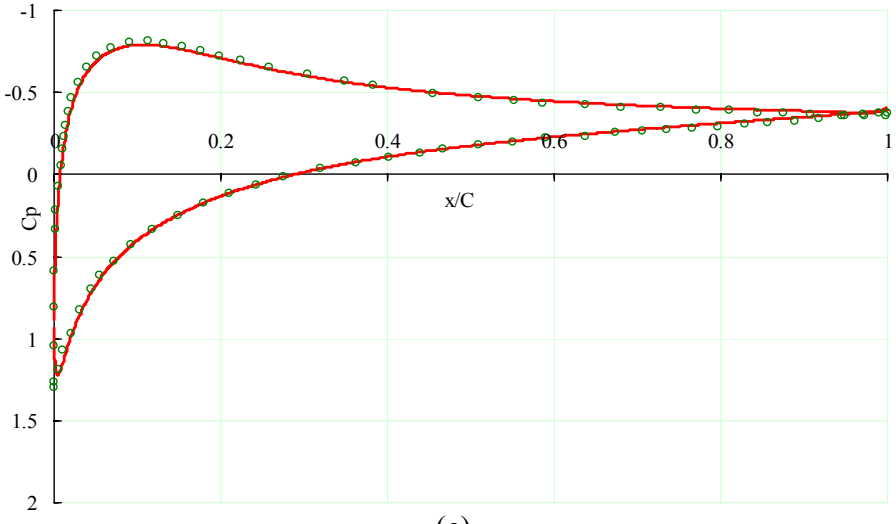

(c)

Fig 6.6 Result plots for subsonic flow over NACA0012 airfoil, (M_∞= 0.8, α = 10º and Re = 500): (a) Mach number contours, (b) pressure contours, (c) Cp-distribution (— LSGS Method, O Tang [91])

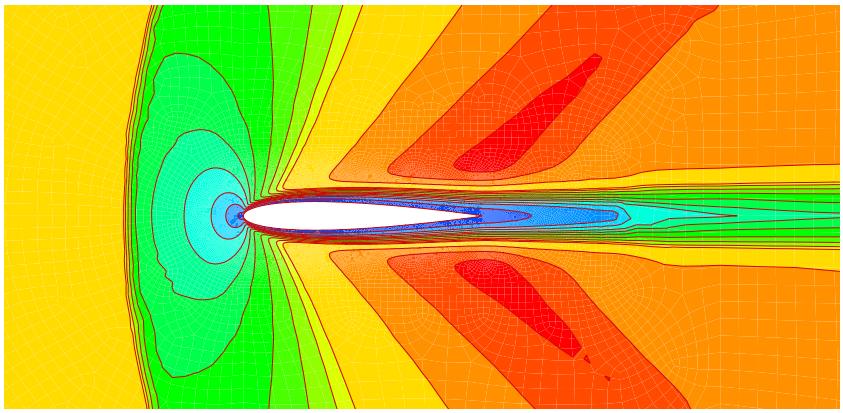

(a)

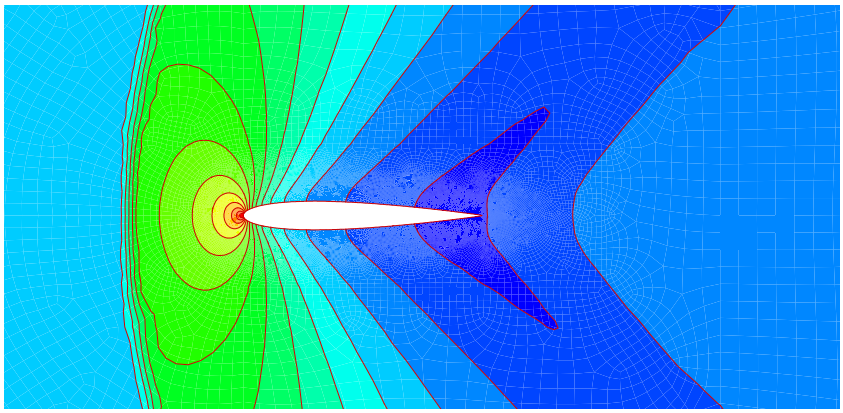

(b)

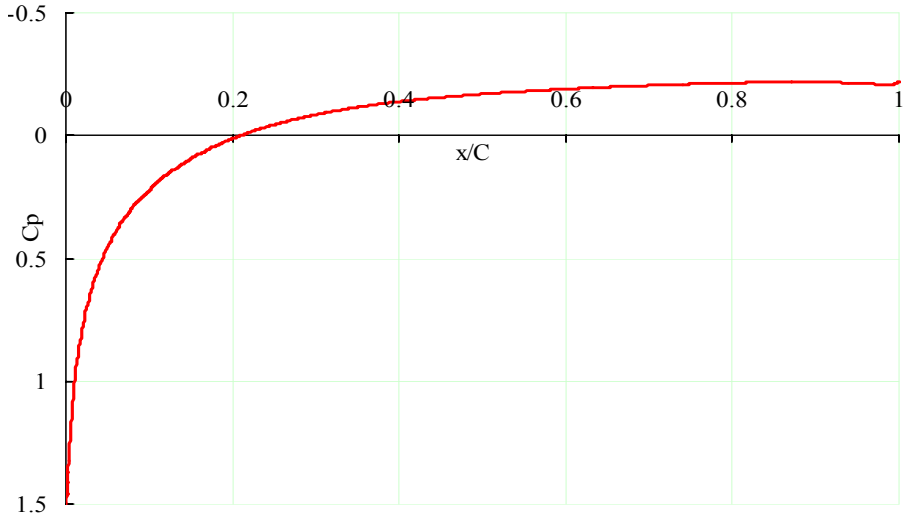

(c)

Fig 6.7 Result plots for subsonic flow over NACA0012 airfoil, (M_∞= 1.2, α = 0º and *Re* = 1000): (a) Mach number contours, (b) pressure contours, (c) *Cp*-distribution

CHAPTER 7

FUTURE AREAS OF RESEARCH

7.1 Introduction

This chapter contains discussion on a few among many possible areas in which work described in previous chapters can be extended. We have considered incompressible flow problems at low to moderate Reynolds numbers and Mach numbers ranging from subsonic to supersonic. LSGS Method can be applied to flow case of vanishingly small Reynolds number, where the viscous forces are much larger than the inertial forces. This interesting flow is called Stokes flow. The fact that there exists exact solution for the Stokes problem can be exploited to carry out convergence study for LSGSFEM.

Presence of significant temperature differences in the flow field makes the flow compressible even at negligible Mach number. The area of low speed compressible flows which is very important in heat transfer problems is a relatively neglected area in FEM. The LSGS method can be applied to simulate Natural convection flows where low Mach number approximation greatly simplifies the governing equations.

All the benchmark problems simulated in present thesis were laminar flow problems at low to moderate Reynolds numbers. As the Reynolds number increases above a critical value, flow becomes turbulent and we must use Governing equations

with turbulence terms. Majority of the flows of practical importance are turbulent flows. LSGS method can be developed for turbulent flows.

In the thesis the system of linear equations was solved using pre-conditioned conjugate gradient method. The number of inner iterations depends on the type of pre-conditioner used. We used diagonal pre-conditioner, which is the simplest and crude pre-conditioner. The performance of the method can be greatly enhanced by using more sophisticated and efficient pre-conditioner. In the following segments above mentioned works will be explained in more detail.

Majority of the practical problems are three-dimensional, therefore the next logical step would be to extend the LSGS method to 3D applications.

7.2 Few Possible Future Areas of Research

7.2.1 Application of LSGS Method to Stokes Flow

Flow of a fluid in the limit of vanishingly small *Re*, where the viscous forces are much larger than the inertial forces is called Stokes Flow. It assumes that the flow is low speed, so that the convective effects can be neglected. It is also known as '*Creeping Flow*'. It is a limiting case of Navier-Stokes flow and given as

$$\begin{aligned} &\frac{\partial u}{\partial x}+\frac{\partial v}{\partial y}=0 \\ &\frac{\partial u}{\partial t}+\frac{\partial p}{\partial x}-\frac{1}{Re}\nabla^2 u=0 \\ &\frac{\partial v}{\partial t}+\frac{\partial p}{\partial y}-\frac{1}{Re}\nabla^2 v=0 \end{aligned} \qquad (7.1)$$

The variables are non-dimensionalized and *Re* is the Reynolds number. Applying LSGS method to above equations gives following Euler-Lagrange form of equations

Continuity:

$$\left(\frac{\{N\}}{\Delta t}\frac{\partial\{N\}^T}{\partial x}\right)U^{n+1}+\left(\frac{\{N\}}{\Delta t}\frac{\partial\{N\}^T}{\partial y}\right)V^{n+1}+\left(\frac{\partial\{N\}}{\partial x}\frac{\partial\{N\}^T}{\partial x}+\frac{\partial\{N\}}{\partial y}\frac{\partial\{N\}^T}{\partial y}\right)P^{n+1}=0 \tag{7.2}$$

x-momentum:

$$\begin{aligned}&\left(\frac{\{N\}\{N\}^T}{\Delta t^2}+\frac{\partial\{N\}}{\partial x}\frac{\partial\{N\}^T}{\partial x}-\frac{1}{\Delta t}\frac{\partial\{N\}}{\partial x}\frac{\partial\{N\}^T}{\partial x}-\frac{1}{\Delta t}\frac{\partial\{N\}}{\partial y}\frac{\partial\{N\}^T}{\partial y}\right)U^{n+1}+\left(\frac{\partial\{N\}}{\partial x}\frac{\partial\{N\}^T}{\partial y}\right)V^{n+1}\\&+\left(\frac{\{N\}}{\Delta t}\frac{\partial\{N\}^T}{\partial x}\right)P^{n+1}=\left(\frac{\{N\}\{N\}^T}{\Delta t^2}\right)U^n\end{aligned} \tag{7.3}$$

y-momentum:

$$\begin{aligned}&\left(\frac{\partial\{N\}}{\partial y}\frac{\partial\{N\}^T}{\partial x}\right)U^{n+1}+\left(\frac{\{N\}\{N\}^T}{\Delta t^2}+\frac{\partial\{N\}}{\partial y}\frac{\partial\{N\}^T}{\partial y}-\frac{1}{\Delta t}\frac{\partial\{N\}}{\partial x}\frac{\partial\{N\}^T}{\partial x}-\frac{1}{\Delta t}\frac{\partial\{N\}}{\partial y}\frac{\partial\{N\}^T}{\partial y}\right)V^{n+1}\\&+\left(\frac{\{N\}}{\Delta t}\frac{\partial\{N\}^T}{\partial y}\right)P^{n+1}=\left(\frac{\{N\}\{N\}^T}{\Delta t^2}\right)V^n\end{aligned} \tag{7.4}$$

We have exact solution for the Stokes problem. One such exact solution is for polynomial divergence –free velocity-pressure field studied by Oden and Jacquotte [80]

$$\begin{aligned}u(x,y)&=x^2(1-x)^2\left(2y-6y^2+4y^3\right)\\v(x,y)&=y^2(1-y)^2\left(-2x+6x^2-4x^3\right)\\p(x,y)&=x^2-y^2\end{aligned} \tag{7.5}$$

Since we have exact solution for Stokes problem, This aspect can be exploited for convergence study of LSGS method.

7.2.2 Application of LSGS Method to Low Speed Compressible Flows

Natural convection flows, despite being low speed flows are compressible due to temperature and density variation. These buoyancy-driven flows, especially two-dimensional cases have been the subject of intense study over last few decades. It has

been extensively explored in finite differences and finite volume methods less so in finite element methods. Buoyancy-driven flow inside a square domain serves as model for many practically important real life applications. For example strong heat radiation inside chemical and nuclear reactors causes low speed compressible flows.

Many researchers have studied buoyancy-driven flows inside a square cavity with differentially heated vertical side walls. Studies by Davis [55], Chenoweth [56] are important in this regard. Other important works are those by Tang [61] and Yu [20] who used LSFEM to solve natural convection flow inside a square domain.

LSGS Method can be applied to solve natural convection flow inside a square domain using low Mach number approximation which greatly simplifies the governing equations. The governing equations for time-dependent two-dimensional compressible viscous flow with thermal convection can be written in non-dimensional form as:

$$
\begin{aligned}
&\frac{\partial \rho}{\partial t}+u\frac{\partial \rho}{\partial x}+v\frac{\partial \rho}{\partial y}+\rho\left(\frac{\partial u}{\partial x}+\frac{\partial v}{\partial y}\right)=0\\
&\rho\frac{\partial u}{\partial t}+\rho\left(u\frac{\partial u}{\partial x}+v\frac{\partial u}{\partial y}\right)+\frac{\partial p}{\partial x}=\frac{1}{Re}\left(\frac{\partial^2 u}{\partial x^2}+\frac{\partial^2 u}{\partial y^2}+\frac{1}{3}\frac{\partial}{\partial x}\left(\frac{\partial u}{\partial x}+\frac{\partial v}{\partial y}\right)\right)\\
&\rho\frac{\partial v}{\partial t}+\rho\left(u\frac{\partial v}{\partial x}+v\frac{\partial v}{\partial y}\right)+\frac{\partial p}{\partial y}=\frac{1}{Re}\left(\frac{\partial^2 v}{\partial x^2}+\frac{\partial^2 v}{\partial y^2}+\frac{1}{3}\frac{\partial}{\partial y}\left(\frac{\partial u}{\partial x}+\frac{\partial v}{\partial y}\right)\right)-\frac{1}{2\in Fr}\rho\\
&\rho\left(\frac{\partial T}{\partial t}+u\frac{\partial T}{\partial x}+v\frac{\partial T}{\partial y}\right)-(\gamma-1)M_\infty^2\left(u\frac{\partial p}{\partial x}+v\frac{\partial p}{\partial y}\right)=\frac{1}{RePr}\left(\frac{\partial^2 T}{\partial x^2}+\frac{\partial^2 T}{\partial y^2}\right)\\
&\qquad+\frac{2(\gamma-1)M_\infty^2}{Re}\left[\left(\frac{\partial u}{\partial x}\right)^2+\left(\frac{\partial v}{\partial y}\right)^2+\frac{1}{2}\left(\frac{\partial u}{\partial y}+\frac{\partial v}{\partial x}\right)^2\right]\\
&\qquad-\frac{2(\gamma-1)M_\infty^2}{3Re}\left(\frac{\partial u}{\partial x}+\frac{\partial v}{\partial y}\right)^2-\frac{(\gamma-1)M_\infty^2}{2\in Fr}\rho v
\end{aligned}
\tag{7.6}
$$

and the equation of state after considering pressure p as sum of mean background pressure $\overline{p}$ and small variation $\hat{p}$ i.e. $p=\overline{p}+\hat{p}$ such that $\overline{p} = \rho_\infty RT_\infty$, the background pressure can therefore be dropped from spatial derivatives. With this interpretation of pressure we get non-dimensional form of the equation of state as:

$$1+\gamma \hat{p} M_\infty^2 = \rho T \tag{7.7}$$

Appropriate boundary conditions have to be applied. . The symbol $\in$ is the temperature difference parameter given as $\in = \frac{\Delta T}{2T_\infty} = \frac{T_H - T_C}{T_H + T_C}$. This also means that reference temperature can be taken as the mean of temperatures at the two walls. The symbols M_∞, *Pr, Re* and *Fr* are the dimensionless numbers called Mach number, Prandtl number, Reynolds number and Froude number respectively. These are given as: $M_\infty = \frac{U_\infty}{\sqrt{\gamma RT_\infty}}, Pr = \frac{\nu}{\alpha}$, $Re = \sqrt{\frac{RaFr}{Pr}}$ and $Fr = \frac{U_\infty^2}{2 \in gL}$ respectively. Here *Ra*, Rayleigh number is another dimensionless number associated with the heat transfer within the fluid and assumes importance here due to buoyancy-driven convection. The Rayleigh number, given as $Ra = \frac{2 \in gL^3}{\nu\alpha}$ is the ratio of the buoyancy force to the viscous force in a medium. Thermal diffusivity, α and ratio of specific heats, γ are given as $\alpha = \frac{k}{\rho_\infty C_p}$ *and* $\gamma = \frac{C_p}{C_v}$ respectively. Now we apply low Mach number approximation. For very low speeds $M_\infty \approx 0$, therefore all the terms in the governing

equations (7.6) and (7.7) containing M_∞ can be dropped and the simplified governing equations become:

$$\begin{aligned}
&\frac{\partial \rho}{\partial t}+u\frac{\partial \rho}{\partial x}+v\frac{\partial \rho}{\partial y}+\rho\left(\frac{\partial u}{\partial x}+\frac{\partial v}{\partial y}\right)=0\\
&\rho\frac{\partial u}{\partial t}+\rho\left(u\frac{\partial u}{\partial x}+v\frac{\partial u}{\partial y}\right)+\frac{\partial p}{\partial x}=\frac{1}{Re}\left(\frac{\partial^2 u}{\partial x^2}+\frac{\partial^2 u}{\partial y^2}+\frac{1}{3}\frac{\partial}{\partial x}\left(\frac{\partial u}{\partial x}+\frac{\partial v}{\partial y}\right)\right)\\
&\rho\frac{\partial v}{\partial t}+\rho\left(u\frac{\partial v}{\partial x}+v\frac{\partial v}{\partial y}\right)+\frac{\partial p}{\partial y}=\frac{1}{Re}\left(\frac{\partial^2 v}{\partial x^2}+\frac{\partial^2 v}{\partial y^2}+\frac{1}{3}\frac{\partial}{\partial y}\left(\frac{\partial u}{\partial x}+\frac{\partial v}{\partial y}\right)\right)-\frac{\rho}{2\in Fr}\\
&\rho\left(\frac{\partial T}{\partial t}+u\frac{\partial T}{\partial x}+v\frac{\partial T}{\partial y}\right)=\frac{1}{Re\,Pr}\left(\frac{\partial^2 T}{\partial x^2}+\frac{\partial^2 T}{\partial y^2}\right)
\end{aligned} \tag{7.8}$$

with equation of state now taking form,

$$\rho=\frac{1}{T} \tag{7.9}$$

From equation (7.9), we have $\partial\rho=-\frac{1}{T^2}\partial T$, which along with equation (7.9) can be used to eliminate ρ from the governing equations and after some rearrangements we can write them in the final form as:

$$\begin{aligned}
&\frac{\partial u}{\partial x}+\frac{\partial v}{\partial y}=\left(\frac{\partial^2 T}{\partial x^2}+\frac{\partial^2 T}{\partial y^2}\right)\\
&\frac{\partial u}{\partial t}+\left(u\frac{\partial u}{\partial x}+v\frac{\partial u}{\partial y}\right)+T\frac{\partial p}{\partial x}=\frac{T}{Re}\left(\frac{\partial^2 u}{\partial x^2}+\frac{\partial^2 u}{\partial y^2}+\frac{1}{3}\frac{\partial}{\partial x}\left(\frac{\partial u}{\partial x}+\frac{\partial v}{\partial y}\right)\right)\\
&\frac{\partial v}{\partial t}+\left(u\frac{\partial v}{\partial x}+v\frac{\partial v}{\partial y}\right)+T\frac{\partial p}{\partial y}=\frac{T}{Re}\left(\frac{\partial^2 v}{\partial x^2}+\frac{\partial^2 v}{\partial y^2}+\frac{1}{3}\frac{\partial}{\partial y}\left(\frac{\partial u}{\partial x}+\frac{\partial v}{\partial y}\right)\right)-\frac{1}{2\in Fr}\\
&\frac{\partial T}{\partial t}+u\frac{\partial T}{\partial x}+v\frac{\partial T}{\partial y}=\frac{T}{Re\,Pr}\left(\frac{\partial^2 T}{\partial x^2}+\frac{\partial^2 T}{\partial y^2}\right)
\end{aligned} \tag{7.10}$$

LSGS method can easily be applied to above equations simplified using the low Mach-number approximation

7.2.3 Application of Turbulence Modeling on LSGS Method

A flow can be classified as laminar or turbulent. Below a critical Reynolds number (depending on the particular flow conditions and geometry), the flow is laminar and remains smooth and regular. At this critical value called '*critical Reynolds number*' flow enters a transition region in which the instabilities begin to appear. These instabilities cause turbulence as the Reynolds number increases further.

Turbulence has various important consequences such as increased skin friction, delay in flow separation, increased heat and mass transfer etc. In principle, turbulent solutions may be obtained from the unsteady Navier-Stokes equations. However, with the exception of few simple flows this would require a very fine grid and vast expenditure of computational resources. Instead, average values for the unknown variables are sought, by means of time (or Reynolds) averaged Navier-Stokes equations. These contain additional terms, which are modeled by further equations either algebraic of differential.

7.2.3.1 Reynolds Averaged Navier-Stokes Equations

We wish to obtain time-averaged values of unknowns, ignoring the fluctuations caused by turbulent effects. Hence we split the unknowns (e.g. u) into two parts

$$u = \overline{u} + u' \tag{7.11}$$

where $\overline{u}$ is either the time average

$$\overline{u}(t) = \frac{1}{\mathcal{T}} \int_{t-\frac{\mathcal{T}}{2}}^{t+\frac{\mathcal{T}}{2}} u(\mathcal{T}) d\mathcal{T} \tag{7.12}$$

for a suitable time-scale $\mathcal{T}$, or ensemble average

$$\bar{u}(t) = \lim_{N \to \infty} \frac{1}{N} \sum_{i=1}^{N} u^i(t) \tag{7.13}$$

which is obtained by repeating the transient process many times. Here $u^i(t)$ denotes the measured value of u at time t in the ith experiment. These two averaging techniques are generally equivalent for most of the turbulent flow cases. It follows that for the fluctuating term u',

$$\bar{u}' = 0 \tag{7.14}$$

This type of averaging is adequate for incompressible flows, but for compressible flows, the resulting averaged equations contain some complex terms which can be avoided by using Favre averaging, where the unknowns are weighted by the density. In this case

$$u = \tilde{u} + u'' \tag{7.15}$$

where $\tilde{u}$ is Favre average

$$\tilde{u}(t) = \frac{1}{\bar{\rho}\mathcal{T}} \int_{t-\frac{\mathcal{T}}{2}}^{t+\frac{\mathcal{T}}{2}} \rho(t) u(\tau) d\tau \tag{7.16}$$

or in ensemble form,

$$\tilde{u}(t) = \lim_{N \to \infty} \frac{1}{\bar{\rho} N} \sum_{i=1}^{N} \rho^i(t) u^i(t) \tag{7.17}$$

We may also write (from 7,16)

$$\tilde{u}(t) = \frac{\overline{\rho u}}{\bar{\rho}} \tag{7.18}$$

Using the conservative form of the Navier-Stokes equations, we wish to rewrite the equations in terms of the averaged quantities $\bar{\rho}, \tilde{u}, \tilde{v}, \tilde{e}, \tilde{T}$ and $\tilde{p}$. This is done by averaging the entire equation then simplifying. For example the continuity equation

becomes

$$\overline{\rho_{,t} + (\rho u_i)_i} = 0 \tag{7.19}$$

where "$,t$" and "$,i$" denotes partial differentiation by t and x_i respectively. Making use of (7.18) this can be written as

$$\overline{\rho}_{,t} + (\overline{\rho}\widetilde{u}_i)_{,i} = 0 \tag{7.20}$$

No new term is introduced in continuity equation, but this is not the case in other equations due to the presence of the non-linear terms. The Reynolds averaged momentum equations

$$\overline{(\rho u_i)_{,t} + (\rho u_i u_j + p\delta_{ij}) - \mu S_{ij}(\vec{V})_{,j}} = 0 \tag{7.21}$$

where μ is the molecular viscosity and $S_{ij}(\vec{V}) = u_{i,j} + u_{j,i} - \frac{2}{3}\delta_{ij}u_{k,k}$ after rearranging terms becomes

$$(\overline{\rho}\widetilde{u}_i)_{,t} + (\overline{\rho}\widetilde{u}_i\widetilde{u}_j + \overline{\rho}\widetilde{u}_i''\widetilde{u}_j'' + \overline{p}\delta_{ij})_{,j} - \mu S_{ij}(\widetilde{V})_{,j} = 0 \tag{7.22}$$

introducing the Reynolds stress tensor $\overline{\rho}\widetilde{u}_i''\widetilde{u}''$ which has to be modeled. Similarly Reynolds averaged energy equation may be written as

$$\begin{aligned}&(\overline{\rho}\widetilde{E})_{,t} + \left(\overline{\rho}\widetilde{u}_i\widetilde{E} + \overline{\rho}\widetilde{u}_i''\widetilde{E}_j'' + \overline{p}\widetilde{u}_i + \overline{pu_i''}\right)_{,i} \\ &- \mu\left(S_{ij}(\widetilde{V})\widetilde{u}_j + S_{ij}(\widetilde{V})\widetilde{u}_j'' + S_{ij}(\overline{V''})\widetilde{u}_j + \overline{S_{ij}(V'')\widetilde{u}_j''} + k\overline{T}_{,i}\right)_{,i} = 0\end{aligned} \tag{7.23}$$

This introduces more extra terms to be modeled. We are now faced with the well known closure problem - six equations and many more unknowns to be determined, including the four (in 2D) components of Reynolds stress tensor and the turbulent flux terms appearing in (7.23).

A common approach is to make the assumption about the Reynolds stress tensor that it may be described in the same way as molecular viscous effects (the eddy viscosity hypothesis [82]), so that

$$\overline{\rho}\widetilde{u}_i''\widetilde{u}_j'' = -\mu_T S_{ij}\left(\widetilde{V}\right) + \frac{2}{3}\overline{\rho}K\delta_{ij} \tag{7.24}$$

where μ_T is the eddy viscosity and the turbulent kinetic energy K is defined by

$$K = \frac{1}{2}\widetilde{u}_i''\widetilde{u}_i'' \tag{7.25}$$

Similarly the eddy diffusivity hypothesis assumes that the turbulent fluxes are proportional to the gradient of the mean values, so for example

$$\overline{\rho}\widetilde{u}_i''\widetilde{E}'' = \frac{\mu_T}{\mathrm{Pr}_T}\widetilde{E}_{,i} \tag{7.26}$$

With the help of above we can write momentum and energy equations as

$$\left(\overline{\rho}\widetilde{u}_i\right)_{,t} + \left(\overline{\rho}\widetilde{u}_i\widetilde{u}_j + \left(\overline{p} + \frac{2}{3}\overline{\rho}K\right)\delta_{ij}\right)_{,j} - \left(\mu + \mu_T\right)S_{ij}(\widetilde{V})_{,j} = 0 \tag{7.27}$$

and

$$\begin{aligned}&\left(\overline{\rho}\widetilde{E}\right)_{,t} + \left(\overline{\rho}\widetilde{u}_i\widetilde{E} + \left(\overline{p} + \frac{2}{3}\overline{\rho}K\right)u_i\right)_{,i} \\ &- \left(\left(\mu + \mu_T\right)\widetilde{u}_j S_{ij}(\widetilde{V}) + \left(k + k_T\right)\overline{T}_{,i} + \left(\mu + \frac{\mu_T}{\mathrm{Pr}_T}\right)K_{,i}\right)_{,i} = 0\end{aligned} \tag{7.28}$$

The turbulent Prandtl number Pr_T is a constant and the turbulent thermal conductivity is defined by

$$k_T = \gamma c_v \frac{\mu_T}{\mathrm{Pr}_T} \tag{7.29}$$

This set of equations (7.20), (7.27) and (7.28) now only require additional modeling of the turbulent kinetic energy K and the eddy viscosity μ_T. Turbulence models which approximate these values are categorized by the number of additional differential equations they consist of. The most common types are zero, one, two equation models, but all models contain several constants which need to be empirically determined, by measuring quantities experimentally involving simple turbulent flows.

7.2.3.2 Types of Turbulence Models

This section contains discussion of the models used to obtain the eddy viscosity μ_T and the turbulent kinetic energy K, which are then used in the Reynolds averaged Navier-Stokes equations.

7.2.3.2.1 Zero-Equation Models

Models in this category use only algebraic expressions to approximate the turbulent quantities. Typically the eddy viscosity is modeled as

$$\mu_T = \rho l_T u_T \tag{7.30}$$

where l_T is the turbulent length scale and u_T is the turbulent velocity scale, which are obtained from local mean flow quantities. It is common to rewrite the Reynolds-Averaged Navier-Stokes equations so that the term $\frac{2}{3}\bar{\rho}K$ appearing in (7.26) and (7.27) is absorbed into the definition of pressure and the diffusive term involving K is no longer present.

This type of model is more suited for flow near the wall, where diffusive effects dominate, since transport effects are ignored. One early model is that of Cebeci and

Smith [82], which splits the boundary layer into two regions, and defines the eddy viscosity for each region separately. One disadvantage of this model is the need to locate the boundary layer in order to determine the length scale in the outer region. The Baldwin-Lomax model [83] avoids this need, instead using the distribution of the vorticity to obtain the length scale.

For high Re flows which remain attached to the wall, these models produce good results, but can not accurately predict highly separated flows and turbulence in the wake. Since they are essentially algebraic models, they are computationally inexpensive, but require turbulent length and velocity scales. This requires the knowledge of the distance of each point from the wall surface (y) which is easily available when using structured mesh, but not when the mesh is unstructured. Mavripilis [84] introduced a method for using Baldwin-Lomax model with unstructured meshes by generating lines normal to the wall and interpolating solution values from the unstructured mesh points onto the normal mesh lines in order to obtain the necessary length scales.

7.2.3.2.2 One-Equation Models

One-equation models, like algebraic models, make the approximation of (7.30) but in this case the turbulent velocity scale is usually defined to be

$$u_T = \sqrt{K} \tag{7.31}$$

where the turbulent kinetic energy K is found from a transport equation. It is common to introduce the turbulence dissipation rate ε to indirectly represent l_T, via the following equation

$$l_T = C\frac{K^{\frac{3}{2}}}{\varepsilon} \tag{7.32}$$

for some constant C. The one-equation model of Wolfshtein [85] consists of a p.d.e. with K as unknown, with the length scale being determined in terms of *y*, the distance from the wall. Jansen et al [86] used the Norris-Reynolds model within the context of Galerkin least-squares finite element method.

All the models mention so far approximate the length scale in terms of *y*, hence are less suitable for unstructured mesh. In general, one equation models can cope with a wider range of flows than the algebraic models, although at extra expense, and some models like Baldwin-Barth model [87] have the ability to be used on unstructured meshes with relative ease.

7.2.3.2.3 Two-Equation Models

Two-equation models eliminate the need to find the velocity and the length scales and instead rely on two transport equations to obtain values from which μ_T may be found. The most common model is *K*-*ε* model where the two equations involve K and ε, the rate of dissipation of turbulent kinetic energy. The eddy viscosity is then determined from

$$\mu_T = \rho C\frac{K^2}{\varepsilon} \tag{7.33}$$

The standard *K*-*ε* model is generally applicable in regions of fully developed turbulence, but not near wall boundaries. There are two ways of overcoming this. A low Reynolds number model incorporates extra terms into the *ε* equation, and redefines the eddy viscosity near walls. This approach requires particularly fine grid near the wall. The

second idea is to either employ a separate simplified model or impose logarithmic wall laws near the wall (a high Re model).

K-ε model by Jones and Launder [88] is one of the well known two-equation models. It can either be used as a low *Re*-model or can be simplified and used as high *Re*-model.

The advantages of two-equation models such as *K*-ε model are that they are applicable to a wide range of flows, and have been in use for over twenty years, so that their uses and limitations are well understood. However they are more difficult to implement than zero and one-equation models. Because they don't require length scales to be determined algebraically from wall distances, *K*-ε models can be used on unstructured grids.

7.2.4 Extension of LSGSFEM to 3D Applications

Only 2-d problems have been considered, but majorities of the practical problems are 3-d problems. Extension of LSGS method to 3-d should not be difficult although it would be a little complex.

The Navier-Stokes equations in 3-d are very similar to the 2-d version, with an additional momentum equation. The Various terms in the equation now have an addition term coming due to the third dimension. For example, the energy dissipation term in equation (6.4) in chapter 6 now becomes

$$F(\nabla V)=\frac{4}{3}\left[\left(\frac{\partial u}{\partial x}\right)^2+\left(\frac{\partial v}{\partial y}\right)^2+\left(\frac{\partial w}{\partial z}\right)^2-\frac{\partial u}{\partial x}\frac{\partial v}{\partial y}-\frac{\partial u}{\partial x}\frac{\partial w}{\partial z}-\frac{\partial v}{\partial y}\frac{\partial w}{\partial z}\right] + \left(\frac{\partial u}{\partial y}+\frac{\partial v}{\partial x}\right)^2+\left(\frac{\partial v}{\partial z}+\frac{\partial w}{\partial y}\right)^2+\left(\frac{\partial w}{\partial x}+\frac{\partial u}{\partial z}\right)^2 \tag{7.34}$$

where $V = (u, v, w)^T$ now.

In 2-d, we use triangles and quadrilaterals to form unstructured meshes, in 3-d it is going to be the tetrahedral and hexahedral elements. In 2-d we used Gaussian integration over the element-area, in 3-d it has to be carried out over the volume of the element. The assembly of the global stiffness matrix and the load vector remains the same.

So in principle, application to 3-d remains relatively simple, although the process would be far more expensive as we would be dealing with huge number of nodes. Parallel computation would be a required for 3-d applications.

7.2.5 Incorporation of a More Sophisticated Pre-Conditioner

The Pre-conditioned Conjugate Gradient solver was used with diagonal pre-conditioner. Diagonal pre-conditioner is the simplest and crudest of pre-conditioners. The performance of the method and convergence greatly depends on the pre-conditioner used. With more sophisticated pre-conditioner like block pre-conditioner would greatly enhance the performance of the method.

CHAPTER 8

SUMMARY

In this thesis we presented a novel yet simple finite element method for incompressible and compressible Navier-Stokes equations. This method treats the first order terms in the governing equations the least-squares way and the second order derivative terms the Galerkin way by exploiting the benefits of integration by parts. The way it is formulated, it tends to combine the positives of both the least-squares method and Galerkin method and get rid of the negative aspects of them. The method is unconditionally stable for fully implicit and semi-implicit formulation. The stability analysis of the method has been done on the split time formulation, the precursor of LSGSFEM. This was possible because both the formulations give the same element stiffness matrices except for one term which has division by 2 which does not affect the stability characteristics.

When the unsteady form of the governing equations is used, a streamline upwinding term is introduced naturally by the least-squares method. The method is stable for convection-dominated flows and allows for equal-order basis functions for both pressure and velocity. In addition, the resulting system of equations **is always symmetric** and is solved using the conjugate gradient method with sparse matrix storage and standard pre-conditioners. Non-linear terms are treated effectively by

linearization in time. The stability and accuracy of the method have been demonstrated with preliminary results of few benchmark convection-diffusion and incompressible flow problems solved using low-order C^0 continuous elements [28, 29]

The method has been amply validated for both incompressible and compressible flow regimes. In incompressible flow regime both steady as well as transient problems have been simulated and results compare very well with the published results. Apart from that method has been successfully applied to simulate the complex natural convection flow with Boussinesq approximation.

But few aspects need to be improved. Firstly, we have used a very simple and crude pre-conditioner. A more sophisticated pre-conditioner like block pre-conditioner would greatly enhance the convergence characteristics. So far we have applied LSGSFEM to two-dimensional problems at low to moderate Reynolds numbers. Most of the practical problems are three-dimensional and at high Reynolds numbers. Therefore the next logical direction for the method would be to incorporate turbulence modeling and application to 3D problems.

APPENDIX A

STABILITY ANALYSIS OF LSGS METHOD

Let us first consider the diffusion equation

$$\frac{T^{n+\frac{1}{2}}-T^{n}}{\Delta t}-k\nabla^{2}T=0 \tag{1}$$

After θ discretization and subsequent resolution of second order term, we can write

$$\frac{\mathrm{T}^{n+\frac{1}{2}}-\mathrm{T}^{n}}{\Delta \mathrm{t}}-\mathrm{k}\theta\frac{\partial^{2}\mathrm{T}^{n+\frac{1}{2}}}{\partial \mathrm{x}^{2}}-\mathrm{k}(1-\theta)\frac{\partial^{2}\mathrm{T}^{n+\frac{1}{2}}}{\partial \mathrm{x}^{2}}=0$$

$$\mathrm{T}^{n+\frac{1}{2}}-\mathrm{T}^{n}-\mathrm{k}\theta\Delta \mathrm{t}\frac{(\mathrm{T}_{i+1}^{n+\frac{1}{2}}-2\mathrm{T}_{i}^{n+\frac{1}{2}}+\mathrm{T}_{i-1}^{n+\frac{1}{2}})}{\Delta \mathrm{x}^{2}}-\mathrm{k}(1-\theta)\Delta \mathrm{t}\frac{(\mathrm{T}_{i+1}^{n}-2\mathrm{T}_{i}^{n}+\mathrm{T}_{i-1}^{n})}{\Delta \mathrm{x}^{2}}=0$$

$$(\mathrm{T}^{n+\frac{1}{2}}-\mathrm{T}^{n})-\theta \mathrm{d}\,\delta^{2}\mathrm{T}^{n+\frac{1}{2}}-(1-\theta)\mathrm{d}\,\delta^{2}\mathrm{T}^{n}=0 \tag{2}$$

where d is the diffusion number given as $\frac{\mathrm{k}\Delta \mathrm{t}}{\Delta \mathrm{x}^{2}}$, and $\delta^{2}\mathrm{T}=\mathrm{T}_{i+1}-2\mathrm{T}_{i}+\mathrm{T}_{i-1}$. Using table 3.1 of reference [35], equation (2) can be written as

$$(1+4\theta \mathrm{d}\sin^{2}\xi/2)\mathrm{T}^{n+\frac{1}{2}}=(1+4(1-\theta)\mathrm{d}\sin^{2}\xi/2)\mathrm{T}^{n} \tag{3}$$

Amplification factor is given as

$$\mathrm{G}_{1}=\frac{\mathrm{T}^{n+\frac{1}{2}}}{\mathrm{T}^{n}}=\frac{1+4(1-\theta)\mathrm{d}\sin^{2}\xi/2}{1+4\theta \mathrm{d}\sin^{2}\xi/2} \tag{4}$$

Similarly for the convection equation we have, for a linear case:

$$\frac{T^{n+1}-T^{n+\frac{1}{2}}}{\Delta t}+a\nabla T=0 \tag{5}$$

θ-discretization and subsequent treatment lead to

$$\frac{\mathrm{T}^{n+1}-\mathrm{T}^{n+\frac{1}{2}}}{\Delta \mathrm{t}}+\mathrm{a}\theta\frac{\partial \mathrm{T}^{n+1}}{\partial \mathrm{x}}+\mathrm{a}(1-\theta)\frac{\partial \mathrm{T}^{n+\frac{1}{2}}}{\partial \mathrm{x}}=0$$

$$\mathrm{T}^{n+1}-\mathrm{T}^{n+\frac{1}{2}}+\mathrm{a}\theta\Delta \mathrm{t}\frac{(\mathrm{T}_{i}^{n+1}+\mathrm{T}_{i-1}^{n+1})}{\Delta \mathrm{x}}+\mathrm{a}(1-\theta)\Delta \mathrm{t}\frac{(\mathrm{T}_{i}^{n+\frac{1}{2}}+\mathrm{T}_{i-1}^{n+\frac{1}{2}})}{\Delta \mathrm{x}}=0$$

$$(T^{n+1}-T^{n+\frac{1}{2}})+\frac{\theta C}{2}(\delta T^{n+1}-\delta^2 T^{n+1})+\frac{(1-\theta)C}{2}(\delta T^{n+\frac{1}{2}}-\delta^2 T^{n+\frac{1}{2}})=0 \tag{6}$$

Where C is CFL number given by $C=\frac{a\,\Delta t}{\Delta x}$ and

$$\delta^2 T=T_{i+1}-2T_i+T_{i-1},\ \delta T=T_{i+1}-T_{i-1}\ ,\ T_i-T_{i-1}=\frac{1}{2}(\delta T-\delta^2 T) \tag{7}$$

Again with the help of Table 3.1, ref [35] equation (6) can be written as

$$(1+i\theta C\sin\xi+2\theta C\sin^2\xi/2)\,T^{n+1}=(1-i(1-\theta)C\sin\xi-2(1-\theta)C\sin^2\xi/2)\,T^{n+\frac{1}{2}}$$

where ξ is the dimensionless wave number and the amplification factor is given as

$$G_2=\frac{T^{n+1}}{T^{n+\frac{1}{2}}}=\frac{1-i(1-\theta)C\sin\xi-2(1-\theta)C\sin^2\xi/2}{1+i\theta C\sin\xi+2\theta C\sin^2\xi/2} \tag{8}$$

The overall amplification factor

$$G=G_1\cdot G_2=\frac{1+4(1-\theta)d\sin^2\xi/2}{1+4\theta d\sin^2\xi/2}\cdot\frac{1-i(1-\theta)C\sin\xi-2(1-\theta)C\sin^2\xi/2}{1+i\theta C\sin\xi+2\theta C\sin^2\xi/2} \tag{9}$$

For Euler backward Scheme, $\theta = 1$, So

$$G=\frac{1}{1+4d\sin^2\xi/2}\cdot\frac{1}{1+iC\sin\xi+2C\sin^2\xi/2},\quad \text{For stability } |G|\le 1$$

$$\Rightarrow\left|\frac{1}{1+4d\sin^2\xi/2}\cdot\frac{1}{1+iC\sin\xi+2C\sin^2\xi/2}\right|\le 1$$

as $\frac{1}{1+4d\sin^2\xi/2}\le 1$ therefore $|G|\le 1\ \Rightarrow\left|\frac{1}{1+iC\sin\xi+2C\sin^2\xi/2}\right|\le 1$

$$\begin{aligned}&\Rightarrow\ 1+2C\sin^2\xi/2+iC\sin\xi\ge 1\\ &\quad(1+2C\sin^2\xi/2)^2+(C\sin\xi)^2\ \ge 1\end{aligned} \tag{10}$$

which after simplification the stability condition becomes

$$C\left(\sin^2 \xi/2+\cos^2 \xi/2\right) \geq 0 \tag{11}$$

Which is always true, Therefore backward Euler scheme is unconditionally stable.

Similarly, for θ = 1/2, the Crank-Nicolson scheme, equation (9) becomes

$$G = \frac{1-C\sin \xi/2\left(\sin \xi/2+i\cos \xi/2\right)}{1+C\sin \xi/2\left(\sin \xi/2+i\cos \xi/2\right)}$$

For stability $|G| \leq 1$

$$\Rightarrow \left|\frac{1-C\sin \xi/2\left(\sin \xi/2+i\cos \xi/2\right)}{1+C\sin \xi/2\left(\sin \xi/2+i\cos \xi/2\right)}\right| \leq 1$$

Therefore the stability condition is

$$\left|1-C\sin \xi/2\left(\sin \xi/2+i\cos \xi/2\right)\right| \leq \left|1+C\sin \xi/2\left(\sin \xi/2+i\cos \xi/2\right)\right| \tag{12}$$

Which is always true, therefore Crank-Nicolson scheme is also unconditionally stable.

APPENDIX B

SYSTEM MATRIX EQUATIONS FOR LSGS METHOD APPLIED TO INCOMPRESSIBLE FLOWS

The Governing equations for two-dimensional incompressible laminar flow is given by

$$\begin{aligned}
&\frac{\partial u}{\partial x}+\frac{\partial v}{\partial y}=0\\
&\frac{\partial u}{\partial t}+\vec{V}\cdot\nabla u+\frac{\partial p}{\partial x}-\frac{1}{Re}\nabla^2 u=0\\
&\frac{\partial v}{\partial t}+\vec{V}\cdot\nabla v+\frac{\partial p}{\partial y}-\frac{1}{Re}\nabla^2 v=0
\end{aligned} \tag{B1}$$

From chapter 4, after discretizing spatial derivative using θ-method and the unsteady terms using Euler backward differences we write the weak form of the system as

$$\int_\Omega (\mathscr{S}N)^T(\mathscr{L}U^{n+1}-f)d\Omega=0 \tag{B2}$$

Where L and $\mathscr{S}$ are the governing equation operator and weighting operator respectively given by

$$\mathscr{L}=\begin{bmatrix}
\dfrac{\partial}{\partial x} & \dfrac{\partial}{\partial y} & 0\\
I+\theta\Delta t\vec{V}^n\cdot\nabla-\dfrac{\theta\Delta t}{Re}\nabla^2 & 0 & \theta\Delta t\dfrac{\partial}{\partial x}\\
0 & I+\theta\Delta t\vec{V}^n\cdot\nabla-\dfrac{\theta\Delta t}{Re}\nabla^2 & \theta\Delta t\dfrac{\partial}{\partial y}
\end{bmatrix} \tag{B3}$$

and $\mathscr{S}$ which is obtained from taking first order terms of governing equations i.e. Euler equation part given by

$$\mathscr{S}=\begin{bmatrix}
\dfrac{\partial}{\partial x} & \dfrac{\partial}{\partial y} & 0\\
I+\theta\Delta t\vec{V}^n\cdot\nabla & 0 & \theta\Delta t\dfrac{\partial}{\partial x}\\
0 & I+\theta\Delta t\vec{V}^n\cdot\nabla & \theta\Delta t\dfrac{\partial}{\partial y}
\end{bmatrix} \tag{B4}$$

Introducing the finite element approximation

$$U^{n+1} \approx U_h^{n+1} = \sum_i^m N_i U_i^{n+1} \tag{B5}$$

Where m is the number of nodes per element and N_i is the element shape function associated with i^{th} node. Substituting the approximation into the weak formulation in (B2) leads to linear algebraic equations

$$[K]\{U^{n+1}\} = \{F\} \tag{B6}$$

Global stiffness matrix $[K]$ and the vector $\{F\}$ result from assembling the element stiffness matrices and vectors respectively given by

$$ke = \int_{\Omega_e} (\mathscr{S} N_i)^T (\mathscr{L} N_j)\, d\Omega; \qquad fe = \int_{\Omega_e} (\mathscr{S} N_i)^T f\, d\Omega.$$

The element stiffness matrix ke is given as

$$[ke] = \begin{bmatrix} k_{11} & k_{12} & k_{13} \\ k_{21} & k_{22} & k_{23} \\ k_{31} & k_{32} & k_{33} \end{bmatrix}$$

where each k_{ij} is a 3×3 matrix with i = 1, . 3 and j = 1, . 3. These are given as

$$k_{11} = [M] + \theta\Delta t\left([C] + [C]^T\right) + [K_x] + \theta^2 \Delta t^2 [K_{UP}] + \frac{\theta\Delta t}{Re}[K_D] \tag{B7}$$

$$k_{12} = [K_{xy}] \tag{B8}$$

$$k_{13} = \theta\Delta t[M_x] + \theta^2 \Delta t^2 [C_x]^T \tag{B9}$$

$$k_{21} = [K_{xy}]^T \tag{B10}$$

$$k_{22} = [M] + \theta\Delta t\left([C] + [C]^T\right) + [K_y] + \theta^2 \Delta t^2 [K_{UP}] + \frac{\theta\Delta t}{Re}[K_D] \tag{B11}$$

$$k_{23} = \theta\Delta t[M_y] + \theta^2 \Delta t^2 [C_y]^T \tag{B12}$$

$$k_{31} = \theta\Delta t[M_x]^T + \theta^2 \Delta t^2 [C_x] \tag{B13}$$

$$k_{32} = \theta \Delta t \left[M_y \right]^T + \theta^2 \Delta t^2 \left[C_y \right] \tag{B14}$$

$$k_{33} = \theta^2 \Delta t^2 \left[K_D \right] \tag{B15}$$

where:

$$\begin{aligned}
\left[M \right] &= \int_\Omega \{N\}\{N\}^T \, d\Omega, \\
\left[C \right] &= \int_\Omega \{N\}\left\{ (\vec{V} \cdot \nabla) N \right\}^T \, d\Omega, \\
\left[K_D \right] &= \int_\Omega \{\nabla N\}\{\nabla N\}^T \, d\Omega, \\
\left[K_{UP} \right] &= \int_\Omega \left\{ (\vec{V} \cdot \nabla) N \right\}\left\{ (\vec{V} \cdot \nabla) N \right\}^T \, d\Omega, \\
\left[M_x \right] &= \int_\Omega \{N\}\left\{ \frac{\partial N}{\partial x} \right\}^T \, d\Omega, \\
\left[M_y \right] &= \int_\Omega \{N\}\left\{ \frac{\partial N}{\partial y} \right\}^T \, d\Omega \\
\left[C_x \right] &= \int_\Omega \left\{ \frac{\partial N}{\partial x} \right\}\left\{ (\vec{V} \cdot \nabla) N \right\}^T \, d\Omega \\
\left[C_y \right] &= \int_\Omega \left\{ \frac{\partial N}{\partial y} \right\}\left\{ (\vec{V} \cdot \nabla) N \right\}^T \, d\Omega \\
\left[K_x \right] &= \int_\Omega \left\{ \frac{\partial N}{\partial x} \right\}\left\{ \frac{\partial N}{\partial x} \right\}^T \, d\Omega \\
\left[K_y \right] &= \int_\Omega \left\{ \frac{\partial N}{\partial y} \right\}\left\{ \frac{\partial N}{\partial y} \right\}^T \, d\Omega \\
\left[K_{xy} \right] &= \int_\Omega \left\{ \frac{\partial N}{\partial x} \right\}\left\{ \frac{\partial N}{\partial y} \right\}^T \, d\Omega
\end{aligned} \tag{B16}$$

APPENDIX C

SYSTEM MATRIX EQUATIONS FOR LSGS METHOD APPLIED TO INCOMPRESSIBLE FLOWS WITH BOUSSINESQ-APPROX.

The Governing equations for two-dimensional buoyancy-driven incompressible laminar flow in non-dimensional form is given by

$$\begin{aligned}
&\frac{\partial u}{\partial x}+\frac{\partial v}{\partial y}=0\\
&\frac{\partial u}{\partial t}+u\frac{\partial u}{\partial x}+v\frac{\partial u}{\partial y}=-\frac{\partial p}{\partial x}+Pr\left(\frac{\partial^2 u}{\partial x^2}+\frac{\partial^2 u}{\partial y^2}\right)\\
&\frac{\partial v}{\partial t}+u\frac{\partial v}{\partial x}+v\frac{\partial v}{\partial y}=-\frac{\partial p}{\partial y}+Pr\left(\frac{\partial^2 v}{\partial x^2}+\frac{\partial^2 v}{\partial y^2}\right)+RaPrT\\
&\frac{\partial T}{\partial t}+u\frac{\partial T}{\partial x}+v\frac{\partial T}{\partial y}=\left(\frac{\partial^2 T}{\partial x^2}+\frac{\partial^2 T}{\partial y^2}\right)
\end{aligned} \tag{C1}$$

with boundary conditions described in chapter 5. After discretizing unsteady terms and spatial derivative terms using Euler backward method the weak form of the system is

$$\int_\Omega (\mathscr{S}N)^T(\mathscr{L}U^{n+1}-f)d\Omega=0 \tag{C2}$$

Where L and $\mathscr{S}$ are the governing equation operator and weighting operator respectively given by

$$\mathscr{L}=\begin{bmatrix}
\frac{\partial}{\partial x} & \frac{\partial}{\partial y} & 0 & 0\\
I+\Delta t\vec{V}^n\cdot\nabla-\Delta t\,Pr\nabla^2 & 0 & \Delta t\frac{\partial}{\partial x} & 0\\
0 & I+\Delta t\vec{V}^n\cdot\nabla-\Delta t\,Pr\nabla^2 & \Delta t\frac{\partial}{\partial y} & 0\\
0 & 0 & 0 & I+\Delta t\vec{V}^n\cdot\nabla-\Delta t\nabla^2
\end{bmatrix} \tag{C3}$$

and

$$\mathscr{S}=\begin{bmatrix}
\frac{\partial}{\partial x} & \frac{\partial}{\partial y} & 0 & 0\\
I+\Delta t\vec{V}^n\cdot\nabla & 0 & \Delta t\frac{\partial}{\partial x} & 0\\
0 & I+\Delta t\vec{V}^n\cdot\nabla & \Delta t\frac{\partial}{\partial y} & 0\\
0 & 0 & 0 & I+\Delta t\vec{V}^n\cdot\nabla
\end{bmatrix} \tag{C4}$$

The weighting operator $\mathscr{S}$ is obtained by taking first order terms of governing equations and f in (C2) is the right hand side vector given by

$$f = \begin{Bmatrix} 0 \\ u^n \\ v^n + \Delta t Ra \Pr T^n \\ T^n \end{Bmatrix} \tag{C5}$$

Introducing the finite element approximation

$$U^{n+1} \approx U_h^{n+1} = \sum_i^m N_i U_i^{n+1} \tag{C6}$$

Where m is the number of nodes per element and N_i is the element shape function associated with i^{th} node. Substituting the approximation into the weak formulation in (C2) leads to linear algebraic equations

$$[K]\{U^{n+1}\} = \{F\} \tag{C7}$$

Global stiffness matrix $[K]$ and the vector $\{F\}$ result from assembling the element stiffness matrices and vectors respectively given by

$$ke = \int_{\Omega_e} (\mathscr{S} N_i)^T (\mathscr{S} N_j)\, d\Omega; \qquad fe = \int_{\Omega_e} (\mathscr{S} N_i)^T f\, d\Omega. \tag{C8}$$

The element stiffness matrix ke is given as

$$[ke] = \begin{bmatrix} k_{11} & k_{12} & k_{13} & k_{14} \\ k_{21} & k_{22} & k_{23} & k_{24} \\ k_{31} & k_{32} & k_{33} & k_{34} \\ k_{41} & k_{42} & k_{43} & k_{44} \end{bmatrix} \tag{C9}$$

where each k_{ij} is a 4×4 matrix with i = 1, . 4 and j = 1, . 4. These are given as

$$k_{11} = [M] + \Delta t\left([C] + [C]^T\right) + [K_x] + \Delta t Pr [K_D] + \Delta t^2 [K_{UP}] \tag{C10}$$

$$k_{12} = [K_{xy}] \tag{C11}$$

$$k_{13} = \Delta t[M_x] + \Delta t^2[C_x]^T, \quad k_{14} = [0] \tag{C12}$$

$$k_{21} = [K_{xy}]^T \tag{C13}$$

$$k_{22} = [M] + \Delta t([C] + [C]^T) + [K_y] + \Delta t Pr[K_D] + \Delta t^2[K_{UP}] \tag{C14}$$

$$k_{23} = \Delta t[M_y] + \Delta t^2[C_y]^T, \quad k_{24} = [0] \tag{C15}$$

$$k_{31} = \Delta t[M_x]^T + \Delta t^2[C_x] \tag{C16}$$

$$k_{32} = \Delta t[M_y]^T + \Delta t^2[C_y], \quad k_{34} = [0] \tag{C17}$$

$$k_{41} = k_{42} = k_{43} = [0] \tag{C18}$$

$$k_{44} = [M] + \Delta t([C] + [C]^T) + [K_y] + \Delta t[K_D] + \Delta t^2[K_{UP}] \tag{C19}$$

The element load vector, *fe*, each element of which is a 4×1 column vector is given as

$$fe = \begin{Bmatrix} (N_i + \Delta t V.\nabla N_i)u^n \\ (N_i + \Delta t V.\nabla N_i)(v^n + \Delta t Ra Pr T^n) \\ \Delta t \dfrac{\partial N_i}{\partial x} u^n + \Delta t \dfrac{\partial N_i}{\partial y}(v^n + \Delta t Ra Pr T^n) \\ (N_i + \Delta t V.\nabla N_i)T^n \end{Bmatrix}$$

APPENDIX D

SYSTEM MATRIX EQUATIONS FOR LSGS METHOD APPLIED TO COMPRESSIBLE FLOWS

The governing equations for compressible flows in $(\rho, u, v, T)^T$ form can be written similar to Bristeau [78] as:

$$\begin{aligned}
&\frac{\partial \rho}{\partial t}+u\frac{\partial \rho}{\partial x}+v\frac{\partial \rho}{\partial y}+\rho\left(\frac{\partial u}{\partial x}+\frac{\partial v}{\partial y}\right)=0\\
&\frac{\partial u}{\partial t}+u\frac{\partial u}{\partial x}+v\frac{\partial u}{\partial y}+(\gamma-1)\frac{T}{\rho}\frac{\partial \rho}{\partial x}+(\gamma-1)\frac{\partial T}{\partial x}=\frac{1}{\rho \mathrm{Re}}\left[\frac{\partial^2 u}{\partial x^2}+\frac{\partial^2 u}{\partial y^2}+\frac{1}{3}\frac{\partial}{\partial x}\left(\frac{\partial u}{\partial x}+\frac{\partial v}{\partial y}\right)\right]+f_x\\
&\frac{\partial v}{\partial t}+u\frac{\partial v}{\partial x}+v\frac{\partial v}{\partial y}+(\gamma-1)\frac{T}{\rho}\frac{\partial \rho}{\partial y}+(\gamma-1)\frac{\partial T}{\partial y}=\frac{1}{\rho \mathrm{Re}}\left[\frac{\partial^2 v}{\partial x^2}+\frac{\partial^2 v}{\partial y^2}+\frac{1}{3}\frac{\partial}{\partial y}\left(\frac{\partial u}{\partial x}+\frac{\partial v}{\partial y}\right)\right]+f_y\\
&\frac{\partial T}{\partial t}+u\frac{\partial T}{\partial x}+v\frac{\partial T}{\partial y}+(\gamma-1)T\left(\frac{\partial u}{\partial x}+\frac{\partial v}{\partial y}\right)=\frac{\gamma}{\rho \mathrm{Re}\,\mathrm{Pr}}\left(\frac{\partial^2 T}{\partial x^2}+\frac{\partial^2 T}{\partial y^2}\right)+\frac{1}{\rho \mathrm{Re}}F(\nabla V)
\end{aligned} \tag{D1}$$

where $F(\nabla V)$ is the energy dissipation term, which in two dimensions is given by

$$F(\nabla V)=\frac{4}{3}\left[\left(\frac{\partial u}{\partial x}\right)^2+\left(\frac{\partial v}{\partial y}\right)^2-\frac{\partial u}{\partial x}\frac{\partial v}{\partial y}\right]+\left(\frac{\partial u}{\partial y}+\frac{\partial v}{\partial x}\right)^2 \tag{D2}$$

Using Euler backward differences for time derivatives as

$$\frac{\partial u}{\partial t}\approx\frac{u^{n+1}-u^{n}}{\Delta t}\quad\text{and}\quad\frac{\partial v}{\partial t}\approx\frac{v^{n+1}-v^{n}}{\Delta t} \tag{D3}$$

Linearization of term $F(\nabla V)$ in time is done as follows

$$\begin{aligned}
F(\nabla V)&=\frac{4}{3}\left[\left(\frac{\partial u}{\partial x}\right)^2+\left(\frac{\partial v}{\partial y}\right)^2-\frac{\partial u}{\partial x}\frac{\partial v}{\partial y}\right]+\left(\frac{\partial u}{\partial y}+\frac{\partial v}{\partial x}\right)^2\\
&=\frac{4}{3}\left[\left|\frac{\partial u}{\partial x}\right|^n\frac{\partial u}{\partial x}+\left|\frac{\partial v}{\partial y}\right|^n\frac{\partial v}{\partial y}-\frac{1}{2}\left(\left|\frac{\partial u}{\partial x}\right|^n\frac{\partial v}{\partial y}+\left|\frac{\partial v}{\partial y}\right|^n\frac{\partial u}{\partial x}\right)\right]+\left|\frac{\partial u}{\partial y}+\frac{\partial v}{\partial x}\right|^n\left(\frac{\partial u}{\partial y}+\frac{\partial v}{\partial x}\right)
\end{aligned} \tag{D4}$$

where terms with $|^n$ are evaluated at the previous time level. Using backward Euler discretization and linearizing rest of non-linear terms in time we get the matrix form of the system

$$\mathscr{L}\, U^{n+1} = f \tag{D5}$$

where $U = (\rho, u, v, T)^T$ is the vector of unknowns, the operator $\mathscr{L}$ is given as

$$\mathscr{L} = \begin{bmatrix} I + \Delta t \vec{V}^n \cdot \nabla & & \Delta t \rho \dfrac{\partial}{\partial x} & \\ \Delta t(\gamma - 1)\dfrac{T}{\rho}\dfrac{\partial}{\partial x} & I + \Delta t \vec{V}^n \cdot \nabla - \dfrac{\Delta t}{\rho Re}\nabla^2 - \dfrac{\Delta t}{3\rho \,\mathrm{Re}}\dfrac{\partial^2}{\partial x^2} & & \\ \Delta t(\gamma - 1)\dfrac{T}{\rho}\dfrac{\partial}{\partial y} & -\dfrac{\Delta t}{3\rho \,\mathrm{Re}}\dfrac{\partial^2}{\partial y \partial x} & & \\ 0 & \Delta t(\gamma - 1)T\dfrac{\partial}{\partial x} - \dfrac{4a\Delta t}{3\rho \,\mathrm{Re}}\dfrac{\partial}{\partial x} - \dfrac{c\Delta t}{\rho Re}\dfrac{\partial}{\partial y} & & \end{bmatrix}$$

$$\begin{bmatrix} \Delta t \rho \dfrac{\partial}{\partial y} & 0 \\ -\dfrac{\Delta t}{3\rho \,\mathrm{Re}}\dfrac{\partial^2}{\partial x \partial y} & \Delta t(\gamma - 1)\dfrac{\partial}{\partial x} \\ I + \Delta t \vec{V}^n \cdot \nabla - \dfrac{\Delta t}{\rho Re}\nabla^2 - \dfrac{\Delta t}{3\rho \,\mathrm{Re}}\dfrac{\partial^2}{\partial y^2} & \Delta t(\gamma - 1)\dfrac{\partial}{\partial y} \\ \Delta t(\gamma - 1)T\dfrac{\partial}{\partial y} - \dfrac{4b\Delta t}{3\rho \,\mathrm{Re}}\dfrac{\partial}{\partial y} - \dfrac{c\Delta t}{\rho Re}\dfrac{\partial}{\partial x} & I + \Delta t \vec{V}^n \cdot \nabla \end{bmatrix} \tag{D6}$$

and the right hand side vector f is given as $\{\rho^n, u^n, v^n, T^n\}^T$. where $\vec{V}^n$ is the velocity field vector at previous time step, I an $m \times m$ identity matrix, m being number of nodes per element. The residual vector is given as

$$\mathscr{R} = \mathscr{L}\, U^{n+1} - f \tag{D7}$$

The residual is minimized using a suitable weighting operator that comes from LSFEM applied to first order terms of the governing equations. As explained in section 3.4, we get the equivalent Galerkin form the Euler-Lagrange formulation resulting from application of LSFEM to first order portion of the governing equations. Once we find the Galerkin form, we add the left out second order terms of the NS equations and apply Galerkin method to complete equation. For linear elements it is equivalent as treating the weighted residual of (D7) with weighting operator $\mathscr{S}$ as

$$\int_{\Omega}(\mathscr{S}N)^{T}(\mathscr{S}U^{n+1}-f)d\Omega=0 \tag{D8}$$

Where $\mathscr{S}$ is obtained from taking first order terms of governing equations i.e. Euler equation part given by

$$\mathscr{S}=\begin{bmatrix} I+\Delta t\vec{V}^{n}\cdot\nabla & 0 & \Delta t\rho\frac{\partial}{\partial x} & 0 \\ \Delta t(\gamma-1)\frac{T}{\rho}\frac{\partial}{\partial x} & I+\Delta t\vec{V}^{n}\cdot\nabla & 0 & \Delta t(\gamma-1)\frac{\partial}{\partial x} \\ \Delta t(\gamma-1)\frac{T}{\rho}\frac{\partial}{\partial y} & 0 & I+\Delta t\vec{V}^{n}\cdot\nabla & \Delta t(\gamma-1)\frac{\partial}{\partial y} \\ 0 & \Delta t(\gamma-1)T\frac{\partial}{\partial x}-\frac{4a\Delta t}{3\rho\,\mathrm{Re}}\frac{\partial}{\partial x}-\frac{c\Delta t}{\rho\,\mathrm{Re}}\frac{\partial}{\partial y} & \Delta t(\gamma-1)T\frac{\partial}{\partial y}-\frac{4b\Delta t}{3\rho\,\mathrm{Re}}\frac{\partial}{\partial y}-\frac{c\Delta t}{\rho\,\mathrm{Re}}\frac{\partial}{\partial x} & I+\Delta t\vec{V}^{n}\cdot\nabla \end{bmatrix} \tag{D9}$$

where a, b, c and d are the simplifying constants introduced. These are given as

$$a=\left(\frac{\partial u}{\partial x}-\frac{1}{2}\frac{\partial v}{\partial y}\right)^n,\ b=\left(\frac{\partial v}{\partial y}-\frac{1}{2}\frac{\partial u}{\partial x}\right)^n \ \ and \ \ c=\left(\frac{\partial v}{\partial x}+\frac{\partial u}{\partial y}\right)^n \tag{D10}$$

where Reynolds number and the Prandtl number given as $\rho_\infty U_\infty L/\mu$ and $\mu C_p/k$ respectively. Introducing the finite element approximation

$$U^{n+1}\approx U_h^{n+1}=\sum_i^m N_i U_i^{n+1} \tag{D11}$$

where m is the number of nodes per element and N_i is the element shape function associated with i^{th} node. Substituting the approximation into the weak formulation in (D8) leads to linear algebraic equations

$$[K]\{U^{n+1}\}=\{F\} \tag{D12}$$

Global stiffness matrix [K] and the vector {F} result from assembling the element stiffness matrices and vectors respectively given by

$$ke=\int_{\Omega_e}(\mathscr{S}\ N_i)^T(\mathscr{L}\ \ N_j)\,d\Omega;\qquad fe=\int_{\Omega_e}(\mathscr{S}\ N_i)^T f\,d\Omega.$$

ke is the element stiffness matrix given by

$$[ke]=\begin{bmatrix}k_{11}&k_{12}&k_{13}&k_{14}\\k_{21}&k_{22}&k_{23}&k_{24}\\k_{31}&k_{32}&k_{33}&k_{34}\\k_{41}&k_{42}&k_{43}&k_{44}\end{bmatrix} \tag{D13}$$

where each k_{ij} is itself a 4×4 matrix with i = 1, . . 4 and j = 1, . . 4. These are given as

$$k_{11}=[M]+\Delta t\left([C]+[C]^T\right)+\Delta t^2[K_{UP}]+\Delta t^2(\gamma-1)^2\frac{T^2}{\rho^2}[K_D] \tag{D14}$$

$$k_{12} = \Delta t\rho[M_x] + \Delta t^2\rho[C_x]^T + \Delta t(\gamma-1)\frac{T}{\rho}[M_x]^T + \Delta t^2(\gamma-1)\frac{T}{\rho}[C_x] \tag{D15}$$

$$k_{13} = \Delta t\rho[M_y] + \Delta t^2\rho[C_y]^T + \Delta t(\gamma-1)\frac{T}{\rho}[M_y]^T + \Delta t^2(\gamma-1)\frac{T}{\rho}[C_y] \tag{D16}$$

$$k_{14} = \Delta t^2(\gamma-1)^2\frac{T}{\rho}[K_D] \tag{D17}$$

$$k_{21} = \Delta t\rho[M_x]^T + \Delta t^2\rho[C_x] + \Delta t(\gamma-1)\frac{T}{\rho}[M_x] + \Delta t^2(\gamma-1)\frac{T}{\rho}[C_x]^T \tag{D18}$$

$$\begin{aligned} k_{22} = {} & [M] + \Delta t\left([C] + [C]^T\right) + \Delta t^2[K_{UP}] + \frac{\Delta t}{\rho\,\mathrm{Re}}[K_D] + \frac{\Delta t}{3\rho\,\mathrm{Re}}[K_x] + \Delta t^2\rho^2[K_x] \\ & + \Delta t^2(\gamma-1)^2T^2[K_x] - \frac{2a\Delta t^2(\gamma-1)T}{3\rho\,\mathrm{Re}}[K_x] + \left(\frac{4a\Delta t}{3\rho\,\mathrm{Re}}\right)^2[K_x] - \frac{c\Delta t^2(\gamma-1)T}{\rho\,\mathrm{Re}}[K_{xy}] \\ & + \frac{4ac\Delta t^2(\gamma-1)}{3\rho^2\,\mathrm{Re}^2}[K_{xy}] - \frac{c\Delta t^2(\gamma-1)T}{\rho\,\mathrm{Re}}[K_{xy}]^T + \frac{4ac\Delta t^2T}{3\rho^2\,\mathrm{Re}^2}[K_{xy}]^T + \left(\frac{c\Delta t}{\rho\,\mathrm{Re}}\right)^2[K_y] \end{aligned} \tag{D19}$$

$$\begin{aligned} k_{23} = {} & \Delta t^2\rho^2[K_{xy}] + \frac{\Delta t}{3\rho\,\mathrm{Re}}[K_{xy}] + \Delta t^2(\gamma-1)^2T^2[K_{xy}] - \frac{4b\Delta t^2(\gamma-1)T}{3\rho\,\mathrm{Re}}[K_{xy}] \\ & - \frac{c\Delta t^2(\gamma-1)T}{\rho\,\mathrm{Re}}[K_x] - \frac{4a\Delta t^2(\gamma-1)T}{3\rho\,\mathrm{Re}}[K_{xy}] + \frac{16ab\Delta t^2}{(3\rho\,\mathrm{Re})^2}[K_{xy}] + \frac{4ac\Delta t^2}{3\rho^2\,\mathrm{Re}^2}[K_x] \\ & - \frac{c\Delta t^2(\gamma-1)T}{\rho\,\mathrm{Re}}[K_y] + \frac{4bc\Delta t^2}{3\rho^2\,\mathrm{Re}^2}[K_y] + \left(\frac{c\Delta t}{\rho\,\mathrm{Re}}\right)^2[K_{xy}]^T \end{aligned} \tag{D20}$$

$$\begin{aligned} k_{24} = {} & \Delta t(\gamma-1)[M_x] + \Delta t^2(\gamma-1)[C_x]^T + \Delta t(\gamma-1)T[M_x]^T + \Delta t^2(\gamma-1)T[C_x] \\ & - \frac{4a\Delta t}{3\rho\,\mathrm{Re}}[M_x]^T - \frac{4a\Delta t^2}{3\rho\,\mathrm{Re}}[C_x] - \frac{c\Delta t}{\rho\,\mathrm{Re}}[M_y]^T - \frac{c\Delta t^2}{\rho\,\mathrm{Re}}[C_y] \end{aligned} \tag{D21}$$

$$k_{31} = \Delta t\rho[M_y]^T + \Delta t^2\rho[C_y] + \Delta t(\gamma-1)\frac{T}{\rho}[M_y] + \Delta t^2(\gamma-1)\frac{T}{\rho}[C_y]^T \tag{D22}$$

$$k_{32} = \Delta t^2 \rho^2 [K_{xy}]^T + \frac{\Delta t}{3\rho \mathrm{Re}}[K_{xy}]^T + \Delta t^2(\gamma-1)^2 T^2 [K_{xy}]^T - \frac{4b\Delta t^2(\gamma-1)T}{3\rho \mathrm{Re}}[K_{xy}]^T$$
$$- \frac{c\Delta t^2(\gamma-1)T}{\rho \mathrm{Re}}[K_x] - \frac{4a\Delta t^2(\gamma-1)T}{3\rho \mathrm{Re}}[K_{xy}]^T + \frac{16ab\Delta t^2}{(3\rho \mathrm{Re})^2}[K_{xy}]^T + \frac{4ac\Delta t^2}{3\rho^2 \mathrm{Re}^2}[K_x] \qquad \text{(D23)}$$
$$- \frac{c\Delta t^2(\gamma-1)T}{\rho \mathrm{Re}}[K_y] + \frac{4bc\Delta t^2}{3\rho^2 \mathrm{Re}^2}[K_y] + \left(\frac{c\Delta t}{\rho \mathrm{Re}}\right)^2 [K_{xy}]$$

$$k_{33} = [M] + \Delta t\left([C] + [C]^T\right) + \Delta t^2 [K_{UP}] + \frac{\Delta t}{\rho \mathrm{Re}}[K_D] + \frac{\Delta t}{3\rho \mathrm{Re}}[K_y] + \Delta t^2 \rho^2 [K_y]$$
$$+ \Delta t^2(\gamma-1)^2 T^2 [K_y] - \frac{2b\Delta t^2(\gamma-1)T}{3\rho \mathrm{Re}}[K_y] + \left(\frac{4b\Delta t}{3\rho \mathrm{Re}}\right)^2 [K_y] - \frac{c\Delta t^2(\gamma-1)T}{\rho \mathrm{Re}}[K_{xy}]^T \qquad \text{(D24)}$$
$$+ \frac{4bc\Delta t^2(\gamma-1)T}{3\rho^2 \mathrm{Re}^2}[K_{xy}]^T - \frac{c\Delta t^2(\gamma-1)T}{\rho \mathrm{Re}}[K_{xy}] + \frac{4bc\Delta t^2 T}{3\rho^2 \mathrm{Re}^2}[K_{xy}] + \left(\frac{c\Delta t}{\rho \mathrm{Re}}\right)^2 [K_y]$$

$$k_{34} = \Delta t(\gamma-1)[M_y] + \Delta t^2(\gamma-1)[C_y]^T + \Delta t(\gamma-1)T[M_y]^T + \Delta t^2(\gamma-1)T[C_y]$$
$$- \frac{4b\Delta t}{3\rho \mathrm{Re}}[M_y]^T - \frac{4b\Delta t^2}{3\rho \mathrm{Re}}[C_y] - \frac{c\Delta t}{\rho \mathrm{Re}}[M_x]^T - \frac{c\Delta t^2}{\rho \mathrm{Re}}[C_x] \qquad \text{(D25)}$$

$$k_{41} = \Delta t^2(\gamma-1)^2 \frac{T}{\rho}[K_D] \qquad \text{(D26)}$$

$$k_{42} = \Delta t(\gamma-1)[M_x]^T + \Delta t^2(\gamma-1)[C_x] + \Delta t(\gamma-1)T[M_x] + \Delta t^2(\gamma-1)T[C_x]^T$$
$$- \frac{4a\Delta t}{3\rho \mathrm{Re}}[M_x] - \frac{4a\Delta t^2}{3\rho \mathrm{Re}}[C_x]^T - \frac{c\Delta t}{\rho \mathrm{Re}}[M_y] - \frac{c\Delta t^2}{\rho \mathrm{Re}}[C_y]^T \qquad \text{(D27)}$$

$$k_{43} = \Delta t(\gamma-1)[M_y]^T + \Delta t^2(\gamma-1)[C_y] + \Delta t(\gamma-1)T[M_y] + \Delta t^2(\gamma-1)T[C_y]^T$$
$$- \frac{4b\Delta t}{3\rho \mathrm{Re}}[M_y] - \frac{4b\Delta t^2}{3\rho \mathrm{Re}}[C_y]^T - \frac{c\Delta t}{\rho \mathrm{Re}}[M_x] - \frac{c\Delta t^2}{\rho \mathrm{Re}}[C_x]^T \qquad \text{(D28)}$$

$$k_{44} = [M] + \Delta t\left([C] + [C]^T\right) + \Delta t^2 [K_{UP}] + \frac{\gamma \Delta t}{\rho \mathrm{Pr}\,\mathrm{Re}}[K_D] + \Delta t^2(\gamma-1)^2 [K_D] \qquad \text{(D29)}$$

and the RHS vector is

$$fe=\begin{Bmatrix} \left(N+\Delta t\vec{V}^{n}\cdot\nabla N\right)\rho^{n}+\Delta t(\gamma-1)\dfrac{T}{\rho}\left(\dfrac{\partial N}{\partial x}u^{n}+\dfrac{\partial N}{\partial y}v^{n}\right) \\ \Delta t\rho^{n}\dfrac{\partial N}{\partial x}\rho^{n}+\left(N+\Delta t\vec{V}^{n}\cdot\nabla N\right)u^{n}+\left(\Delta t(\gamma-1)T\dfrac{\partial N}{\partial x}-\dfrac{4a\Delta t}{3\rho\,\mathrm{Re}}\dfrac{\partial N}{\partial x}-\dfrac{c\Delta t}{\rho\,\mathrm{Re}}\dfrac{\partial N}{\partial y}\right)T^{n} \\ \Delta t\rho^{n}\dfrac{\partial N}{\partial y}\rho^{n}+\left(N+\Delta t\vec{V}^{n}\cdot\nabla N\right)v^{n}+\left(\Delta t(\gamma-1)T\dfrac{\partial N}{\partial y}-\dfrac{4b\Delta t}{3\rho\,\mathrm{Re}}\dfrac{\partial N}{\partial y}-\dfrac{c\Delta t}{\rho\,\mathrm{Re}}\dfrac{\partial N}{\partial x}\right)T^{n} \\ \Delta t(\gamma-1)\left(\dfrac{\partial N}{\partial x}u^{n}+\dfrac{\partial N}{\partial y}v^{n}\right)+\left(N+\Delta t\vec{V}^{n}\cdot\nabla N\right)T^{n} \end{Bmatrix} \quad \text{(D30)}$$

where:

$$[M]=\int_{\Omega}\{N\}\{N\}^{T}d\Omega, \qquad [M_x]=\int_{\Omega}\{N\}\left\{\frac{\partial N}{\partial x}\right\}^{T}d\Omega, \qquad [M_y]=\int_{\Omega}\{N\}\left\{\frac{\partial N}{\partial y}\right\}^{T}d\Omega$$

$$[C]=\int_{\Omega}\{N\}\left\{(\vec{V}\cdot\nabla)N\right\}^{T}d\Omega, \quad [C_x]=\int_{\Omega}\left\{\frac{\partial N}{\partial x}\right\}\left\{(\vec{V}\cdot\nabla)N\right\}^{T}d\Omega, \quad [C_y]=\int_{\Omega}\left\{\frac{\partial N}{\partial y}\right\}\left\{(\vec{V}\cdot\nabla)N\right\}^{T}d\Omega$$

$$[K_D]=\int_{\Omega}\{\nabla N\}\{\nabla N\}^{T}d\Omega, \quad [K_x]=\int_{\Omega}\left\{\frac{\partial N}{\partial x}\right\}\left\{\frac{\partial N}{\partial x}\right\}^{T}d\Omega, \qquad [K_y]=\int_{\Omega}\left\{\frac{\partial N}{\partial y}\right\}\left\{\frac{\partial N}{\partial y}\right\}^{T}d\Omega \quad \text{(D31)}$$

$$[K_{UP}]=\int_{\Omega}\left\{(\vec{V}\cdot\nabla)N\right\}\left\{(\vec{V}\cdot\nabla)N\right\}^{T}d\Omega, \qquad [K_{xy}]=\int_{\Omega}\left\{\frac{\partial N}{\partial x}\right\}\left\{\frac{\partial N}{\partial y}\right\}^{T}d\Omega$$

REFERENCES

[1] Clough, R. W. (1960). "The Finite Element Methods in Plane Stress Analysis." *Proc. 2nd Conf. Electronic Computations*, Pittsburgh, Pa.: ASCE, 345-378.

[2] Zienkiewicz, O. C. and Cheung, Y. K. (1965). "Finite Elements in Solution of Field Problems." *Engineer* 220: 507-510.

[3] Oden, J. T. (1972). *Finite Elements of Nonlinear Continua*, New York: McGraw Hill.

[4] Huebner, K. H. (1975). *Finite Element Method for Engineers*. New York: John Wiley & Sons.

[5] Baker, A. J. (1971). "A Finite Element Computational Theory for the Mechanics and Thermodynamics of a Viscous Compressible Multi-Species Fluid," *Bell Aerospace Research Dept*. 9500-920200

[6] Christie, I., Griffiths, D. F., Mitchell, A. R. and Zienkiewicz, O. C. (1976). "Finite Element Methods for Second Order Differential Equations with Significant First Derivative." *Int. J. Num. Meth. Eng.* 10: 1389-1396.

[7] Heinrich, J. C., Huyakorn, P. S., Zienkiewicz, O. C. and Mitchell, A. R. (1977). "An Upwind Finite Element Scheme for Two Dimensional Convective Transport Equation." *Int. J. Num. Meth. Eng.* 11: 134-143.

[8] Hughes, T. J. R. (1978). "A Simple Scheme for Developing Upwind Finite Elements." *Int. J. Num. Meth. Eng.* 12: 1359-1365.

[9] Hughes, T. J. R. and Atkinson, J. (1978). "A Variational Basis for Upwind Finite Elements." *IUTAM Symposium on Variational Methods in the Mechanics of Solids*, Northwestern University, Evanston, IL.

[10] Heinrich, J. C. and Zienkiewicz, O. C. (1979). "The Finite Element Method and 'Upwinding' Techniques in the Numerical Solution of Convection Dominated Flow Problems." In *Finite Element Methods for Convection Dominated Flows* (T. J. R. Hughes, ed.). New York: ASME AMD; 34: 105-136.

[11] Griffiths, P. M. and Mitchell, A. R. (1979). "On Generating Upwind Finite Element Methods" In *Finite Element Methods for Convection Dominated Flows* (T. J. R. Hughes, ed.), Presented at the Winter Annual Meeting of ASME, New York: ASME AMD; 34: 91-104.

[12] Brooks, A. N. and Hughes, T. J. R. (1982). "Streamline Upwind/Petrov Galerkin Formulations for Convection Dominated Flows with Particular Emphasis on the Incompressible Navier-Stokes Equations." *Comput. Meth. Appl. Mech. Eng.* 32: 199-259.

[13] Johnson, C. (1981). "Finite Element Methods for Convection-Diffusion Problems." *Fifth International Symposium on Computing Methods in Engineering and Applied Sciences*, INRIA, Versailles.

[14] Nävert, U. (1982). *A Finite Element Method for Convection-Diffusion Problems.* PhD Thesis, Dept. of Comp. Sci., Chalmers Univ. of Tech, Goteborg, Sweden.

[15] Hughes, T. J. R. and Tezduyar, T. E. (1984). "Finite Element Methods for First Order hyperbolic Systems with Particular Emphasis on the Compressible Euler Equations." *Comput. Meth. Appl. Mech. Eng.* 45: 217-284.

[16] Hughes, T. J. R., Mallet, M. and Mizukami, A. (1986). "A New Finite Element Formulation for Computational Fluid Dynamics: II. Beyond SUPG." *Comput. Meth. Appl. Mech. Eng.* 54: 341-355.

[17] Hughes, T. J. R and Mallet, M. (1986). "A New Finite Element Formulation for Computational Fluid Dynamics: IV. A Discontinuity Capturing Operator for Multidimensional Advective-Diffusive Systems." *Comput. Meth. Appl. Mech. Eng.* 58: 329-336.

[18] Oden, J. T. (1993). "A Short Course of Finite Element Methods for Computational Fluid Dynamics." Lecture Notes, Knoxville, Tennessee.

[19] Zienkiewicz, O. C. and Wu, J. (1991). "Incompressibility without Tears-How to Avoid Restrictions on Mixed Formulation." *Int. J. Num. Meth. Eng.* 32: 1189-1203.

[20] Yu, Sheng-Tao, Jiang, B. N., Wu, J. and Liu, N. S. (1996). "A Div-Curl-Grad Formulation for Compressible Buoyant Flows Solved by Least-Squares Finite Element Method." *Comput. Meth. Appl. Mech. Eng.* 137: 59-88.

[21] Babuska, I. (1971). "Error Bounds for Finite Element Method." *Num. Math.* 16: 322-333.

[22] Brezzi, F. (1974). "On the Existence, Uniqueness and Approximation of Saddle-point Problems arising from Lagrange Multipliers." *Rech. Oper., Ser. Rouge Anal. Numer.* 8: R-2, 129-151.

[23] Benim, A. C. and Zinser, W. (1986). "A Segregated Formulation of Navier-Stokes Equations with Finite Elements." *Comput. Meth. Appl. Mech. Engg.* **57**: 223-237.

[24] Rice, J. C. and Schnipke, R. J. (1986). "An Equal Order Velocity-Pressure Formulation that does not exhibit Spurious Pressure Modes." *Comput. Meth. Appl. Mech. Engg.* **58**: 135-149.

[25] Jiang, B. N. (1989). "A Least-squares Finite Element Method for Incompressible Navier-Stokes Problem." *NASA TM* 102385, *ICOMP* 89-28.

[26] Jiang, B. N. and Povinelli, L. A. (1989). "A Least-squares Finite Element Method for Incompressible Navier-Stokes Problem." *Proceedings of 12th Canadian Congress of Applied Mechanics*, Carleton university, Ottawa, Ontario, 602-603.

[27] Jiang, B. N. and Povinelli, L. A. (1990). "Least-squares Finite Element Method for Fluid Dynamics." *Comput. Meth. Appl. Mech. Engg.* **81**: 13-37.

[28] Dennis, B. H. and Rajeev Kumar (2007). "A Least-Squares/Galerkin Finite Element Method for Incompressible and Compressible Viscous Flows." *14th International Conference on Finite Elements in Flow Problems,* Santa Fe, New Mexico 26-28, March.

[29] Dennis, B. H. and Rajeev Kumar (2008). "A Least-Squares/Galerkin Split Finite Element Method for Incompressible Navier-Stokes Problems", *ASME International Design Engineering Technical Conferences & Computers and*

Information in Engineering Conference IDETC/CIE 2008, Brooklyn, New York 3-6, August.

[30] Karniadakis, G. E. and Sherwin, S. J. (1999) *Spectral/hp Element Methods for CFD*. Oxford University Press, NY

[31] Taghaddosi, F., Habashi, W. G., Guevremont, G. and Ait-Ali-Yahia, D. (1999). "An Adaptive Least-squares Method for the Compressible Euler Equations." *Int. J. Num. Meth. Fluids* **31**: 1121 - 1139.

[32] Xue, J. and Liao, G. (2005). "Least-squares Finite Element Method with Adaptive Grids for pdes with Shocks." *Wiley Interscience* Online Publication (www.interscience.wiley.com) DOI 10.1002/Num 20087.

[33] Cai, X., Fleitas, D. L., Jiang, B. N. and Liao, G. (2004). "Adaptive Grid Generation based on Least-squares Finite Element Methods." *Comput. Math. Appl*. 48: 1077-1085.

[34] Fleitas, D. L., Cai, X., Liao, G. and Jiang, B. N. (2005). "The Least-Squares Finite Element Method on Overlapping Elements." *J. Comput. Inf. Sys* 1:**2**: 203-213.

[35] Donea, J. and Huerta, A. (2003). *Finite Element Methods for Flow Problems*, Wiley Publishers, Chichester, England.

[36] Leij, F. J. and Dane, J. H. (1990). "Analytical Solutions of the One-Dimensional Advection Equation and Two- or Three-Dimensional Dispersion Equation." *Water Resources Research*, **26** (7): 1475-1482.

[37] Elman, H., Silvester, D. and Wathen, A. (2005). *Finite Elements and Fast Iterative Solvers: with Applications in Incompressible Fluid Dynamics*, Oxford University Press, New York.

[38] Huyakorn, P. S., Taylor, C., Lee, R. L. and Gresho, P. M. (1978). "A Comparison of Various Mixed-Interpolation Finite Elements in the Velocity-Pressure Formulation of the Navier-Stokes Equations." *Computers and Fluids,* **6**: 33-35.

[39] Carey, G. F. and Oden, J. T. (1986). "Finite Elements: Fluid Mechanics.", *Prentice Hall*, **IV**.

[40] Girault, V. and Raviart P. A. (1986). "Finite Element Method for Navier-Stokes Equation.", *Springer Verlag.*

[41] Ghia, U., Ghia, K. N. and Shin, C. T. (1982). "High Re Solutions for Incompressible Flow using the Navier-Stokes Equation and a Multigrid Method." *J. Comput. Phys.*, **48**: 387-411.

[42] Schreiber, R. and Keller, H. B. (1983), "Driven Cavity Flows by Efficient Numerical Techniques." *J. Comput. Phys.* **49**

[43] Bruneau, C. H. and Saad, M. (2006). "The 2D Lid-Driven Cavity Problem Revisited." *Comput. Fluids* **35**: 326-348.

[44] Armaly, B. F., Durst F., Pereira, J. C. F. and Schonung, B. (1982). "Experimental and Theoretical Investigation of Backward-Facing Step Flow." *J. Fluid Mech*. **127**: 473-496.

[45] Sohn, J. L. (1988). "Evaluation of FIDAP on Some Classical Laminar and Turbulent Benchmarks." *Int. J. Num. Meth. Fluids* **8**: 1469 - 1490.

[46] Gartling, D. K. (1990). "A Test Problem for Outflow Boundary Conditions-Flow over a Backward-Facing Step." *Int. J. Num. Meth. Fluids* **11**: 953 – 967.

[47] Kaiksis, L., Karniadakis, G. E. and Orszag, S. A. (1991). "Onset of Three-Dimensionality, Equilibria and Early Transition in Flow Over a Backward-Facing Step." *J. Fluid Mech.* **231**: 501 – 528.

[48] Runchal, A. W. (1992). "ANSWER: A Benchmark Study of Backward-Facing Step." in: Blackwell, B. and Pepper, D. W. (eds). (1992). "Benchmark Problems for Heat Transfer Codes." *Winter Annual Meeting ASME*, Anaheim, CA :13-30.

[49] Torczynski, J., R. (1993). "A Grid-Refinement Study of Two-Dimensional Transient Flow over a Backward-Facing Step using a Spectral Element Method." *Separated Flows*, *ASME Fluids Eng. Div*. **149**: 1 – 7.

[50] Okajima, A. (1982). "Strouhal Numbers of Rectangular Cylinders." . *J. Fluid Mech.* **123**: 379-398.

[51] Buscaglia, G. C. and Dari, E. A. (1992). "Implementation of the Lagrange-Galerkin Method for the Incompressible Navier-Stokes Equations." *Int. J. Num. Meth. Fluids* **15**: 23 – 36.

[52] Ostrach, S. (1988). "Natural Convection in Enclosures." *ASME Trans. J. Heat Transfer* **110**: 1175-1190.

[53] Gebhart, B. (1979). "Buoyancy-induced Fluid Motion Characteristics of Applications in Technology: The 1979 Freeman Scholar Lecture." *ASME Trans. J. Fluid Eng.* **101**: 5-28.

[54] Hoogendoorn, C. J. (1986). "Natural Convection in Enclosures." *Proc. Eighth Int. Heat Transfer Conf.* Hemisphere Publishing Corp., San Francisco **I**: 111-120.

[55] Davis Vahl, G. De (1983). "Natural Convection of Air in a Square Cavity: A Benchmark Numerical Solution." *Int. J. Num. Meth. Fluids* **3**: 249-264.

[56] Chenoweth, D.R. and Paolucci, S. (1986). "Natural Convection in an Enclosed Vertical Air Layer with Large Horizontal Temperature Differences." *J. Fluid Mech*. **169**: 173-210.

[57] Vierendeels, J., Merci, B. and Dick, E. (2003). "Benchmark Solutions for the Natural Convective Heat Transfer Problem in a Square Cavity with Large Horizontal Temperature Differences." *Int. J. Num. Meth. Heat Fluid Flow* **13**: 1057-1078.

[58] Chen, Y., Ohashi, H. and Akiyama, M. (1994). "Thermal Lattice Bhatnagar-Gross-Krook Model without Nonlinear Deviations in Macrodynamic Equations." *Phys. Rev. E* **50**: 2776-2783.

[59] Eggels, J. G. M. and Somers, J. A. (1995). "Numerical Simulation of Free Convection Flow using Lattice Boltzmann Scheme." *Int. J Heat Fluid Flow* **16:** 357-364.

[60] Dixit, H. N. and Babu, V. (2006). "Simulation of High Rayleigh Number Natural Convection in a Square Cavity using Lattice Boltzmann Method." *Int. J. Heat and Mass Transfer* **49**: 727-739.

[61] Tang, L.Q. and Tsang, T.T. (1993). "A Least-Squares Finite Element Method for Time-dependent Incompressible Flows with Thermal Convection." *Int. J. Num. Meth. Fluids*, **17**: 271-289.

[62] Tezduyar, T. E., Behr, M., Mittal, S. and Liou, J. (1992). "A new Strategy for Finite Element Computations Involving Moving Boundaries and Interfaces- The Deforming Spatial-Domain/ Space Time Procedure: II. Computation of Free-Surface .. Cylinders." *Comput. Meth. Appl. Mech. Eng.*, **94** : 353-371.

[63] Tezduyar, T. E. and Hughes, T. J. R. (1982). "Development of Time-Accurate Finite Element Techniques for First Order Hyperbolic Systems with Particular Emphasis on Compressible Euler Equations." *NASA TR NASA-CR*-204772.

[64] Hughes, T. J. R., Mallet, M. and Mizukami, A. (1986). "A New Finite Element Formulation for Computational Fluid Dynamics: II. Beyond SUPG." *Comput. Meth. Appl. Mech. Eng.*, **54** : 341-355.

[65] Le Beau, G. J. and Tezduyar, T. E. (1991a). "Finite Element Computation of Compressible Flows with the SUPG Formulation." *Advances in Finite Element Analysis in Fluid Dynamics,* FED **123**: 21-27 New York, ASME.

[66] Shakib, F. and Hughes, T. J. R. (1991). "A New Finite Element Formulation for Computational Fluid Dynamics: IX. Fourier Analysis of Space-Time Galerkin/Least Squares Algorithms." *Comput. Meth. Appl. Mech. Eng.* **87**: 35-58.

[67] Shakib, F., Hughes, T. J. R. and John, Z. (1991). "A New Finite Element Formulation for Computational Fluid Dynamics: X. The Compressible Euler and Navier-Stokes Equations" *Comput. Meth. Appl. Mech. Eng.* **89**: 141-219.

[68] Jansen, K. E. (1990). "A Stabilized Finite Element Method for Computing Turbulence." *Comput. Meth. Appl. Mech. Eng.* **174**: 299-317.

[69] Jansen, K. E. and Hughes, T. J. R. (1995). "A Stabilized Finite Element Method for the Reynolds-averaged Navier-Stokes Equations." *Surveys on Mathematics for Industry*, **4**: 279-317.

[70] Jansen, K. E., John, Z. and Hughes, T. J. R. (1993). "Implementation of a One-Equation Turbulence Model within a Stabilized Finite Element Formulation of a Sym. Advective-Diffusive Sys." *Comput. Meth. Appl. Mech. Eng.* **105**: 405-433.

[71] Hauke, G. (1995). *A Unified Approach to Compressible and Incompressible Flows and a new Entropy-consistent Formulation of the k-ε Model*. PhD Thesis, Mechanical Engineering Department, Stanford University.

[72] Le Beau, G. J. and Tezduyar, T. E. (1991b). "Finite Element Solution of Flow-problems with Mixed-time Integration." *J. Engineering Mech.* **117**: 1311-1330.

[73] Tezduyar, T. E., Aliabadi, S., Behr, M., Johnson, A., Kalro, B. and Litke, M. (1996). "Flow Simulation and High Performance Computing." *Computational Mech.* **18**: 397-412.

[74] Tezduyar, T. E., Aliabadi, S. K., Behr, M., Johnson, A. and Mittal, S. (1993). "Parallel Finite Element Computation of 3D Flows." *Computer* **26**(10): 27-36.

[75] Tezduyar, T. E., Aliabadi, S. K., Behr, M. and Mittal, S. (1994). "Massively Parallel Finite Element Simulation of Compressible and Incompressible Flows." *Comput. Meth. Appl. Mech. Eng.* **119**: 157-177.

[76] Mittal, S. and Tezduyar, T. E. (1998). "A unified Finite Element Formulation for Compressible and Incompressible Flows using Augmented Conservation Variables." *Comput. Meth. Appl. Mech. Eng.* **161**: 229-243.

[77] Mittal, S., Aliabadi, S. K. and Tezduyar, T. E. (1999). "Parallel Computation of Unsteady Compressible Flows with the EDICT." *Computational Mechanics* **23**:151-157.

[78] Bristeau, M. O., Glowinski, R., Dutto, L., Periaux, J. and Roge, G. (1990). "Compressible Viscous Flow Calculations Using Compatible Finite Element Approximations." *Int. J. Num. Meth. Fluids* **11**: 719 – 749.

[79] Carter, J. E. (1972). "Numerical Solutions of the Navier-Stokes Equations for the Supersonic Laminar Flow over a Two-Dimensional Compression Corner." *NASA-TR-R*-385.

[80] Oden, J. T. and Jacquotte, O. P. (1984). "Stability of Some Mixed Finite Element Methods for Stokesian Flows." *Comput. Meth. Appl. Mech. Eng.* **43**(2): 231-248.

[81] Cebeci, T. and Bradshaw, P. (1977). *Momentum Transfer in Boundary Layers*, McGraw-Hill , New York.

[82] Cebeci, T. and Smith, A. M. O. (1970). "A Finite-Difference Method for Calculating Compressible Laminar and Turbulent Boundary Layers." *J. Basic Eng*. **92**(3): 523-535

[83] Baldwin, B. S. and Lomax, H. (1978). "Thin-layer Approximation and Algebraic Model for Separated Turbulent Flows." *AIAA*, 78-257.

[84] Mavripilis, D. J. (1991). "Turbulent Flow Calculations using unstructured and Adaptive Meshes." *Int. J. Num. Meth. Fluids*, **13**: 1131-1152.

[85] Wolfshtein, M. (1992). "The Velocity and Temperature Distribution in One-dimensional Flow with Turbulence Augmentation and Pressure Gradient." *Int. J. Heat Mass Transfer*, **12**: 301-312.

[86] Jansen, K., Johan, Z. and Hughes, T. J. R. (1993). "Implementation of a One-equation Turbulence Model within a Stabilized Finite Element Formulation of a Symmetric Advective-Diffusive System." *Comput. Meth. Appl. Mech. Eng.* **105**: 405-433.

[87] Baldwin, B. S. and Barth, T. J. (1978). "A One-equation Turbulence Transport Model for High Reynolds Number Wall-bounded Flows." *AIAA TR* 91-0610.

[88] Jones, W. P. and Launder, B. E. (1972). "The Prediction of Laminarization with a 2-equation Model of Turbulence." *Int. J. Heat Mass Transfer*, **15**: 301-314.

[89] Kubota, T. and Ko, D. R. S. (1967). "A Second Order Wake-Interaction Expansion for Moderately Hypersonic Flow Past a Flat Plate." *AIAA J.* **5**(10): 1915-1917.

[90] Mavriplis, D. J. (1989). "Zonal Multigrid Solution of Compressive Flow Problems on Unstructured and Adaptive Meshes." *ICASE* Rep. No. 89-37 NASA CR-181848.

[91] Tang, C. and Hafez, M. (2001). "Numerical Simulation of Steady Compressive Flows using a Zonal Formulation. Part II: Viscous Flows." *Comput. Fluids* **30**: 1003-1016.

BIOGRAPHICAL INFORMATION

Rajeev Kumar received his Bachelor of Engineering degree from Punjab University, Chandigarh, India in 1992 and Master of Engineering degree from Indian Institute of Science, Bangalore, India in 2000 and his Ph. D. degree from University of Texas at Arlington in 2008, all in Aerospace Engineering. He worked for ten years as a research scientist in National Aerospace Laboratories, Bangalore, India as an experimental aerodynamicist. He worked in the fields of turbulent drag reduction, base drag characteristics of aerodynamic bodies with and without jet exhaust and flow visualization. He received Hermann Doctoral Fellowship and Kalpana Chawla Memorial Scholarship at University of Texas Arlington. He is a member of tau beta pi honor society and a student member of ASME, AIAA. His current research interests include Finite Element Methods, Turbulence Modeling and Heat Transfer.